To be published as a chapter in
book "Advances in Electrochemistry
and Electrochemical Engineering" Vol. 9
R. Muller, ed. (Interscience)

LBL-187
Preprint

PRINCIPLES OF ELLIPSOMETRY

Rolf H. Muller

December 1971

AEC Contract No. W-7405-eng-48

TWO-WEEK LOAN COPY

This is a Library Circulating Copy which may be borrowed for two weeks. For a personal retention copy, call Tech. Info. Division, Ext. 5545

LBL-187

DISCLAIMER

This document was prepared as an account of work sponsored by the United States Government. While this document is believed to contain correct information, neither the United States Government nor any agency thereof, nor the Regents of the University of California, nor any of their employees, makes any warranty, express or implied, or assumes any legal responsibility for the accuracy, completeness, or usefulness of any information, apparatus, product, or process disclosed, or represents that its use would not infringe privately owned rights. Reference herein to any specific commercial product, process, or service by its trade name, trademark, manufacturer, or otherwise, does not necessarily constitute or imply its endorsement, recommendation, or favoring by the United States Government or any agency thereof, or the Regents of the University of California. The views and opinions of authors expressed herein do not necessarily state or reflect those of the United States Government or any agency thereof or the Regents of the University of California.

PRINCIPLES OF ELLIPSOMETRY

Contents

Abstract iii

I. Introduction 1

II. Polarized Light 3

1. Linear Polarization 3

2. Elliptic Polarization 3

A. s and p Components 3

B. Geometric and Physical Parameters 4

C. Poincaré Sphere 7

III. Optical Reflection 9

1. Reflection from Bare Surfaces 9

A. Complex Amplitude 9

B. Fresnel Equations 10

C. Equations of Ellipsometry 14

D. Data for Reflection from Bare Surfaces 16

2. Reflection from Film-Covered Surfaces 17

A. Drude Equations 17

B. Computations 20

C. Double Beam Model for Transparent Films 22

D. Multiple Films 23

3. Conventions and Definitions 24

IV. Ellipsometer Arrangements 26

1. Measurement With or Without Compensation 26

2. Fixed and Variables Compensators 26

3. Linear and Elliptic Polarization Incident 29

4. Application of Poincaré Sphere 31

A. Linear Polarization Incident 31

B. Elliptic Polarization Incident 33

C. Error Propagation 34

5. Other Ellipsometer Arrangements 36

6. Modern Instrumentation 36

A. Self-Compensating Ellipsometers 36

B. Non-Compensating Ellipsometers 39

V. Experimental Aspects 40

1. Four Zones 40

2. Sixteen Zones 42

3. Zone Averaging 44

4. Alignment and Calibration 45

5. Other Sources of Errors 47

6. Manual Ellipsometer Operation 50

VI. Outlook 51

1. Theoretical Problems 51

2. Instrumental Problems 53

3. Conclusions 54

References 55

Figure Captions 63

Figures 72

PRINCIPLES OF ELLIPSOMETRY

Rolf H. Muller

Inorganic Materials Research Division, Lawrence Berkeley Laboratory and
Department of Chemical Engineering: University of California
Berkeley, California

ABSTRACT

Theoretical principles of ellipsometry, capabilities and limitations of the technique for the study of surfaces and thin films are reviewed. Factors which need to be considered in the operation of ellipsometers of present design are considered and directions of future developments are indicated.

PRINCIPLES OF ELLIPSOMETRY

I. Introduction

Ellipsometry derives its name from the measurement of elliptically polarized light which results from optical reflection. More precisely, the change in the state of polarization due to reflection is measured and interpreted in terms of properties of the reflecting surface. The utility of ellipsometry for electrochemical purposes is largely due to its capability for examining surfaces in any optically transparent environment. Electrode surfaces can therefore often be observed in situ, without exposing them to conditions (e.g. vacuum, heat, electron impact) which might alter their properties. Previous reviews of ellipsometry (7,16,144) and proceedings from two conferences (13,98) are available.

Two parameters are measured in ellipsometry: the change in relative amplitude and relative phase of two orthogonal components of light due to reflection. The fact that relative, rather than absolute measurements are made is one reason for the high resolution of ellipsometry. The technique employs a built-in reference, so to speak, which largely eliminates effects due to external fluctuations, such as those of the light source. The other reason for the high resolution lies in the fact that the measured quantities are usually azimuth angles (i.e. angles resulting from rotation around an optic axis), and angular measurements can easily be made with high resolution. For example, an angle of 0.01°, the resolution of currently available research instruments, represents 3×10^{-5} of a full turn, the largest measurement possible.

From the measured two quantities, change in relative amplitude and phase at constant wavelength, two parameters of the reflecting surface can be derived. For a bare surface, this can be real and imaginary parts of

the refractive index. For a surface covered with a transparent film, thickness and refractive index of the film can be determined, if the optical constants of the substate are known. If sufficiently narrow limits can be imposed on acceptable solutions, it is sometimes possible to determine more than two unknowns, e.g. thickness and complex refractive index of an absorbing film. Additional data have been generated by immersion in media of different refractive index and reflectivity measurements at normal incidence (79).

In many cases, an increase in film thickness by one wavelength results in an azimuth change of a full turn. Under these conditions, an angular resolution of 0.01° results in an average resolution in film thickness of 3×10^{-5} wavelengths or about 0.2Å.

The availability of high-speed computers and comprehensive programs (84) has been an important factor for the renewed interest in ellipsometry, which has been in existence at least since 1888 (55). The exact classical equations, presently used for the interpretation of results, cannot be solved explicitly (130) and, despite their simple algebraic form, are too tedious for hand calculations in all but a few special cases. Approximations, introduced in earlier days, have more recently been found to be often not reliable (31).

In the following, a brief account of the classical theory of ellipsometry, its used and limitations will be given. Detailed derivations of electromagnetic theory on which this theory is based, would exceed the scope of this chapter. Instead, it will be attempted to provide primarily a physical understanding of the optical phenomena involved and of the principles of ellipsometer measurements.

II. POLARIZED LIGHT

1. Linear Polarization

The complete description of a monochromatic light wave, in addition to frequency, phase, propagation direction and amplitude, has to include information on the orientation of electric and magnetic vectors in space (Fig. 1). Since the two vectors are orthogonal, it is usually sufficient to consider the electric vector only. If the electric vector, along a wave in space, lies in a plane, the light is called linearly polarized. The connecting line between the end-points of the vectors shows the sinusoidal electric field distribution along the propagation direction z at a fixed instant in time (Fig. 2). At a given point in space, the tip of the electric vector oscillates along a straight line as a function of time, hence the name. Polarization is a direct consequence of the transverse nature of light. In the present literature, the plane which contains the electric vectors in space is called the plane of polarization. Superposition of two linearly polarized waves which are in phase results in another linear polarization (Fig. 3). Linear polarization is the best known state of polarization of light and often simply referred to as polarized light.

2. Elliptic Polarization

A. s and p Components

In analyzing the reflection of light, it is convenient to decompose incident and reflected waves into two orthogonal linear components. One of these components has its electric vector oriented parallel to the plane which contains incident and reflected beams (or wave normals), called the plane of incidence. This component is usually denoted by a subscript p. The other component, denoted by a subscript s, has its electric vector oriented normal to the plane of incidence (Fig. 4).

Both components suffer different changes in phase and amplitude upon reflection.

B. Geometric and Physical Parameters

The superposition of linearly polarized s and p components of the same frequency, but different phase and amplitude, in general, results in elliptic polarization (96,111,122, 141). The tip of the electric vector now describes a helix in space or, at a given location, it traces an ellipse as a function of time (Fig. 5).

$$E_{tp} = |E_p| \cos(\omega t + \varepsilon_p) \tag{1}$$

$$E_{ts} = |E_s| \cos(\omega t + \varepsilon_s) \tag{2}$$

This ellipse also results from the projection of the helix on a plane normal to the propagation direction. The ellipse possesses a positive (counterclockwise) or negative (clockwise) sense of rotation, as seen looking into the beam, and is inscribed in a rectangle (if we limit these considerations to orthogonal components) with sides parallel to the planes of polarization of both components and lengths equal to twice their amplitudes (Fig. 5, top). A detailed review of the analysis of elliptic polarization, using matrix methods, has been given by Richartz and Hsue (104).

Elliptic polarization is the most general state of polarization, with circular and linear polarization being limiting cases. The state of polarization, independent of light intensity, can be characterized by either of two sets of two parameters each, which can be measured as azimuth angles with an ellipsometer.

The physical parameters, already mentioned, are the ratio of the

electric field amplitudes $|E|$ of p and s components, expressed as the tangent of an angle ψ

$$\frac{|E_p|}{|E_s|} = \tan \psi \tag{3}$$

and the difference Δ of the time independent phase ε of the two components

$$\varepsilon_p - \varepsilon_s = \Delta \tag{4}$$

The quantities ψ and Δ are indicated in the upper part of Fig. 5. The range of values for the two physical parameters are

$$0° \leqslant \psi \leqslant 90° \tag{5}$$

$$0° \leqslant \Delta \leqslant 360° \tag{6}$$

A range of ±180° for Δ is equivalent to the one given in Eq. 6. For reflection from bare surfaces the ranges of ψ and Δ values are further restricted (see section D).

The <u>geometric parameters</u> characterize elliptic polarization by the shape and orientation of the ellipse. They are the angle θ, which the major axis of the ellipse forms with the plane of incidence (measured counterclockwise)

$$\theta = \text{orientation of major axis} \tag{7}$$

and the excentricity of the ellipse

$$\tan \gamma = \frac{\text{minor axis}}{\text{major axis}} \tag{8}$$

The angle γ is measured in the sense of the rotation of the ellipse and can therefore assume positive and negative values. The angles γ and θ are indicated in the lower part of Fig. 5. The ranges of the geometric parameters are

$$0° \leqslant \theta < 180° \tag{9}$$

$$-45° \leqslant \gamma \leqslant 45° \tag{10}$$

Physical and geometric parameters of elliptic polarization can be mutually converted either graphically by use of the Poincaré sphere (see below) or algebraically with the following expressions (27,47,96,111,134), which can be derived by coordinate transformations.

$$\sin 2\gamma = \sin 2\psi \sin \Delta \tag{11}$$

$$\tan \Delta = \frac{\tan 2\gamma}{\sin 2\theta} \tag{12}$$

$$\tan 2\theta = -\tan 2\psi \cos \Delta \tag{13}$$

$$\cos 2\psi = -\cos 2\gamma \cos 2\theta \tag{14}$$

All the angles except the relative phase Δ appear doubled in the above relations.

Orientation and sense of rotation of the ellipse are determined by the phase difference Δ between both components (47,63). A few examples are given in Fig. 6, where the azimuth angles representing different parameters are also indicated. It can be seen that a phase difference of 0°, 180° etc. produces linear polarization, while a phase difference of 90° (or a quarter wavelength), 270° etc. results in the ellipse axis to be oriented parallel to the planes of polarization of the two components. Fast and slow components, mutually out of phase by 90° are indicated for a general ellipic polarization in Fig. 5. This fact will be used later. The orientations of the ellipse shown in Fig. 6 are valid only for the coordinate system indicated, the relative phase Δ as defined in Eq. 4 and the phase ε as formulated in Eqs 1 and 2. The same figures have been obtained with different definitions of Δ and ε (47).

Unpolarized light can be pictured as a superposition or rapid sequence of different states of polarization which may be linear or elliptic each (96).

C. Poincaré Sphere

The state of polarization of any light wave of unit intensity may be represented by a point E on the surface of a unit sphere, known as Poincaré sphere (18,64,82,112, 128). The features of this representation can be derived from the Stokes parameters (27,82,85,122). A coordinate grid for the geometic parameters of polarization (Fig. 7, top) is established, with longitude 2 θ, measured on the "equator" counterclockwise, as seen from pole L, from point H, which signifies the plane of incidence, and latitude 2 γ. Points on the "northern" hemisphere (o), with positive γ values, represent left hand (positive)rotation of the ellipse, points on the "southern" hemisphere (x) right hand rotation. The two poles represent left and right hand circular polarization, while points on the equator signify linear polarization states of different azimuth, θ, with pure p polarization represented by point H, pure s by point V.

A similar coordinate grid can be established to represent the physical parameters of polarization (Fig. 7, center). Point H forms one pole of this coordinate grid. Great circles represent lines of constant relative phase Δ, which is measured from the "equator" in a positive (counterclockwise) sense of rotation, as seen from point H. Lines of constant paramter 2 ψ are small circles with the origin at the pole V opposite to H. This pole represents the plane normal to the plane of incidence, or pure s polarization. Points on the circle of

$2\psi = 90°$ (which is also a great circle through poles L and R) represent states of polarization of equal amplitude of p and s components.

It should be noted that all angles, except phase angles appear doubled on the Poincaré sphere, as in equations 9 to 12, which can also be derived from the two coordinate grids by use of spherical trigonometry.

The equator of the Poincaré sphere is also used to indicate the orientation of polarizer and analyzer transmission axis P and A and the fast axis F of the compensator. Their azimuth angles p, a and q (measured counterclockwise from the plane of incidence) are also doubled on the sphere and have the same value as the quantity θ.

A superposition of the coordinate girds for geometric and physical parameters provides a graphical conversion between the two. For this purpose, and other applications of the Poincaré sphere to follow, the use of a stereographic projection of the sphere, indicated in the right hand column of Fig. 7, is best suited (141). The stereographic projection provides an angle-true representation of the surface of a sphere. It is obtained by a central projection of a hemisphere from the opposite pole on a plane through the equator. Stereographic grids (polar and equatorial, Wulff's net) are commonly used in crystallography (11).

The third coordinate grid, indicated on the bottom of Fig. 7, represents the effect of a retardation plate. The orientation of the fast axis of this compensator plate, chosen to be of azimuth 45° in the figure, is represented by point F on the equator of the sphere. The retardation δ_Q of the plate results in a positive rotation on the sphere, as seen from F. This grid is identical to the one for Δ with the fast axis F taking the place of the plane of incidence H, its use will become clearer in some sections to follow.

III. OPTICAL REFLECTION

1. Reflection from Bare Surfaces

A. Complex Amplitude

The complex notation provides a simple formalism for the description of oscillations and waves (47,62,121). Its advantages are best seen in the addition of two waves of different phase which can be performed as an addition of two vectors in the complex plane without the use of tedious trigonometric formulas.

The instantaneous amplitude of a harmonic oscillation can be formulated trigonometrically (Eq. 1) as

$$E_t = |E| \cos(\omega t + \varepsilon) \tag{15}$$

According to the Gauss equation

$$e^{ix} = \cos x + i \sin x \tag{16}$$

the exponential formulation (Eq. 17) has the same real part as Eq. 15. (The imaginary unit $\sqrt{-1}$ is designated by the letter i.)

$$|E| \; e^{i(\omega t + \varepsilon)} = |E| \; [\cos(\omega t + \varepsilon) + i \sin(\omega t + \varepsilon)] \tag{17}$$

For this reason, it is used to represent the cosine formulation, with the understanding that the real part represents the oscillation.

$$E_t = |E| \; e^{i(\omega t + \varepsilon)} \tag{18}$$

The time-dependent factor in Eq. 18

$$e^{i\omega t}$$

is not particularly important and often disregarded in considerations of monochromatic light. The time-independent part of Eq. 18 is called the complex amplitude E:

$$E = |E|\ e^{i\varepsilon} \tag{19}$$

Its modulus $|E|$ is the real amplitude, its argument ε the phase of the oscillation relative to a reference.

B. Fresnel Equations

The reflection of light on a dielectric (non-absorbing) interface can be described by the Fresnal (amplitude) reflection coefficients r. These coefficients represent the ratio of reflected to incident electric field amplitude, they are different for s and p components

$$r_p = \frac{E''_p}{E_p} \tag{20}$$

$$r_s = \frac{E''_s}{E_s} \tag{21}$$

As indicated in Fig. 8, double-primed quantities refer to the reflected, unprimed to the incident wave. The Fresnel equations (27,63,126,128,134, 139), in their simplest form relate the amplitude reflection coefficients to the angles of incidence and refraction, indicated in Fig. 8.

$$r_p = \frac{\tan(\phi - \phi')}{\tan(\phi + \phi')} \tag{22}$$

$$r_s = -\frac{\sin(\phi - \phi')}{\sin(\phi + \phi')} \tag{23}$$

The angle of refraction ϕ' can be obtained from the angle of incidence ϕ and the refractive indices of both media at the interface by use of Snell's law

$$\sin\ \phi' = \frac{n_o}{n_1} \sin\ \phi \tag{24}$$

Fresnel coefficients of negative sign signify a phase change of 180°

($\exp i\pi = -1$) of the reflected with respect to the incident wave at the reflecting surface.

Application of electromagnetic theory (19,26,27,37,68,72,80,106,123) shows that the Fresnel equations can be adapted to describe reflection from absorbing media by introduction of a complex refractive index n_c in place of n_1

$$n_c = n - i\,k \tag{25}$$

If n_c is defined here to be a material constant, independent of angle of incidence (41,90), application of Snell's law

$$n_o \sin\phi = n_c \sin\phi_c' \tag{26}$$

results in a complex angle of refraction ϕ_c', which provides a valid formalism, but has no recognizable physical meaning.

The resulting complex reflection coefficients can be cast in exponential form

$$r_p = \frac{|E_p''|}{|E_p|}\, e^{i(\varepsilon_p'' - \varepsilon_p)} \tag{27}$$

$$r_s = \frac{|E_s''|}{|E_s|}\, e^{i(\varepsilon_s'' - \varepsilon_s)} \tag{28}$$

with the modulus representing the amplitude attenuation $|r|$

$$|r_p| = \frac{|E_p''|}{|E_p|}$$

$$|r_s| = \frac{|E_s''|}{|E_s|} \tag{30}$$

and the argument representing the (absolute) change in phase δ due to reflection

$$\delta_p = \varepsilon''_p - \varepsilon_p \tag{31}$$

$$\delta_s = \varepsilon''_s - \varepsilon_s \tag{32}$$

Thus, the complex Fresnel reflection coefficients can also be expressed as

$$r_p = |r_p| \, e^{i\delta p} \tag{33}$$

$$r_s = |r_s| \, e^{i\delta s} \tag{34}$$

As shown by Koenig (68) the use of complex arithmetic to derive the above quantities can be avoided by the introduction of expressions involving only real quantities. For the present conventions and definitions these expressions are (51,88):

$$|r_s| = \sqrt{\frac{A^2 + B^2 - 2A \cos\phi + \cos^2\phi}{A^2 + B^2 + 2A \cos\phi + \cos^2\phi}} \tag{35}$$

$$|r_p| = |r_s| \sqrt{\frac{A^2 + B^2 - 2A \sin\phi \tan\phi + \sin^2\phi \tan^2\phi}{A^2 + B^2 + 2A \sin\phi \tan\phi + \sin^2\phi \tan^2\phi}} \tag{36}$$

$$\delta_s = \tan^{-1}\left[- \frac{2B \cos\phi}{A^2 + B^2 - \cos^2\phi} \right] \tag{37}$$

$$\delta_p = \tan^{-1}\left[\frac{2B \cos\phi \, (A^2 + B^2 - \sin^2\phi)}{A^2 + B^2 - \frac{1}{n_o^4} (n^2 + k^2)^2 \cos^2\phi} \right] \tag{38}$$

with the intermediate variables A and B defined as

$$A = \sqrt{\frac{1}{2\,n_o^2}\left[\sqrt{(n^2 - k^2 - n_o^2 \sin^2\phi)^2 + 4n^2k^2} + (n^2 - k^2 - n_o^2 \sin^2\phi)\right]} \quad (39)$$

$$B = \sqrt{\frac{1}{2\,n_o^2}\left[\sqrt{(n^2 - k^2 - n_o^2 \sin^2\phi)^2 + 4n^2k^2} - (n^2 - k^2 - n_o^2 \sin^2\phi)\right]} \quad (40)$$

When the direction of propagation of the refracted wave (the physical, real angle of refraction ϕ_r') has to be known, e.g. for determining the penetration depth at non-normal incidence, an alternate complex refractive index

$$n_c' = n' - ik' \quad (41)$$

which depends on the angle of incidence can be defined (41). The real part of this refractive index and the real angle of refraction ϕ_r' satisfy Snell's law

$$n_o \sin\phi = n' \sin\phi_r' \quad (42)$$

The imaginary part describes the decay of the electric field amplitude with increasing distance z normal to the surface

$$E \sim e^{-\frac{2\pi}{\lambda_o} k' z} \quad (43)$$

where λ_o is the vacuum wavelength.

The distance at which the square of the electric field amplitude (a measure of light intensity) decreases by a factor 1/e is the (intensity) penetration depth

$$z = \frac{\lambda_o}{4\pi\ k'} \quad (44)$$

Some penetration depth data are given in Fig. 9. For most metals, z is a few hundred Angstrom units. The complex refractive index and its alternate are related (41) by

$$n^2 - k^2 = n'^2 - k'^2 \tag{45}$$

$$nk = n' k' \quad \cos \phi_r' \tag{46}$$

The dependence of the alternate optical constants on the angle of incidence has been illustrated elsewhere (90). For many metals the change is small. At normal incidence the two quantities become identical. The angle-dependent optical constants have deliberately been used by Vašíček (133).

C. Equations of Ellipsometry

The ellipsometer determines the ratio ρ of the (complex) reflection coefficients for p and s components

$$\rho = \frac{r_p}{r_s} \tag{47}$$

The use of equations 27 and 28 and re-arranging of terms results in

$$\rho = \frac{\frac{|E_p''|}{|E_s''|}}{\frac{|E_p|}{|E_s|}} \; e^{i[(\varepsilon_p'' - \varepsilon_s'') - (\varepsilon_p - \varepsilon_s)]} \tag{48}$$

The modulus of this expression contains the relative amplitudes of p and s components in reflected (subscript r) and incident (subscritp i) waves, which can be formulated according to Eq. 3 as

$$\tan \psi_r = \frac{|E_p''|}{|E_s''|} \tag{49}$$

$$\tan \psi_i = \frac{|E_p|}{|E_s|} \tag{50}$$

The argument of Eq. 48 contains the relative phase of p and s components in reflected and incident waves. According to Eq. 4 they can be formulated as

$$\Delta_r = \varepsilon''_p - \varepsilon''_s \tag{51}$$

$$\Delta_i = \varepsilon_p - \varepsilon_s \tag{52}$$

Thus, Eq. 48 becomes the basic equation of ellipsometry

$$\rho = \frac{\tan \psi_r}{\tan \psi_i} e^{i(\Delta_r - \Delta_i)} \tag{53}$$

which is often given in a simplified form as

$$\rho = \tan \psi \, e^{i\Delta} \tag{54}$$

For the sake of simplicity, the present usage of ellipsometers employs equal amplitudes of p and s components in the incident light, so that $\tan \psi_i = 1$. The relative phase between the two components may be zero in the incident or reflected beam.

With the formulation of Eqs. 33 and 34 Eq. 47 can also be written as

$$\rho = \frac{|r_p|}{|r_s|} e^{i(\delta_p - \delta_s)} \tag{55}$$

comparison with Eq. 54 leads to the definitions

$$\tan \psi = \frac{|r_p|}{|r_s|} \tag{56}$$

$$\Delta = \delta_p - \delta_s \tag{57}$$

Expressions for relative phase and amplitude change due to reflection from a bare surface using only real quantities (51,68,88) are:

$$\Delta = \tan^{-1}\left(-\frac{2B \sin\phi \tan\phi}{A^2 + B^2 - \sin^2\phi \tan^2\phi}\right) \tag{58}$$

$$\psi = \tan^{-1}\left\{\sqrt{\frac{A^2 + B^2 - 2A \sin\phi \tan\phi + \sin^2\phi \tan^2\phi}{A^2 + B^2 + 2A \sin\phi \tan\phi + \sin^2\phi \tan^2\phi}}\right\} \tag{59}$$

The intermediate variables A and B have been defined in Eqs. 39 and 40.

Conversely, the optical constants of a bare surface can be determined from the parameters ψ and Δ by

$$n = n_o \sqrt{1/2 \left\{(G^2 - E^2 + \sin^2\phi) + \sqrt{(G^2 - E^2 + \sin^2\phi)^2 + 4G^2E^2}\right\}} \tag{60}$$

$$k = n_o \sqrt{1/2 \left\{-(G^2 - E^2 + \sin^2\phi) + \sqrt{(G^2 - E^2 + \sin^2\phi)^2 + 4G^2E^2}\right\}} \tag{61}$$

With the intermediate variables G and E (equal to A and B in Eqs. 39, 40) defined as

$$G = \frac{\sin\phi \tan\phi \cos 2\psi}{1 + \sin 2\psi \cos\Delta} \tag{62}$$

$$E = \frac{\sin\phi \tan\phi \sin 2\psi \sin\Delta}{1 + \sin 2\psi \cos\Delta} \tag{63}$$

D. Data for Reflection from Bare Surfaces

In the following, some results of numerical computations for refections from bare surfaces (88) are presented in graphical form in order to provide a better idea of the relationships between the optical and ellipsometric quantities discussed.

Figure 10 illustrates the dependence of ellipsometer parameters and complex reflection coefficients on angle of incidence (40,63,126). It also shows the effect of an increased imaginary part of the refractive index, starting with dielectric reflection as a limiting case. For an incident dielectric medium of refractive index n_o, n and k/n have to be

divided by n_o (72,128). Similar data based on different conventions can be found in the literature (27,124). The sensitivity for determining metal optical constants greatly depends on angle of incidence (75,91).

The dependence of the same four quantities on the optical constants n and k/n of the reflecting surface is illustrated in Figs. 11-18 for angles of incidence 2°, 45° and 75°. The data for 2° are a close approximation to normal incidence, where indeterminate values resulting from the computations would have to be resolved by a limiting process. At normal incidence, s and p components become indistinguishable. The difference in phase of 180° between s and p components shown in Figs. 11 and 12 is due to the choice of coordinate system (Fig. 8). Not all combinations of optical constants shown are physically realizable. Computed nets of n, k vs ψ, Δ values for bare surfaces (14,71, 139) and detailed data for dielectric reflection (69) as well as the use of reflectance (19,43,113) can be found in the literature.

2. Reflection from Film-Covered Surfaces

A. Drude Equations

The classical theory of optical reflection from a film-covered surface assumes a planar substrate covered with a plano-parallel, homogeneous, isotropic film. Application of electromagnetic theory to this geometry provides solutions for waves traveling in incident medium, film and substrate in the directions indicated in Fig. 19b. These waves are equivalent to the summation of multiple reflections shown in Fig. 19a (56,74,80,131). The resultant reflected wave is described in the (exact) Drude equations (Eqs. 64,65) by an overall, complex reflection coefficient r, which depends on the reflection coefficients r_1 and r_2 of the two interfaces and the phase delay D due to the travel of the light in the film (42).

$$r_p = \frac{E''_p}{E_p} = \frac{r_{1p} + r_{2p}\, e^{-iD}}{1 + r_{1p}\, r_{2p}\, e^{-iD}} \tag{64}$$

$$r_s = \frac{E''_s}{E_s} = \frac{r_{1s} + r_{2s}\, e^{-iD}}{1 + r_{1s}\, r_{2s}\, e^{-iD}} \tag{65}$$

The delay in the film of refractive index n_{cf} and thickness L is

$$D = \frac{4\pi}{\lambda_o} L\, n_{cf} \cos \phi_{cf} \tag{66}$$

where λ_o is the vacuum wavelength of the light and ϕ_{cf} the complex angle of refraction in the film (equal to ϕ'_c of Eq. 26). The reflection coefficients r_1 and r_2 are the Fresnel coefficients for the two interfaces considered seperately (with an infinitely thick film). With the electric field designations given in Fig. 20 they are defined as

$$r_1 = \frac{E_1}{E} \tag{67}$$

$$r_2 = \frac{E'''}{E'} \tag{68}$$

with Eqs. 20 and 23 they can be formulated as

$$r_{1p} = \frac{\tan(\phi - \phi_{cf})}{\tan(\phi + \phi_{cf})} \tag{69}$$

$$r_{2s} = -\frac{\sin(\phi - \phi_{cf})}{\sin(\phi + \phi_{cf})} \tag{70}$$

$$r_{2p} = \frac{\tan(\phi_{cf} - \phi_{cm})}{\tan(\phi_{cf} + \phi_{cm})} \tag{71}$$

$$r_{2s} = - \frac{\sin(\phi_{cf} - \phi_{cm})}{\sin(\phi_{cf} + \phi_{cm})} \tag{72}$$

where ϕ_{cf} and ϕ_{cm} are the complex angles of propagation in film and substrate, obtained by applying Snell's law (Eq. 26) to the two interfaces

$$n_o \sin \phi = n_{cf} \sin \phi_{cf} \tag{73}$$

$$n_{cf} \sin \phi_{cf} = n_{cm} \sin \phi_{cm} \tag{74}$$

Drude has also derived a linearized form (31,42,80) of Eqs. 64 and 65 which are sometimes called <u>the</u> Drude equations (56,134). To avoid confusion, this nomenclature should be discontinued. Other approximations have been developed since (3,5,36,77). The exact equations are, however, easily handled by a computer and are now mostly used.

B. Computations

With the Drude equations for reflection from a film-covered surface, the basic equation of ellipsometry becomes

$$\rho = \frac{(r_{1p}+r_{2p}e^{-iD})(1+r_{1s}r_{2s}e^{-iD})}{(r_{1s}+r_{2s}e^{-iD})(1+r_{1p}r_{2p}e^{-iD})} = \tan\psi\, e^{i\Delta} \tag{75}$$

For given values of the optical constants of the three media involved (Fig. 20) and the thickness of the film, the ellipsometer parameters ψ and Δ can be computed by use of Eq. 75 (83). Examples for different classes of film-covered surfaces, with film thickness (in Angstrom units) indicated as a parameter along the curve, are given in Figs. 21-24.

It is typical for dielectric films that the ellipsometer parameters ψ and Δ repeat themselves after an increment of one wavelength optical path (or an increment of 2π in phase delay D) in the film. According to Eq. 66 one wavelength optical path usually requires a film thickness of about half a wavelength. A dielectric film on a metallic substrate (Fig. 22) produces, in general, a greater change in Δ and ψ than a dielectric film on a dielectric substrate (Fig. 21). In both cases, the curves are closed. Good agreement with measurements has been reported for the optical constants used in Fig. 22 (71).

With absorbing films, the effect of the substrate material is increasingly obscured, with increasing film thickness, by the light absorption in the film, and the ellipsometer parameters ψ and Δ approach the values representative of bulk film material. The ψ vs. Δ curve is

therefore not closed but runs from a point representing the bare substrate to a point representing the bare film material. Extremely thin absorbing films on a dielectric substrate (Fig. 23) can be expected to produce particularly large changes in ψ and Δ, because of the large difference in optical constants of the two materials. Since the optical properties of a metal film and a metal substrate are more similar to each other, the ellipsometer parameters are much less sensitive to film thickness for such a combination (Fig. 24).

The effect of film thickness (in the 100Å range) on changes in ψ and Δ depends on the angle of incidence for each film-substrate combination and may even change sign. The optimum angle of incidence lies usually in the range of 60-80° (7,91,117,139).

In practice, one is usually interested in determining the thickness L and refractive index n_{cf} of a film on a substrate of known properties from measured values of ψ and Δ. The above procedure for calculating ψ and Δ for various combinations of n_f, k_f and L can be used, until satisfactory agreement with measurement is found. Computed parametric curves (7,15,16,23,82,99) or computer-generated visual displays (92) can assist in this process. If an appreciable range of each of the three variables has to be covered in the search for a solution, the number of computations soon becomes too large to evaluate manually.

A more efficient determination of film thickness and refractive index from ellipsometer measurements (82,84). makes use of the fact that Eq. 75 can be solved explicitly for L as a function of n_{cf}, ψ and Δ (this is, however, not possible for n_{cf}). This solution involves a quadratic equation and therefore provides two values of L which should

be a real quantity. In practice, the solution with the smaller imaginary part is chosen to represent the physical situation.

C. Double Beam Model for Transparent Films

Since s and p components of reflected light are delayed to the same extent by the optical path in a film (Eq. 51), it is not obvious why the resulting state of polarization should depend on film thickness. The following double beam approximation to reflection from a transparent film on a metal substrate is intended to illustrate the physical basis of the ellipsometry of film-covered surfaces. The present approach is more easily understandable than a graphical computation (139) and a multiple beam model (44) employed before.

As an example for this approach, a tantalum oxide film on a tantalum surface will be considered. The multiple beam model of reflection (Fig. 25), which involves the summation of an infinite series of beams, will be approximated by the sum of the zero order reflection r_o, which involves only a dielectric reflection and r_∞, the resultant of all higher order reflections, which involve at least one metallic reflection.

For an incident wave of unit amplitude, r_o and r_∞ are complex reflected amplitudes which can be added vectorially in the complex plane to form the resultant r. This process is carried out in Fig. 26, for s and p components for a film of negligible thickness. With the known Fesnel coefficient r_o, for the film material, r_∞ is chosen in such a way that the resultant r agrees with the known Fresnel coefficient for the

bare substrate surface. The relative phase Δ between p and s components is directly visible in the figure, the relative amplitude attenuation $\tan \psi$ has to be formed from the ratio of the lengths of the resultant p and s vectors.

An increase in film thickness results in an increased delay D, or a decrease in phase of r_∞ indicated by the double-arrows in Fig. 26. This delay is equal for s and p components. (It will be assumed that the amplitude of r_∞ remains constant.) Phase and amplitude of r_o, on the other hand, are independent of film thickness. The sequence in Fig. 27 illustrates how the resultant s and p components are affected differently by the increase in film thickness and, thus, ψ and Δ values change. A comparison of results obtained graphically by this method with exact computations (Fig. 28) indicates that the double beam model provides a reasonable approximation to reality.

D. Multiple Films

The optical effect of several different layers of film stacked up on a substrate can be computed by recursion formulas (38,84) or matrix methods (97, 139,132). Inhomogeneous films with continuously varying optical properties in the direction normal to the substrate surface (1, 132) can be represented by multiple films (83). Evidence for the existence of multiple or inhomogeneous films cannot be obtained by ellipsometry alone and considerable leeway usually exists in the choice of the additional parameters describing such films.

3. Conventions and Definitions

Numerical values of most of the parameters which appear in the theory of ellipsometry, or result from measurements, depend on the choice of arbitrary conventions and definitions. The effect of nine two-fold choices (resulting in 512 possible combinations) and their past usage has been discussed elsewhere (90).

Depending on the choices made, reflection from any given surface can be represented by 8 numerically different combinations of ellipsometer parameters ψ and Δ. Conversely, from any measured set of ψ and Δ values, 16 different combinations of optical constants of a bare surface can be derived.

The preferred usage, determined at the International Ellipsometry Conference in Nebraska, and used throughout this chapter is:

(1) Definition of the relative amplitude parameter ψ

$$\tan \psi = \frac{|r_p|}{|r_s|} \qquad \left(\text{alternative: } \frac{|r_s|}{|r_p|}\right)$$

(2) Definition of the relative phase parameter Δ

$$\Delta = \delta_p - \delta_s \qquad (\text{alternative: } \delta_s - \delta_p)$$

(3) Definition of complex relative amplitude attentuation

$$\rho = \tan \psi \, e^{i\Delta} \quad (\text{alternative: } \tan \psi \, e^{-i\Delta})$$

(4) Choice of time dependence factor

$$E \sim e^{i\omega t} \qquad (\text{alternative: } e^{-i\omega t})$$

(5) Definition of absolute phase

$$E \sim e^{i(\omega t+\delta)} \qquad \text{(alternative: } e^{i(\omega t-\delta)}\text{)}$$

(6) Positive coordinate directions for p-component as shown in Fig. 8 (alternative: E''_p of opposite direction).

(7) Positive coordinate directions for s-component as shown in Fig. 8 (alternative: E''_s of opposite direction).

(8) Formulation of complex refractive index

$$n_c = n - ik \qquad \text{(alternative: } n_c = n(1-i\kappa)\text{)}$$

(9) Definition of complex refractive index

$$n_c = n - ik \qquad \text{(alternative: } n'_c = n' - i\,k'\text{)}$$

Azimuth angles of polarizers and analyzers are measured counter clockwise from the plane of incidence to the transmission direction for the electric field vector. Azimuth angles of compensators are measured counterclockwise from the plane of incidence to the fast axis of the compensator. In both cases the observer looks into the beam.

IV. ELLIPSOMETER ARRANGEMENTS

1. Measurement With or Without Compensation

Elliptically polarized light (Fig. 5) can be analyzed by measuring the intensity transmitted by a rotating linear polarizer (analyzer) as a function of its azimuth angle (30). The azimuth of the intensity maximum represents the orientation θ of the major ellipse axis, the ratio of the square roots of intensity minimum to maximum represents the excentricity tan γ of the ellipse. (Fig. 29). This measurement without compensation requires absolute intensity determinations and therefore does not take full advantage of some of the inherent capabilities of ellipsometry.

The measurement of elliptic polarization with compensation is based on the restoration of linear polarization by the introduction of a known phase difference between two orthogonal components of the elliptic polarization. This phase difference is generated by a compensator (wave plate) and can have a fixed or variable value. The restored linear polarization is recognized by the extinction with a (linear) analyzer. In practice, a minimum in the transmitted light intensity is sought.

2. Fixed and Variable Compensators

Conceptually the simplest ellipsometer arrangement, although not normally used in practice, employs linearly polarized light from a polarizer P of azimuth a = 45° incident on the reflecting surface. Thus, s and p components of the incident light are in phase and of equal amplitude. (In the basic ellipsometer equation (Eq. 53)

$\tan \psi_i = 1$ and $\Delta_i = 0$.) As indicated in Fig. 30, reflection of this light results in elliptic polarization, due to a change in relative phase and amplitude of p and s components. e.g. the p component may now be ahead of the s component and be of smaller amplitude. (For the sake of simplicity, Δ is assumed to have a value between 0 and 90°, ψ between 0 and 45° in Figs. 30-33. With bare metal surfaces this case is realized at angles of incidence above the principal angle.)

The phase difference between the two components can be restored by a compensator of variable retardation and fixed azimuth (Babinet-Soleil compensator, symbolized by a wedge C in Fig. 30), which introduces a relative phase change δ_C between p and s components which is equal but of opposite sign to that due to reflection (15,16). For this purpose, the fast axis F of the compensator is aligned with the component which has been retarded in reflection (e.g. the s-component) and a retardation is chosen such that linear polarization is restored. The plane of this polarization forms the diagonal of a rectangle, in contrast to the diagonal of a square shown for the incident polarization, because p and s components, have been attenuated differently during reflection. Thus, the change in relative phase Δ due to reflection is obtained from the retardation δ_C of the compensator, while the change in relative amplitude, $\tan \psi$, is obtained from the azimuth of the restored linear polarization. In practice the latter is derived from the azimuth a of the analyzer A at extinction, as indicated in Fig. 30.

The elliptic polarization which results from the reflection of linearly polarized light can also be compensated with a compensator of fixed retardation and variable azimuth, as illustrated in Fig. 31. The elliptic polarization, in this case, is decomposed into components parallel to the major and minor axis of the ellipse. As had been pointed out in the discussion of Fig. 6, these two components are mutually out of phase by 90° or a quarter wavelength. Linear polarization can therefore be restored by the introduction of a quarter wave phase difference between these components by means of a quarter wave plate (Sénarmont compensator Q). Thus, the azimuth ψ of the quarter wave plate at extinction is a measure of the orientation θ of the major ellipse axis, the azimuth of the restored linear polarization is a measure of the excentricity $\tan \gamma$ of the ellipse. In contrast to the first arrangement, which provided a direct measurement of the physical parameters of elliptic polarization, this arrangement therefore provides the geometrical parameters.

Presently available compensators of variable retardation allow one to determine retardation only with a resolution of approx. 1°, because the measurement involves a translatory movement, in contrast to the rotatory movement employed with a compensator of fixed retardation. If a compensator of variable retardation is used in practice (e.g. for spectral work), it is therefore preferable not to change its retardation during a measurement, but to set it to quarter wave and rotate it like a compensator of fixed retardation. Optical imperfections are more prevalent in variable than in fixed compensators and may also

affect the accuracy of such measurements. If reliable variable compensators of high resolution become available (e.g. electro-optic devices) some of the presently unused ellipsometer arrangements, such as the one in Fig. 32 may become of practical interest.

3. Linear and Elliptic Polarization Incident

Both ellipsometer arrangements described above employ linearly polarized light incident on the specimen and the elliptic polarization resulting from the reflection is converted back to linear polarization. A reversal of the sequence of optical elements results in elliptically polarized light incident on the specimen. The elliptic polarization is then chosen so that reflection results in linear polarization. If s and p components of the incident light are again chosen to be of equal amplitude, the use of compensators with variable or fixed retardation results in the following ellipsometer arrangements.

A compensator of variable retardation, shown in Fig. 32, introduces a phase difference δ_C between p and s components before reflection. This phase difference is of equal magnitude but opposite sign compared to the one due to reflection on the specimen. Linear polarization is therefore restored by reflection. As with the arrangement of Fig. 30, the parameters Δ and ψ, characteristic of the reflecting surface, are derived from the retardation δ_C of the compensator and the azimuth a of the analyzer.

The use of a quarter wave compensator with elliptic incidence is illustrated in Fig. 33. This arrangement is presently the preferred one for practical use. The 45° azimuth q of the quarter wave plate

results in equal amplitudes of p and s components incident on the specimen. At extinction, the polarizer azimuth p is a measure of Δ, the analzyer azimuth a a measure of ψ due to the reflection. These features will be more apparent by use of the Poincaré sphere (Fig. 37).

4. Appliciation of Poincaré Sphere

A. Linear Polarization Incident

The state of polarization can easily be traced on the Poincaré sphere (34) through the elements of an ellipsometer (140) operated in the four modes shown above. The stereographic projection of the sphere, looking down on the "north" (L) pole, will be used for this purpose. The effect of reflection is represented by two separate steps, one affecting only Δ, the other only ψ. The following symbols are used

H - plane of incidence (origin of azimuth measurements), p component

V - plane of s-component

L - left hand circular pole of sphere

P - polarizer transmission axis, azimuth p (angle to plane of incidence)

Δ - change in relative phase introduced by reflection between p and s components.

E - elliplic state of polarization before or after reflection

(ψ)- change in relative amplitude ψ due to reflection

δ_C- change in relative phase between fast and slow axis, introduced by a compensator of variable retardation

δ_Q- change in relative phase introduced by a quarter wave plate.

F - compensator fast axis, azimuth q

A'- restored linear polarization, azimuth a'

A - analyzer transmission axis, aximuth a (at extinction)

—o- circles and points on the upper hemisphere (left hand polarization).

---x - circles and points on the lower hemisphere (right hand polarization)

With linear polarization incident and a variable compensator, the state of polarization through an ellipsometer, arranged as shown in Fig. 30 is given in Fig. 34. The linear polarization produced by the polarizer of fixed 45° azimuth is represented by point P on the equator (angle from plane of incidence H doubled). Reflection on the specimen results in a change of relative phase Δ and relative amplitude ($\tan \psi$). (As in Figs. 30-33, Δ is assumed to have a value between 0 and 90° and ψ is assumed to lie between 0 and 45°.) Point E on the sphere represents the elliptic state of polarization after reflection. Introduction of the phase change δ_C (equal but opposite to Δ), between fast and slow axis of the variable compensator of fixed orientation of its fast axis F, results in the restored linear polarization A', which forms the angle ψ (doubled on the sphere) with the direction V of the s-component (coincides here with F). In practice, ψ is derived from the azimuth a of analyzer A (2a measured counterclockwise from H to A).

Figure 35 similarly traces the state of polarization for linear incident polarization and a compensator of fixed retardation (140). In this case, the elliptic polarization E has to be converted to a linear polarization with a compensator of $\delta_Q = 90°$ retardation (quarter wave plate, Mac Cullagh method of compensation (105)). This is accomplished by choosing F on a great circle through L and E (parallel to a principal ellipse radius of azimuth θ). A 90° rotation in the positive direction, as seen from F then brings point E to A'. The difference in azimuth q between the fast axis F of the compensator and the aximuth a' of the restored linear polarization A' is the geometric ellipse parameter γ.

B. Elliptic Polarization Incident

Elliptic incident polarization, produced by a compensator of variable retardation, is illustrated in Fig. 36. The polarizer P is again in a 45° azimuth (90° from point H on the sphere). The effect δ_C of the compensator (positive rotation as seen from F) results in right hand elliptic polarization incident on the specimen. Point E, representing this state of polarization lies on the lower half of the Poincaré sphere and is represented by a cross in Fig. 36. The phase change Δ due to reflection is equal and opposite to δ_C, the unequal amplitude attenuation in reflection results in the linear polarization state A'. The angle ψ is derived from the azimuth of analyzer A.

Elliptic incident polarization, produced with a quarter wave plate, is illustrated in Fig. 37 (140). This is the most important ellipsometer arrangement in practice. In this case, the incident elliptic state of polarization E, identical to the one in Fig. 36, is obtained from the linear state P (determined by the polarizer azimuth p) by the action of the quarter wave plate with fast axis F of azimuth q = 45° (90° from H on the sphere). The effect of the quarter wave plate on the Poincaré sphere is a 90° positive (counterclockwise) rotation on a small circle around F. As in Fig. 36, phase and amplitude change during reflection result in the restored linear state of polarization A' which is extinguished by the analyzer A of azimuth a.

The above argument assumes ideal, perfectly aligned optical components. In particular, the quarter wave plate is assumed to

introduce a retardation of exactly 90° and not to change the relative amplitude. Deviations from these conditions can be determined (60) and employed in the computations (82,84). Averaging measurements in "four zones" (to be discussed) also serves to reduce the effect of some errors (82).

C. Error Propagation

The operation of an ellipsometer with a quarter wave compensator requires the rotation in azimuth of two components to reach extinction. For precise measurements, it is important that small deviations in azimuth from the correct (final) setting of one component do not affect the azimuth of the other component for minimum transmitted light intensity.

The ellipsometer arrangements of Figs. 31 and 33 differs in this respect. With incident linear polarization (Fig. 38a) any deviation in the quarter wave plate azimuth from the correct value q_1 results in a proportionate displacement of the analyzer aximuth a for intensity minimum, and vice versa. Compensator and analyzer azimuth therefore hunt each other in search for the deepest intensity minimum, which is not very well defined and often affected by noise in the photodetector circuit.

With incident elliptic polarization, on the other hand, the analyzer azimuth a for minimum intensity is not affected by deviations in the polarizer azimuth from the final value p_1, the minima are not as low, but occur at the same angle. The same is true for intensity

as a function of polarizer azimuth with the analyzer in different orientations. The lack of propagation of errors from one azimuth reading to the other is the reason for the preferred usage of the arrangement shown in Figs. 33 and 37.

The difference in error propagation can be demonstrated on the Poincaré sphere. With linear polarization incident (Fig. 39a), a compensator of fast axis F_2, which is different from the correct location F_1 results in a restored polarization A_2', (indicated by x) which is slightly elliptical. The major axis of the ellipse is indicated by a great circle through x and L, which appears as a diameter of the circle in the projection. A minimum in transmitted intensity is reached with the transmission direction of the analyzer in orientation A_2, parallel to the minor axis of the ellipse. Thus, in first approximation, the difference in compensator azimuths between F_1 and F_2 is shown to be transmitted to the analyzer azimuths of A_1 and A_2, as shown by experiment (Fig. 38).

The situation with elliptic polarization incident is illustrated in Fig. 39b. A polarizer P_2 of an azimuth which is different from the correct setting P_1, results, in first approximation, in a restored slightly elliptic polarization A_2' with major axis parallel to the correctly restored linear polarization A_1'. Thus, the polarizer azimuths A_1 and A_2 for minimum transmitted intensity are shown to be the same, in agreement with experiment.

A similar analysis for the variable compensators, used as shown in Figs. 30 and 32, shows that errors in retardation δ_C do not propagate to the azimuth of the analyzer A.

For a more general analysis of the amplitude transmitted by an analyzer (82,103,139,141), a right triangle can be inscribed in the Poincaré sphere, with the three corners representing transmission and absorption directions of the analyzer and the state of polarization incident on it. The length of the side of the triangle opposite to the transmission of the analyzer (a chord on the sphere) is then a measure of the transmitted amplitude (82).

5. Other Ellipsometer Arrangements

The four ellipsometer arrangements discussed employ equal amplitudes of p and s components incident on the specimen (state of polarization represented by a point on the horizontal diameter of the circle, showing a great circle through pole L, in Figs. 34 to 37). In principle, any two optical elements can be adjusted to reach extinction, with the others remaining unchanged, and many more modes of operation are feasible. The derivation of results from the measured quantities is, however, somewhat more complicated if incident p and s components are not of equal amplitude. Arrangements with incident linear polarization and quarter wave plate of fixed azimuth (65) as well as the use of an optimum compensator azimuth (109) have been described.

6. Modern Instrumentation

A. Self-Compensating Ellipsometers

The manual operation of an ellisometer is quite slow. To find extinction with good precision, several minutes are required for a measurement in one zone. A considerable fraction of this time is used for the repeated reading of azimuth circles. Mechanizing this process,

e.g. by use of digital angle position encoders, seems to be a promising route which has not been taken yet to speed up the response of manually operated ellipsometers. With optical modulation techniques and mechanized azimuth readout, manual operation with response times of a few seconds appears feasible. A manually operated instrument with azimuth and phase modulation by use of Faraday and piezo optic cells has been described by Wilmans (138).

Self-compensating ellipsometers, for the most part, simulate manual operation at a greater speed and maintain the precision inherent in compensating measurements. Two kinds of mechanically operated self-balancing instruments have been described. One, by Ord (93,94), is controlled by the intensity of the photodetector output. Compensation is reached in about a second. Another one, by Takasaki (127) is controlled by the phase of the photodetector output. A modulation in the state of polarization is introduced by two electro-optic elements (Pockels cells). Compensation takes several seconds.

Instead of by mechanical rotation of a polarizing prism, the plane of polarization of light can also be rotated electronically by a magneto-optic element (Faraday cell). This approach has been used by Layer (73) for an automatic ellipsometer, designed to respond within approx. 10^{-3} sec. A slew rate of $4°$/sec has been demonstrated. Unfortunately, no final analysis of the performance of this instrument is available. The use of Faraday and Pockels cells for automatic ellipsometers has been suggested by several authors (137,140).

Several new designs of self-compensating ellipsometers would be made possible by the availability of a reliable electronic compensator of measurably variable retardation. Future forms of electro-optic or piezo-optic (61,66,95) devices may be useful for this purpose.

B. Non-Compensating Ellipsometers

Off-balance intensity changes of the transmitted light can be used as a measure of changes in ellipsometer parameters (70,102, 118). Depending on the azimuth settings chosen, the output is primarily due to changes in ψ or Δ, provided that the changes are of limited extent. Time resolution of less than 10^{-3} sec should be realizable by this approach.

As had been explained with Fig. 29, an elliptic state of polarization can also be determined from the transmitted light intensity as a function of the analyzer azimuth (103). An instrument which employs a rotating analyzer has been reported by Cahan and Spanier (33).

It must be remembered that the use of light intensity measurements in ellipsometry, common to all non-compensating techniques, to some extent negates one of the basic advantages of the technique: its use of the state of polarization, rather than the intensity of reflected light. To what extent this fact affects the reliability of results obtained from such measurements has to be analyzed for each specific case.

V. EXPERIMENTAL ASPECTS

1. Four Zones

The following discussion will be restricted to the use of a compensator of fixed retardation, a quarter wave plate, and elliptic incident polarization which are at present most commonly employed. Similar classifications can be derived for other modes of operation.

A given pair of values ψ and Δ, due to reflection, can be determined by 32 different combinations of polarizer, analyzer and compensator azimuth settings. These combinations can be organized in four groups or "zones" (82), which are identified by the quadrant on the "equator" of the Poincaré sphere (with origin H), in which the polarizer is located (Table I).

Table I

Definition of zone numbering

Zones	Azimuth p of polarizer transmission axis
1	0-45°
2	45°-90°
3	90°-135°
4	135°-180°

The algebraic expressions which relate the azimuth readings, p, q and a of polarizer, quarter wave plate and analyzer, with the desired quantities ψ and Δ are slightly different for different ranges of the

value of Δ. It is therefore convenient to distinguish four groups of zones A to D (Table II).

Table II

Definition of zone groups

Zone Groups	Δ
A	0 - 90°
B	90 - 180°
C	180° - 270°
D	270° - 360°

The reason for the existence of four zones is most easily shown on the Poincaré sphere with a small value of Δ (group A) and is illustrated in Fig. 40. Zone A-1, with the fast axis F of the quarter wave plate in a 45° azimuth, is identical to the arrangement discussed in Fig. 37. The same state of incident polarization is produced in zone A-2 with the quarter wave plate of 135° (or -45°) azimuth and the polarizer in a position symmetrical to the first one around the 45° azimuth. In both cases, the analyzer azimuth at extinction is the same. Zones 3 and 4 are related to each other like zones 1 and 2. The incident state of polarization is now represented by a point on the upper hemisphere (circle).

Because any two azimuth positions of polarizer, quarter wave plate and analyzer 180° apart are optically identical, a measurement in each zone can be obtained by 8 different combinations of azimuth circle

readings, or 32 combinations for all four zones. To avoid this additional multiplicity, all azimuth readings should be restricted (or converted) to values in the range of 0-180°.

2. Sixteen Zones

The derivation of ellipsometer parameters ψ and Δ from the measured azimuth angles in zone A-1 can be seen in Fig. 37 and may be applied to the other zones in group A. If we denote the azimuth angles (measured counterclockwise from the plane of incidence H) of polarizer, quarter wave plate and analyzer by p, q, and a, the algebraic expressions listed in Table III result. The expressions for zone groups B to D can be derived similarly, as indicated in Fig. 41 for zone 1. All azimuth readings are assumed to lie in the range 0 to 180°.

Azimuth circles in ellipsometers often have their origin in the plane of the s, rather than the p component and increase clockwise, rather than counter-clockwise. Readings from such circles will first have to be converted to the azimuth angles defined here, before the expressions for ψ and Δ given in Table III can be used. Alternatively, a new set of expressions for ψ and Δ, which permits the use of instrument readings which do not conform to the definitions, can be derived. In practice, the use of Table III first involves a search for the correct zone, based on the values of polarizer, compensator and analyzer azimuths. Then the appropriate algebraic expressions for deriving ψ and Δ can be used.

Table III

Derivation of ψ and Δ from ellipsometer azimuths of polarizer, Quarter wave plate and analyzer (all angles in degrees). (ψ=0° to 90°, Δ=0 to 360°)

Zone	Range of Polarizer Transmission Azimuth p	Compensator Fast Axis Azimuth q	Range of Analyzer Transmission Azimuth a	ψ	Δ
A-1	0-45	45	90-180	180-a	90-2p
A-2	45-90	135	90-180	180-a	2p-90
A-3	90-135	45	0-90	a	270-2p
A-4	135-180	135	0-90	a	2p-270
B-1	0-45	135	0-90	a	90+2p
B-2	45-90	45	0-90	a	270-2p
B-3	90-135	135	90-180	180-a	2p-90
B-4	135-180	45	90-180	180-a	450-2p
C-1	0-45	45	0-90	a	270-2p
C-2	45-90	135	0-90	a	90+2p
C-3	90-135	45	90-180	180-a	450-2p
C-4	135-180	135	90-180	180-a	2p-90
D-1	0-45	135	90-180	180-a	270+2p
D-2	45-90	45	90-180	180-a	450-2p
D-3	90-135	135	0-90	a	90+2p
D-4	135-180	45	0-90	a	630-2p

3. Zone Averaging

With ideal, perfectly aligned ellipsometer components, the algebraic expressions in table III provide identical ψ and Δ values for a given surface measured in all four zones. In practice, however, the results are different (78,116). If the effect of different errors is investigated on the Poincaré sphere, it can be shown that by using the arithmetic average of results from four zones, errors due to different causes are reduced to different degrees:

--- Errors due to deviations in polarizer and analyzer circle alignment are closely eliminated.

--- Errors due to deviations of the compensator retardation from quarter wave and due to unequal transmission of fast and slow components are partially eliminated.

--- Errors due to deviations in compensator azimuth are not reduced.

Of the optical elements in an ellipsometer, the quarter wave plate usually deviates most from the ideal state. In addition to deviations from 90° retardation (50,52,107) differences in transmittance between fast and slow directions, due to absorption or interference (6,136,142) should be considered. A detailed theory of retardation plates (59) their use and calibration (60) has been given by Holmes and Feucht. Corrections based on measurements in two zones are contained in the computer program by Mc Crackin (84) and corrections of measurements from one, two or four zones have been analyzed by Azzam and Bashara(9).

4. Alignment and Calibration

The mechanical adjustment of azimuth circles (to read zero for the plane of incidence) has been described in detail (82). The procedure is based on the fact that pure s or p polarization remains linearly polarized in reflection from a metal surface, and linear polarization parallel to fast or slow axis of the compensator remains linear upon transmission through it. Dielectric reflection can also be used (8). Most instruments do not provide for a precise adjustment of azimuth circles. One, therefore, has to establish corrections, which are then applied to all the readings.

Less information is available on the alignment of the axes of polarizer, analyzer and compensator (51). The first two elements are often built into collimator and telescope (polarizer and analyzer telescopes), respectively, the axes of which should lie in the same plane and intersect in the surface of the specimen (Fig. 42). If collimator or telescope can be rotated to vary the angle of incidence, the two axes are most easily made parallel to each other by aligning both telescopes with respect to each other in the straight-through position. The axes can then be made to intersect in the specimen surface by use of a mirror with a target on its surface. Iris diaphragms centered on the axes of collimator and telescope (E and J in Fig. 43) are of great help in this operation. The point of intersection also has to coincide with the axis of rotation of the movable telescope (138). Auto-collimation techniques can be used to align the axis of rotation of the specimen table normal to the plane of incidence. The plane of incidence, defined by the two optic axis must be parallel to the plane of rotation of the telescope.

With ellipsometers of fixed angle of incidence,(89) a mirror stand with calibrated angle of rotation or a prism of the desired angle between reflecting faces has to be used for the alignment of collimator and telescope.

Adjustment of the angle of incidence circle, similar to the alignment of opic axis, is also accomplished in the straight-through position for instruments with variable angle of incidence and requires the use of a mirror with calibrated rotation or a prism with reflecting faces at the desired angle for instruments with fixed angle of incidence(51).

In order to employ a narrowly defined angle of incidence in ellipsometer measurements, it is important that the light incident on the specimen is well collimated (a parallel beam). For the use of most light sources, a small diaphragm (pinhole), precisely positioned in the focal plane of the collimator lens, provides the parallel beam. The location of the focal plane can best be found by auto-collimation with a cross-hair in place of the pinhole: In the correct position the cross-hair and its reflected image appear sharp and without parallax. The diameter of the pinhole has to be chosen to result in an acceptable divergence in the collimated beam and a sufficient output of the photodetector. Effects of angle at incidence errors have been discussed (75,110,119).

All adjustments and alignments should be checked periodically. Such complete checks can be quite time-consuming, but it would often be satisfactory to check the over-all reproducibility of an ellipsometer, if a reproducible reflecting surface were available. A totally reflecting glass prism, with faces oriented normal to entering and exiting

beams, has been found very suitable for this purpose. To render the reflecting surface independent of the surrounding medium, it has been coated with an opaque aluminum film, which in turn was protected by a layer of silicon monoxide. Except for some small changes due to aging during the first two weeks after preparation, this surface provided a stable reference. No changes could be detected when the environment of the prism was altered from vacuum to saturated vapors of several solvents.

5. Other Sources of Errors

Cell windows act as a source of errors in several different ways: Reflection adds "parasitic" beams which are reflected by other components into the photodetector. These parasitic beams are not extinguished together with the main beam and result in a broadening of the intensity minimum and possibly a shift in the azimuth at which the minimum is reached. The application of anti-reflective coatings (which must not be polarizing or birefringent) to all reflecting surfaces reduces the intensity of parasitic beams (144), but further reductions are often desired. For this purpose, a pinhole in the focal plane of the analyzer telescope can be used (138). Because of (inadvertent or purposeful) slight misalignment of reflecting surfaces from the axis, parasitic beams are in general not focused on the axis, as the main beam is aligned to be. The pinhole can therefore prevent parasitic beams from reaching the photodetector (Fig. 43).

A pinhole on the axis in the focal plane of the telescope also serves to better define the angle of incidence on the specimen.

Light which is not reflected parallel to the axis, or under an angle of reflection equal to the angle of incidence, (e.g., due to surface roughness) is not accepted for measurement. For this reason alone, the pinhole should be routinely employed. The diameter of the pinhole determines the range of angles of incidence which contribute to the measurement. To avoid unnecessary signal attenuation, the telescope pinhole should be slightly larger than the collimator pinhole (if both lenses are of the same local length). The image of the collimator pinhole must be centered on the telescope pinhole for proper operation. This alignment can easily be achieved by fine-adjusting the reflecting surface to maximize the photodetector output off extinction. Figure 43 also shows two iris diaphragms E and J which control the diameter of the light beam and are used in the alignment procedure. Not shown is a condenser lens, possibly inserted between light source and collimator pinhole, as well as color filters, usually positioned in the same area.

Birefrigence in cell windows, usually caused by stress, is a serious source of error (10,100) which often goes unnoticed, because under most circumstances, it can only be detected by use of a reference surface in place of the specimen. In all-glass equipment, carefully annealed, fused quartz windows have been used successfully (82). Satisfactory constructions for windows on bakeable stainless vacuum chambers still need to be developed. Glass with a low stress-optical coefficient (67) may find a use there.

Even a perfectly isotropic cell window changes the state of polarization of transmitted light which is not incident normal to the

surface of the window (91) Measurements shown in Fig. 44 indicate that a one degree deviation from normal incidence, which is more than the accuracy usually achieved in construction and alignment of cells, can be tolerated. The use of substantial angles ϕ would require, however, that their value be known to a higher degree of accuracy than is usually possible, in order to satisfactorily compute the effect of such cell windows and back it out of measurements (22,23,103).
The optical properties of the window material, including the presence of surface layers, would also have to be known precisely for such computations.

Most of the errors discussed need not be considered if they remain constant during an experiment and only "relative" measurements are made, in which a change in the optical properties of the surface, e.g., due to the formation of a film, is of interest. The interpretation of this change is usually little affected by substantial errors in the absolute magnitude of the measurements (120). "Absolute" measurements, on the other hand (e.g., bare surface optical constants), require careful consideration of all sources of error (9,53,65,110,115).
The availability of an absolute reference surface would be highly desirable for such purposes.

6. Manual Ellipsometer Operation

The use of electronic photodetectors (photomultipliers, phototransistors) for establishing minimum transmitted light intensity (108) has largely displaced half-shade devices (15,104,129) employed earlier for visual operation, although visual observation continues to be indispensable for detecting surface inhomogeneities. As shown in Fig. 38b the minimun in the transmitted light intensity as a function of azimuth setting is flat and therefore not well defined. For precise measurements, advantage is taken of the symmetrical nature of the intensity curve, and the azimuth of minimum intensity is found as the center between the azimuth of two off-minimum readings of equal intensity (4). This technique provides the highest resolution possible with manual operation, but several minutes are required for establishing polarizer and analyzer azimuths in one zone. (Off-minimum readings are also employed in an automatic ellipsometer (93) and the same effect is achieved by modulation of the state of polarization (73,127,138).)

Noise due to the laboratory environment, the light source, the photodetector and its instrumentation are often limiting the resolution obtainable. The use of a phase-sensitive detector and beam modulator (61,91) may be necessary to realize the 0.01° resolution in azimuth reading commonly offered by research-grade ellipsometers.

The physical appearance of a manually operated ellipsometer is shown in Fig. 45. A commercially available instrument (Gaertner L-119) has been extensively modified to provide space for large specimens, facilitate the exchange of light sources and the conversion from elliptic to linear incident polarization. Other additions are iris diaphrams on collimator and telescope, the illumination of circles, a motor-driven, vertically movable specimen table and a light chopper.

VI. OUTLOOK

1. Theoretical Problems

The theory of optical reflection, on which the present theory of ellipsometry is based, employs the macroscopic Maxwell equations (123). Although extrapolations of this theory to atomic dimensions have in many cases been surprisingly successful (see also chapter by Kruger), and good arguments can be made that the ellipsometer measures the amount of material present on a surface (5), a general validity of the theory in this regime can hardly be expected.

A more realistic model for optical reflection from bare surfaces, in place of an ideally flat, continuous interface, will have to consider the effect of surface roughness (17), which is found to be present on most real surfaces, usually on a scale much larger than atomic dimensions (Fig. 46). The representation of roughness as an inhomogeneous surface layer, which is then treated by the present macroscopic theory, has been proposed by Mc Crackin (45). The validity of the assumptions inherent in this model still need to be tested experimentally. A new theoretical approach by Berreman (21) is based on optical scattering from submicroscopic spherical surface irregularities. Computational applications or experimental checks of this theory are also not available yet. Exact solutions for optical reflection from a plug-type model of surface roughness have been obtained by Deriugin (39).

Further information for the prediction of transitional layers on clean surfaces (25), due to the different environment of surface atoms as compared to bulk atoms (dangling bonds) will have to be developed.

The classical theory for ellipsometry of film-covered surfaces is also in need of refinement. Instead of the plano-parallel films of sub-molecular thickness assumed so far, and often successfully interpreted as equivalent films of equal mass (12,20,28,32,87,118), approaches considering arrays of individual oscillators (114,125) may have to be extended to account for the discrete distributions of atoms in films of molecular coverage. A comparison of different models now available for sub-monolayers with measurements has shown a nearly linear relationship between the change in Δ and degree of coverage (24,25).

The effect of submicroscopic patchwise film coverage, or local agglomeration of material, found in many thin films (20,57,58,143), on ellipsometer measurements needs to be analyzed. It may be possible to identify patch size by use of variable lateral coherence in the incident light, because coherent and incoherent superposition of light (54) reflected from bare and film-covered surface elements can be expected to result in different states of polarization (Fig. 47).

The availability of more explicit procedures for the ellipsometry of anisotropic films and substrates (49,139) would be desirable.

Of immediate electrochemical interest is a better understanding of the optical properties of electrolytic double layers (35) and mass transfer boundary layers which are present in most electrochemical situations. Procedures to account for the latter are in principle available but have not been sufficiently used or compared to results from other techniques yet.

2. Instrumental Problems

Automated ellipsometers should soon improve the time-resolution of measurements greatly. Response-times in the order of 10^{-3} sec appear well realizable. Some forms of automated operation should also make it possible to increase azimuth resolution to $10^{-3°}$ or better. Increased sensitivity will be necessary for some of the data interpretations suggested above, such as in the study of patchwise film coverage and surface roughness.

Ellipsometry, as presently constituted, provides information only on one surface element at the time. Size and shape of this element are determined by the beam cross-section. The development of holographic ellipsometry (29,46,76) offers the capability for simultaneously observing many different surface elements of extended objects. No usable instrument of this kind seems to have been operated yet.

Some highly desirable instrumental developments concern the convenient scan in wavelength of the light used in an ellipsometer, and very promising leads in the field of ellipsometric spectroscopy (81) have been developed.

3. Conclusions

Ellipsometry offers some unique possibilities for the study of surfaces and thin films. Some of these possibilities are particularly attractive for electrochemical applications. For the satisfactory use of ellipsometry, some of the principles outlined in this chapter must be considered. Except for precisely repetitive applications, an ellipsometer can therefore not normally be considered a routine analytical tool. Since ellipsometry, in general, provides only two measured parameters, the characterization of complex systems often requires a combination with other techniques (86,135).
Many applications of the ellipsometer in its present form remain to be explored and new possibilities will be opened by instrumental developments presently in progress.

REFERENCES

1. F. Abelès, in Ref. 98, p. 41.
2. R. J. Archer, Phys. Rev. 110, 354 (1958).
3. R. J. Archer, J. Electrochem. Soc. 104, 619 (1957).
4. R. J. Archer, J. Opt. Soc. Am. 52, 970 (1962).
5. R. J. Archer and G. W. Gobeli, J. Phys. Chem. Solids 26, 343 (1965).
6. R. J. Archer and C. V. Shank, J. Opt. Soc. Am. 57, 191 (1967).
7. R. J. Archer, Manual on Ellipsometry, Gaertner Scientific Corp., Chicago, 1968.
8. D. E. Aspnes and A. A. Studna, Appl. Optics 10, 1024 (1971).
9. R. M. A. Azzam and N. M. Bashara, J. Opt. Soc. Am. 61, 600 (1971).
10. R. M. A. Azzam and N. M. Bashara, J. Opt. Soc. Am. 61, 773 (1971).
11. C. S. Barrett, Structure of Metals, McGraw-Hill, New York, 1943, Ch. II.
12. L. S. Bartell and J. F. Betts, J. Phys. Chem. 64, 1075 (1960).
13. N. M. Bashara, A. B. Buckman and A. C. Hall, eds., Recent Developments in Ellipsometry, Proc. Symposium Univ. Nebraska, 1968. Surface Sci. 16 (1969), North-Holland Publ. Co., Amsterdam.
14. J. R. Beattie and G. K. T. Conn, Phil. Mag. 46, 222 (1955).
15. K. H. Beckmann, Ber. Bunsenges. 70, 842 (1966).
16. K. H. Beckmann, Philips Techn. Review 29, 129 (1968).
17. P. Beckmann and A. Spizzichino, The Scattering of Electromagnetic Waves from Rough Surfaces, Pergamon Press, 1963.
18. J. Becquerel, Z. Physik 52, 342 (1928).
19. E. E. Bell, in Encyclopedia of Physics, vol. XXV/2a, S. Fluegge and L. Genzel, eds., Springer-Verlag 1967, p. 1.
20. H. E. Bennett, D. K. Burge, R. L. Peck, and J. M. Bennett, J. Opt. Soc. Am. 59, 675 (1969).

21. D. W. Berreman, J. Opt. Soc. Am. 60, 499 (1970).

22. J. O'M. Bockris, M. A. V. Devanathan and A. K. N. Reddy, Proc. Roy. Soc. [A] 279, 327 (1964).

23. J. O'M. Bockris, A. K. N. Reddy and B. Rao, J. Electrochem. Soc. 113, 1133 (1966).

24. G. A. Bootsma and F. Meyer, Surface Sci. 13, 110 (1969).

25. G. A. Bootsma and F. Meyer, Surface Sci. 14, 52 (1969).

26. M. Born, Optik, Springer-Verlag, 1965, 2nd ed., Ch. 1,6.

27. M. Born and E. Wolf, Principles of Optics, MacMillian Co., New York 1964, 2nd ed., Ch. I, XIII.

28. B. J. Bornong, Surface Sci. 16, 321 (1969).

29. O. Bryngdahl, J. Opt. Soc. Am. 57, 545 (1967).

30. W. Budde, Appl. Optics 1, 201 (1962).

31. D. K. Burge and H. E. Bennett, J. Opt. Soc. Am., 54, 1428 (1964).

32. D. K. Burge, J. M. Bennett, R. L. Peck and H. E. Bennett, Surface Sci. 16, 303 (1969).

33. B. D. Cahan and R. F. Spanier, Surface Sci. 16, 166 (1969).

34. M. L. Chaumont, Ann. de Physique [9], 4, 101 (1915).

35. Y.-C. Chiu and M. A. Genshaw, J. Phys. Chem. 73, 3571 (1969).

36. B. H. Claussen, J. Electrochem. Soc. 111, 646 (1964).

37. E. U. Condon, in Handbook of Physics, E. U. Condon and H. Odishaw, eds., McGraw-Hill Book Co., 1958, Ch. 1.

38. A. W. Cook, J. Opt. Soc. Am. 38, 954 (1948).

39. L. N. Deriugin, Radiotekhnika 15 [2], 15 (1960); 15, [5], 9 (1960).

40. R. W. Ditchburn, J. Opt. Soc. Am. 45, 743 (1955).

41. R. W. Ditchburn, Light, Interscience Publ., 1964, vol. II, p. 590.

42. P. Drude, Ann. Physik u. Chemie, N.F. 36, 865 (1889).

43. A. Engelsrath and E. V. Loewenstein, Appl. Optics 5, 565 (1966).

44. J. A. Faucher, G. M. McManus and H. J. Trurnit, J. Opt. Soc. Am. 48, 51 (1958).

45. C. A. Fenstermaker and F. L. McCrackin, Surface Sci. 16, 85 (1969).

46. M. E. Fourney, A. P. Waggoner and K. V. Mate, J. Opt. Soc. Am. 58, 701 (1968).

47. M. Françon, in Encylcopedia of Physics, vol. XXIV, S. Fluegge, ed. Springer-Verlag, Berlin, 1956, p. 171.

48. T. C. Fry, J. Opt. Soc. Ann. 16, 1 (1928), 22, 307 (1932).

49. R. H. W. Graves, J. Opt. Soc. Am. 59, 1225 (1969).

50. B. R. Grunstra and H. B. Perkins, Appl. Optics 5, 585 (1966).

51. H. Gu, M.S. Thesis, Department of Chemical Engineering, University of California, Berkeley, 1971 (LBL 165).

52. A. C. Hall, J. Opt. Soc. Am. 53, 801 (1963).

53. A. C. Hall, J. Opt. Soc. Am. 55, 911 (1965).

54. A. C. Hall, J. Phys. Chem. 70, 1702 (1966).

55. A. C. Hall, Surface Sci. 16, 1 (1969).

56. O. S. Heavens, Optical Properties of Thin Solid Films, Dover Publ., New York 1956, Ch. 4 and 5.

57. ibid, Ch. 3.

58. G. Henderson and C. Weaver, J. Opt. Soc. Am. 56, 1551 (1966).

59. D. A. Holmes, J. Opt. Soc. Am. 54, 1115 (1964).

60. D. A. Holmes and D. L. Feucht, J. Opt. Soc. Am. 57, 466 (1967).

61. S. N. Jasperson and S. E. Schnatterly, Rev. Sci. Instr. 40, 761 (1969).

62. F. A. Jenkins and H. E. White, Fundamentals of Optics, McGraw-Hill, New York, 1957, 3rd ed., Ch. 14.

63. ibid, Ch. 25.

64. H. G. Jerrard, J. Opt. Soc. Am. 44, 634 (1954).

65. H. G. Jerrard, Surface Sci. 16, 137 (1969).

66. J. C. Kemp, J. Opt. Soc. Am. 59, 950 (1969).

67. R. J. King and M. J. Downs, Surface Sci. 16, 288 (1969).

68. W. Koenig, in Handbuch der Physik, vol. XX, H. Geiger and K. Scheel, eds., Springer, Berlin, 1928, p. 141, p. 240.

69. J. Komrska , Optica Acta 15, 389 (1968).

70. J. Kruger, Corrosion 22, 88 (1966).

71. S. Kumagai and L. Young, J. Electrochem. Soc. 111, 1411 (1964).

72. M. v. Laue, in Handbuch der Experimentalphysik vol. 18, W. Wien and F. Harms, eds., Akademische Verlagsges, Leipzig, 1928.

73. H. P. Layer, Surface Sci. 16, 177 (1969).

74. C. E. Leberknight and B. Lustman, J. Opt. Soc. Am. 29, 59 (1939).

75. D. H. Loescher, Appl. Optics 10, 1031 (1971).

76. A. W. Lohmann, Appl. Optics 4, 1667 (1965).

77. F. A. Lucy, J. Chem. Phys. 16, 167 (1948).

78. F. Lukeš, Surface Sci. 16, 74 (1969).

79. F. Lukeš, W. H. Knausenberger and K. Vedam, Surface Sci. 16, 112 (1969).

80. H. Mayer, Physik duenner Schichten, Wiss. Verlagsges. Stuttgart, 1950, Ch. IV,1.

81. C. L. McBee and J. Kruger, Surface Sci. 16, 340 (1969).

82. F. L. Mc Crackin, E. Passaglia, R. R. Stromberg and H. L. Steinberg, J. Research Natl. Bur. Standards 67A, 363 (1963).

83. F. L. McCrackin and J. P. Colson, in Ref. 98., p. 61.

84. F. L. McCrackin, A. Fortran Program for Analysis of Ellipsometer Measurements, Natl. Bur. Standards, Tech. Note 479, April 1969, U.S. Government Printing Office, Washington, D.C.

85. W. H. McMaster, Am. J. Phys. 22, 531 (1954).

86. A. J. Melmed, H. P. Layer and J. Kruger, Surface Sci. 9, 476 (1968).

87. J. R. Miller and J. E. Berger, J. Phys. Chem. 70, 3070 (1966).

88. J. R. Mowat and R. H. Muller, Reflection of Polarized Light From Absorbing Media, University of California, Lawrence Radiation Laboratory, UCRL-11813, 1966.

89. R. H. Muller, Rev. Sci. Instr. 39, 1593 (1968).

90. R. H. Muller, Surface Sci. 16, 14 (1969).

91. R. H. Muller, R. F. Steiger, G. A. Somorjai, and J. M. Morabito, Surface Sci. 16, 234 (1969).

92. W. G. Oldham, Surface Sci. 16, 97 (1969).

93. J. L. Ord and B. L. Wills, Appl. Optics 6, 1673 (1967).

94. J. L. Ord, Surface Sci. 16, 155 (1969).

95. A. D. F. Palmer, Phys. Rev. 17, 409 (1921).

96. J. R. Partington, An Advanced Treatise on Physical Chemistry, vol. 4. Longmans, Green and Co., London, 1953.

97. E. Partovi, J. Opt. Soc. Am. 52, 918 (1962).

98. E. Passaglia, R. R. Stromberg, and J. Kruger, eds., Ellipsometry in the Measurement of Surfaces and Thin Films, Proc. Symposium Washington 1963, Natl. Bur. Standards, Misc. Publ.256, 1964.

99. E. Passaglia and R. R. Stromberg, J. Research Natl. Bur. Standards 68A, 601 (1964).

100. W. Primak, in Ref. 98, p. 154.

101. G. N. Ramachandran and S. Ramaseshan, in Encylcopedia of Physics, vol. XXV/1, S. Fluegge, ed., Springer-Verlag 1961, p. 1.

102. A. K. N. Reddy, M. A. V. Devanathan and J. O'M. Bockris, J. Electroanal. Chem. 6, 61 (1963).

103. A. K. N. Reddy and J. O'M. Bockris, in Ref. 98, p. 229.

104. M. Richartz and H.-Y. Hsue, J. Opt. Soc. Am. 39, 136 (1949).

105. M. Richartz, J. Opt. Soc. Am. 56, 198 (1966).

106. B. Rossi, Optics, Addison-Wesley Co., Reading, Mass., 1959, 2nd ed., Ch. 7, 8.

107. A. Rothen and M. Hanson, Rev. Sci. Instr. 19, 839 (1948).

108. A. Rothen, Rev. Sci. Instr. 28, 283 (1957).

109. E. Schmidt, J. Opt. Soc. Am. 60, 490 (1970).

110. D. G. Schueler, Surface Sci. 16, 104 (1969).

111. A. V. Shubnikov, Principles of Optical Crystallography, Consultants Bureau, New York, 1960, p. 145.

112. W. A. Shurcliff, Polarized Light, Harvard University Press, 1962, Ch. 2,7.

113. I. Šimon, J. Opt. Soc. Am. 41, 336 (1951).

114. D. V. Sivukhin, Soviet Physics JETP 3, 269 (1956).

115. L. E. Smith and R. R. Stromberg, J. Opt. Soc. Am. 56, 1539 (1966).

116. P.H. Smith, Surface Sci. 16, 34 (1969).

117. R. C. Smith and M. Hacskaylo, in Ref. 98, p. 83.

118. T. Smith, J. Opt. Soc. Am. 58, 1069 (1968).

119. S. S. So, W. H. Knausenberger and K. Vedam, J. Opt. Soc. Am. 61, 124 (1971).

120. R. F. Steiger, J. M. Morabito, G. A. Somorjai and R. H. Muller, Surface Sci. 14, 279 (1969).

121. J. M. Stone, Radiation and Optics, McGraw Hill Co., New York, 1963 , Ch. 2.

122. ibid, Ch. 13.

123. ibid, Ch. 15, 16.

124. ibid, Ch. 16.

125. C. Strachan, Proc. Cambridge Phil. Soc. 29, 116 (1933).

126. J. Strong, Concepts of Classical Optics, W. H. Freeman, Co., San Francisco, 1958 , Ch. III, VI.

127. H. Takasaki, Appl. Optics 5, 759 (1966).

128. L. Tronstad, Det Kgl Norske Videnskabers Selskabs Skrifter (1931) Nr. 1, F. Bruns, Trondheim, 1931.

129. L. Tronstad, J. Sci. Instr. 11, 144 (1934).

130. A. Vašíček, J. Opt. Soc. Am. 37, 145 (1947).

131. A. Vašíček, Optics of Thin Films, North-Holland Publ. Co., Amsterdam, 1960, Ch. 2,3.

132. ibid, Ch. 4.

133. ibid Ch. 5.

134. A. Vašíček, in Ref. 98, p. 25.

135. K. Vedam, W. Knausenberger and F. Lukes J. Opt. Soc. Am. 59, 64 (1969).

136. H. Weinberger and J. Harris, J. Opt. Soc. Am. 54, 552 (1964).

137. J. M. Weingart and A. R. Johnson, in Ref. 98, p. 113.

138. I. Wilmans, Surface Sci. 16, 147 (1969).

139. A. B. Winterbottom, Det Kongelige Norske Videnskabers Selskabs Skrifter (1955) Nr. 1, F. Bruns, Trondheim, 1956.

140. A. B. Winderbottom, in Ref. 98, p. 97.

141. F. E. Wright, J. Opt. Soc. Am. 20, 529 (1930).

142. H. T. Yolken, R. M. Waxler and J. Kruger, J. Opt. Soc. Am. 57, 283 (1967).

143. S. Yoshida, T. Yamaguchi and A. Kinbara, J. Opt. Soc. Am. 61, 463 (1971).

144. K. H. Zaininger and A. G. Revesz, RCA Review, March 1964, p. 85.

FIGURE CAPTIONS

Fig. 1. Electric and magnetic vectors in a linearly polarized light wave.

Fig. 2. Electric vector in linearly polarized light. The plane of polarization contains the electric field vectors in space. At a fixed location, the tip of the electric vector traces a straight line as a function of time.

Fig. 3. Linear polarization resulting from the superposition of two linearly polarized waves in phase with each other. x and y coordinate directions may represent p and s components, respectively.

Fig. 4. Reflection of polarized light. Plane of incidence defined by incident and reflected beam. s and p components indicated in incident light, with electric vector normal and parallel, respectively, to the plane of incidence.

Fig. 5. Elliptic polarization resulting from the superposition of two linear components of different phase and amplitude. Representation as a helix in space or an ellipse in a plane normal to the propagation direction k. Physical parameters ψ, Δ and geometric parameters θ, γ of the state of polarization. E_F, E_{SL} orthogonal fast and slow components ahead or behind each other in phase, respectively, by a quarter wave (90°).

Fig. 6. Dependence of gemetric parameters θ and γ of elliptic polarization on phase difference Δ between p and s components for constant relative amplitude tan ψ.

Fig. 7. Poincaré Sphere (left) and its stereographic projection (right) seen from the left hand circular pole L. Reference point H denotes the plane of incidence. Top: grid for geometrical parameters, θ and γ, center: grid for physical parameters ψ and Δ, bottom: grid for retardation δ_Q of a compensator with fast axis F.

Fig. 8. Reflection and refraction at a dielectric interface. Definition of symbols and of positive coordinate directions for p and s components of electric field vector E in incident, reflected and refracted waves. Circles represent arrows pointing out of the plant of the drawing.

k - propagation direction of the three waves

ϕ - angle of incidence

ϕ' - angle of refraction

n_o - refractive index of incident medium

n_1 - refractive index of reflecting medium,

z - coordinate direction for amplitude attenuation if the reflection medium is absorbing.

Fig. 9. Light penetration into absorbing media of alternate complex refractive index $n_c' = n' - ik'$. Wavelength 5.461×10^{-5} cm.

Fig. 10. Reflection from bare surfaces of complex refractive index n_c as a function of angle of incidence ϕ. a) Argument δ (absolute phase change) and modulus $|r|$ of reflection coefficient for p (——) and s (---) components. b) Ellipsometer parameters Δ (relative phase change) and ψ (relative amplitude attenuation $\tan \psi$).

Identification of curves

1. $n_c = 1.5$ (clear glass)
2. $n_c = 1.5 - 0.15i$ (dark glass)
3. $n_c = 3.3 - 2.31i$ (Tantalum)
4. $n_c = 0.2 - 4.0i$ (Silver)

Fig. 11. Argument δ (absolute phase change) and modulus $|r|$ (amplitude) of reflection coefficient for reflection from a bare metal surface of refractive index $n_c = n - ik$. Angle of incidence 2°, p - component.

Fig. 12. As Fig. 11, s - component.

Fig. 13. As Fig. 11, angle of incidence 45°, p - component.

Fig. 14. As Fig. 11, angle of incidence 45°, s - component.

Fig. 15. As Fig. 11, angle of incidence 75°, p - component.

Fig. 16. As Fig. 11, angle of incidence 75°, s - component.

Fig. 17. Ellipsometer parameters Δ (relative phase change) and ψ (relative amplitude change tan ψ) for reflection from a bare metal surface of refractive index n - ik. Angle of incidence 45°.

Fig. 18. As Fig. 17, angle of incidence 75°.

Fig. 19. Reflection from idealized film-covered surface (a) representation by multiple beam reflections (b) representation by resultant waves.

Fig. 20. Reflection coefficients r_1 and r_2 at both interfaces of a film-covered surface. Designation of refractive indices and electric fields. All the angles of propagation except ϕ are complex (indicated by dotted circles and lines) and cannot be interpreted geometrically.

Fig. 21. Computed values of ψ and Δ (Eq. 60) for 100 Å increments of a dielectric film (CaF_2, $n_f = 1.4339-0i$) on a dielectric substrate (glass, $n_m = 1.519-0i$). Angle of incidence 60°. Incident medium vacuum ($n_o = 1$), wavelength 5461 Å, film thickness in Å indicated along the curve.

Fig. 22. Computed values of ψ and Δ for 100 Å increments of a dielectric film (Ta_2O_5, n_{cf} = 2.26-0i) on an absorbing substrate (Ta, n_{cm} = 3.5-2.4i). Other data as in Fig. 21.

Fig. 23. Computed values of ψ and Δ for an absorbing film (Cr, n_{cf} = 2.96-3.45i) on a dielectric substrate (glass, n_{cm} = 1.519-0i). Other data as on Fig. 21.

Fig. 24. Computed values of ψ and Δ for an absorbing film (Cr, n_{cf} = 2.96-3.45i) on an absorbing substrate (Ni, n_{cm} = 1.4-2.52i). Other data as on Fig. 21.

Fig. 25. Multiple beam model $r_o + r_1 + r_2 + r_3$ etc. and double beam approximation $r_o + r_\infty$ of reflection r from a dielectric film (Ta_2O_5, n_{cf} = 2.26-0i) on an absorbing substrate (Ta, n_{cm} = 3.5-2.4i). Angle of incidence 75°, incident medium vacuum (n_o = 1).

Fig. 26. Double beam model of ellipsometry. Addition of complex amplitudes r_o anf r_∞ for s and p components, Ta_2O_5 on Ta, data as in Fig. 25, negligible film thickness.

Fig. 27. Double beam model of ellipsometry. Effect of increasing film thickness on ellipsometer parameters Δ and $|r_p|/|r_s| = \tan\psi$, Ta_2O_5 film on Ta, data as in Fig. 25.

Fig. 28. Comparison of ellipsometric parameters ψ and Δ obtained graphically by means of the double beam model (dashed curve) with exact computations (solid curve). Ta_2O_5 film (n_{cf} = 2.26-0i) on Ta (n_{cm} = 3.5-2.4i). Angle of incidence 75°, incident medium vacuum.

Fig. 29. Analysis of elliptic polarization with a rotating analyzer.

Fig. 30. Arrangement of components and states of polarization in an ellipsometer with linear polarization incident on the specimen and use of a compensator of variable retardation.

P - polarizer with transmitted electric field direction in fixed 45° azimuth.

S - reflecting specimen surface.

E - elliptic state of polarization after reflection.

C - variable compensator of fixed azimuth (slow and fast axis parallel to p and s directions). Retardation at extinction is a measure of Δ.

A' - restored linear state of polarization.

A - Analyzer with transmitted electric field direction. Azimuth a at extinction is a measure of ψ.

Fig. 31. Ellipsometer with linear polarization incident and compensator of fixed retardation.

P,S,E,A' - as in Fig. 30.

Q - fixed compensator (quarter wave plate) of variable azimuth q (at extinction, fast axis F parallel to major axis of ellipse, $q = \theta$).

A - analyzer with transmitted electric field direction. Azimuth a at extinction is a measure of γ.

Fig. 32. Ellipsometer with elliptic polarization incident and compensator of variable retardation. P, C, S, A', A as in Fig. 30.

E - elliptic state of polarization before reflection.

Fig. 33. Ellipsometer with elliptic polarization incident and compensator of fixed retardation.

P - Polarizer with transmitted electric field direction. Azimuth p at extinction is a measure of Δ.

Q - Fixed compensator (quarter wave plate) of fixed azimuth (fast axis F at 45° to plane of incidence).

E - Elliptic state of polarization before reflection.

S - reflecting specimen surface.

A' - restored linear state of polarization

A - analyzer with transmitted electric field direction. Azimuth a at extinction is a measure of ψ.

Fig. 34. Poincaré representation of the changes in the state of polarization through the components of an ellipsometer arranged as in Fig. 30. Stereographic projection. Symbols listed in text.

Fig. 35. Poincaré representation of ellipsometer arrangement of Fig. 31.

Fig. 36. Poincaré representation of ellipsometer arrangement of Fig. 32.

Fig. 37. Poincaré representation of ellipsometer arrangement of Fig. 33.

Fig. 38. Propagation of azimuth errors with quater wave compensator. Transmitted light intensity as a function of analyzer azimuth. Stainless steel surface in air, angle of incidence 75°, Photomultiplier RCA 931A,-800V. (a) linear polarization incident polarizer azimuth 135°, compensator azimuth $q_1 = 96.87°$, $q_2 = 95.87°$, $q_3 = 95.37°$ (b) elliptic polarization incident, compensator azimuth 45°, polarizer azimuth $p_1 = 0.33°$, $p_2 = 1.33°$, $p_3 = 1.83°$.

Fig. 39. Propagation of azimuth errors with quarter wave compensator, Poincaré representation. (a) linear Polarization incident. (b) elliptic polarization incident.

Fig. 40. Four zones for elliptic incident polarization and quarter wave compensator. Zone group A (Δ = 0 to 90°). Measurement of the same values ψ and Δ due to reflection. Stereographic projection of Poincaré sphere.

Fig. 41. Four zone groups for elliptic incident polarization and quarter wave compensator. Zone 1 (p = 0 to 45°). Sterographic projection of Poincaré sphere.

Fig. 42. Errors in alignment of axes of collimator (A) and telescope (C). (a) plan vue with intersection of axes in front of specimen surface (B). (b) side view with axes intersecting in specimen but not parallel to each other (c) side view with axes parallel but not in the same plane.

Fig. 43. Effect of pinhole in analyzer telescope. Ellipsometer for elliptic incident polarization with quarter wave compensator.

A - light source

B - collimator pinhole

C - collimator lens

D - polarizer prism

E, J - iris diaphragms

F - quarter wave plate

G, I - cell windows

H - reflecting specimen

K - analyzer prism

L - telescope lens

M - telescope pinhole

N - photodetector

____ main beam

--- parasitic beam

Fig. 44. Effect of non-normal incidence on a 3/8 in. thick cell window on the state of polarization of transmitted light.

Fig. 45. Modified ellipsometer, elliptic polarization incident.

A - movable carriage for light sources

B - exchangeable monochromatic light sources

C - light chopper and generator of reference signal for phase-sensitive detector

D - collimator tube with pinhole entrance

E - polarizer circle with illuminated scale

G - cell with specimen surface

H - iris diaphragm for control of observed specimen area

I - polarizer circle with illuminated scale

K - telescope tube with pinhole exit

L - photomultiplier

M - base plate for exchange of light sources and conversion to linear polarization incident

N - angle of incidence circle

O - specimen table with vertical movement

P - motor drive controle unit for specimen table.

Fig. 46. Models for optical reflection from a rough surface (a) triangular ridge model of surface profile (b) peak to peak variations in surface profile represented by a homogeneous transitional layer (c) inhomogeneous transitional layer with optical properties varying in the vertical direction.

Fig. 47. Reflection from patch-wise distributed films, variation of lateral coherence (indicated by width of wave fronts) in incident light. (a) coherent superposition of polarization states due to reflection on bare and film-covered surface elements. (b) incoherent superposition of polarization states.

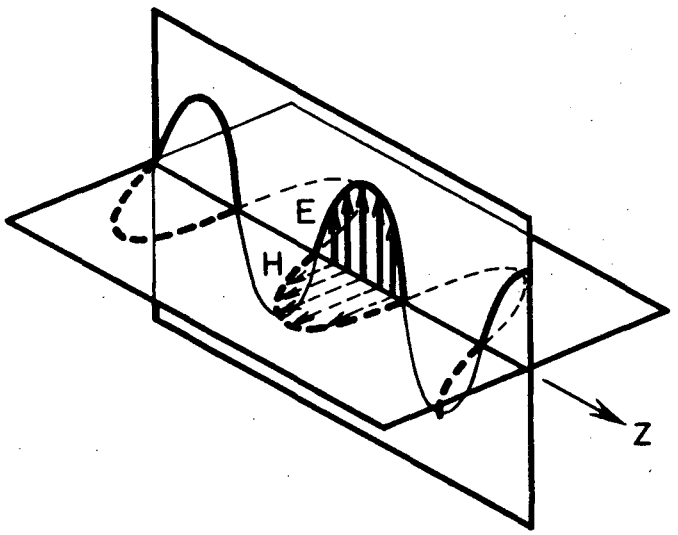

Fig. 1

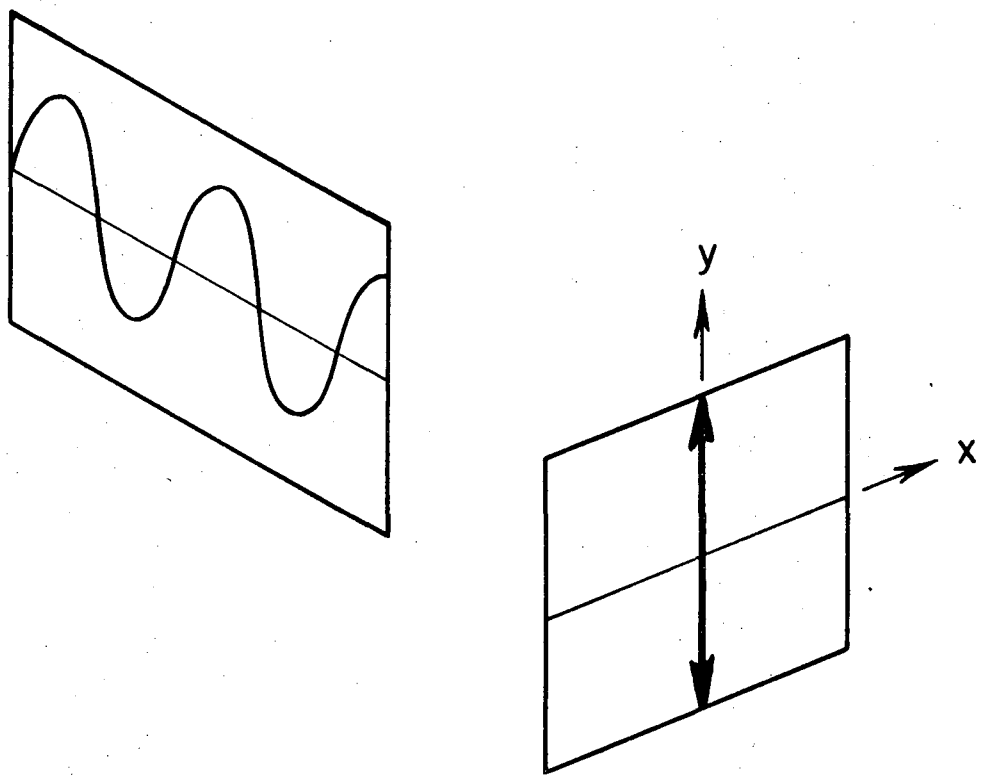

MUB-8163

Fig. 2

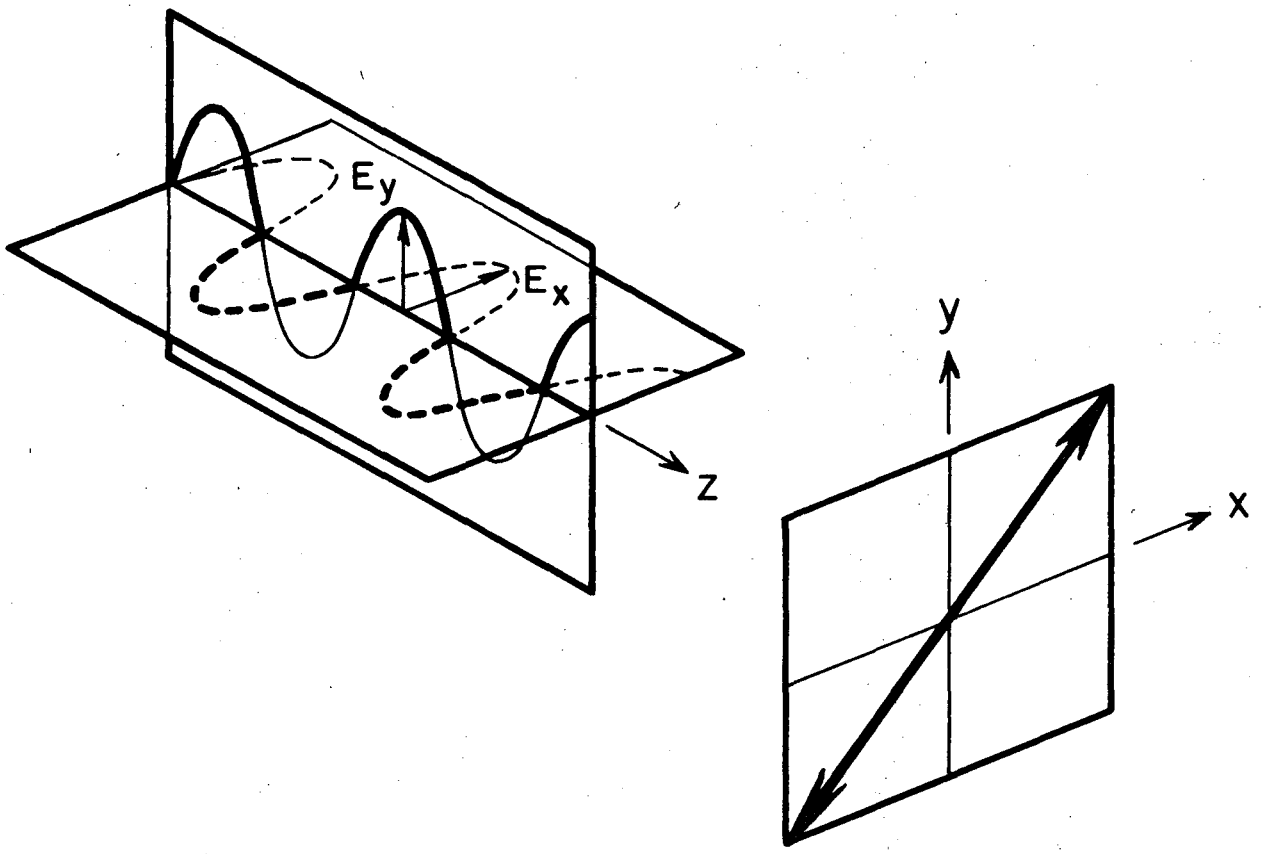

MUB-8164

Fig. 3

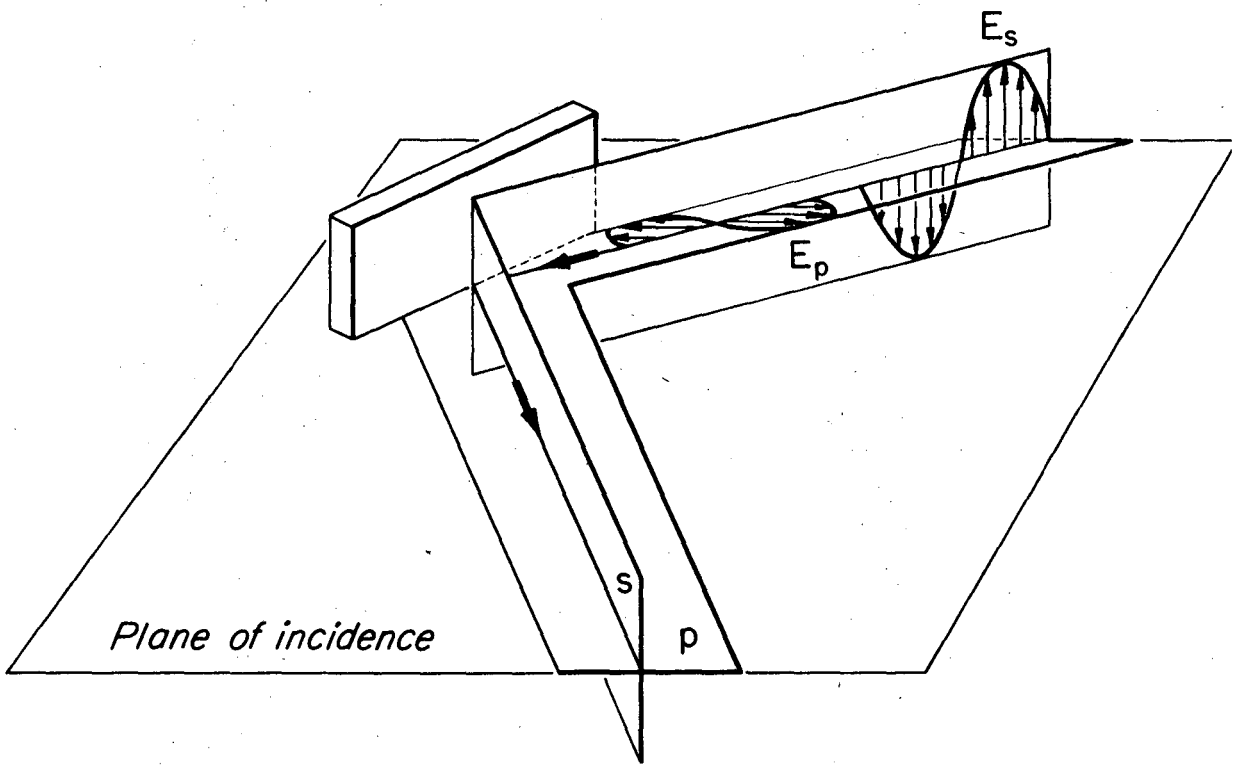

XBL719-4288

Fig. 4

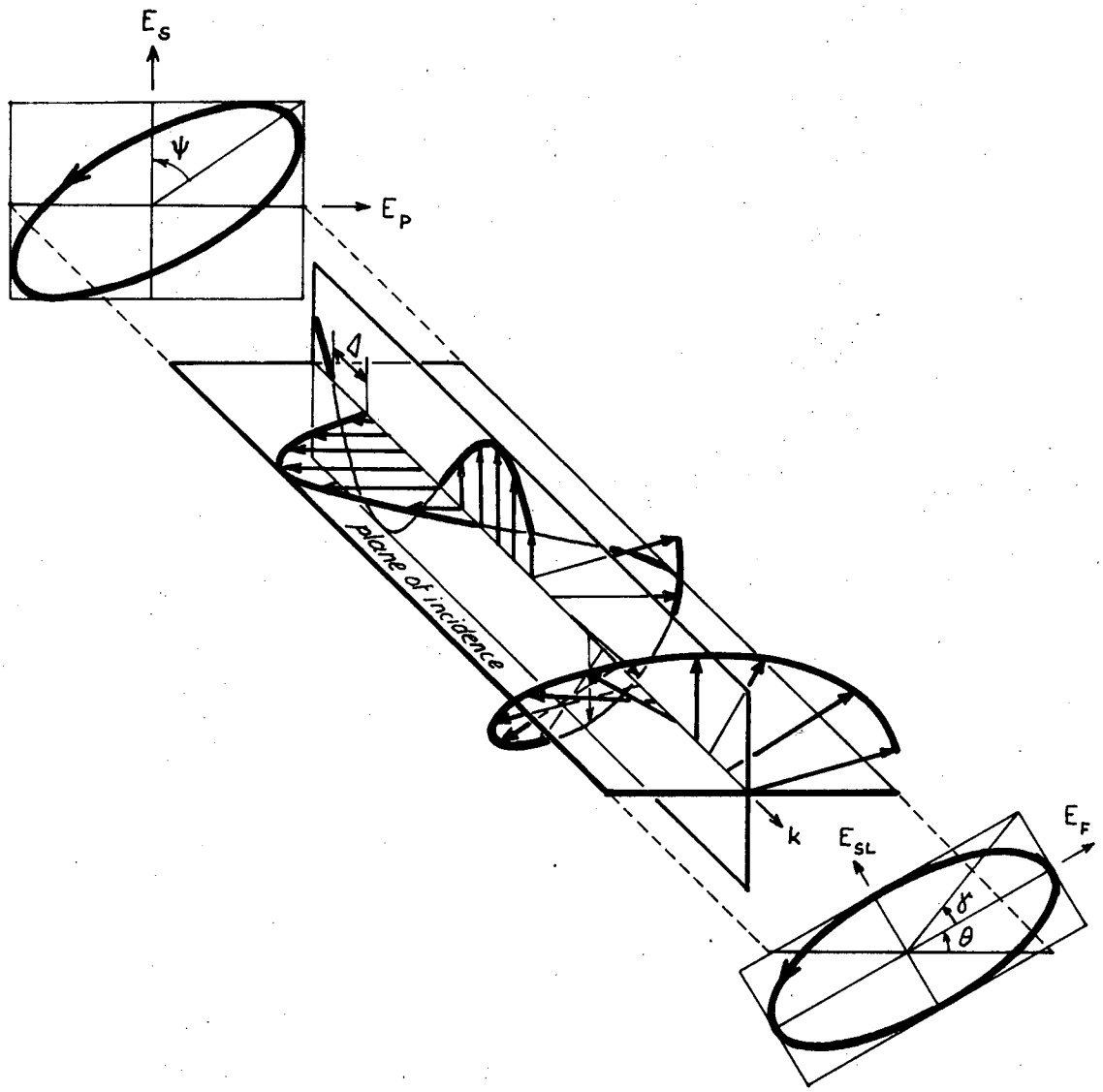

XBL 681-59A

Fig. 5

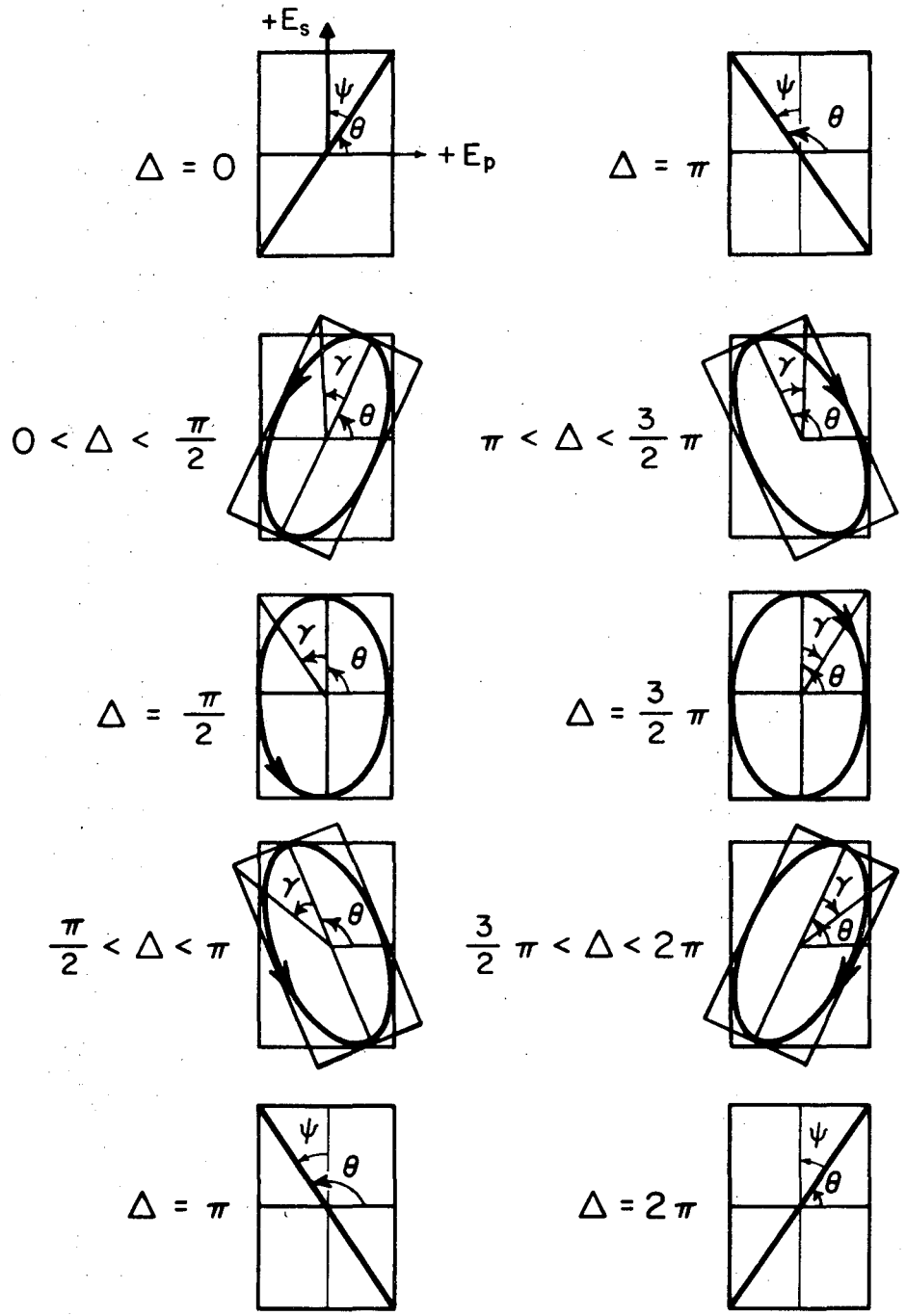

MUB-8168-B

Fig. 6

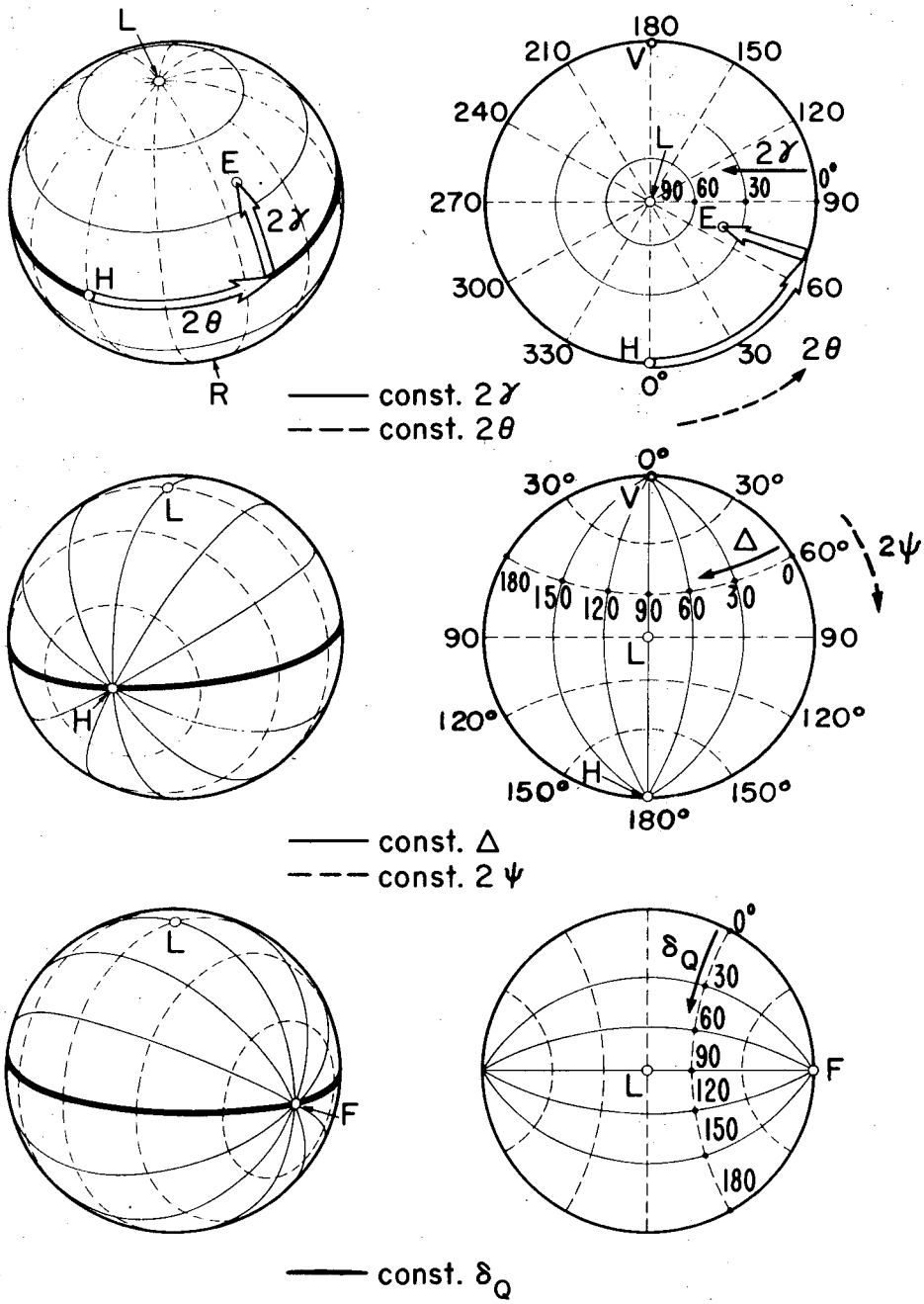

XBL685-2759-A

Fig. 7

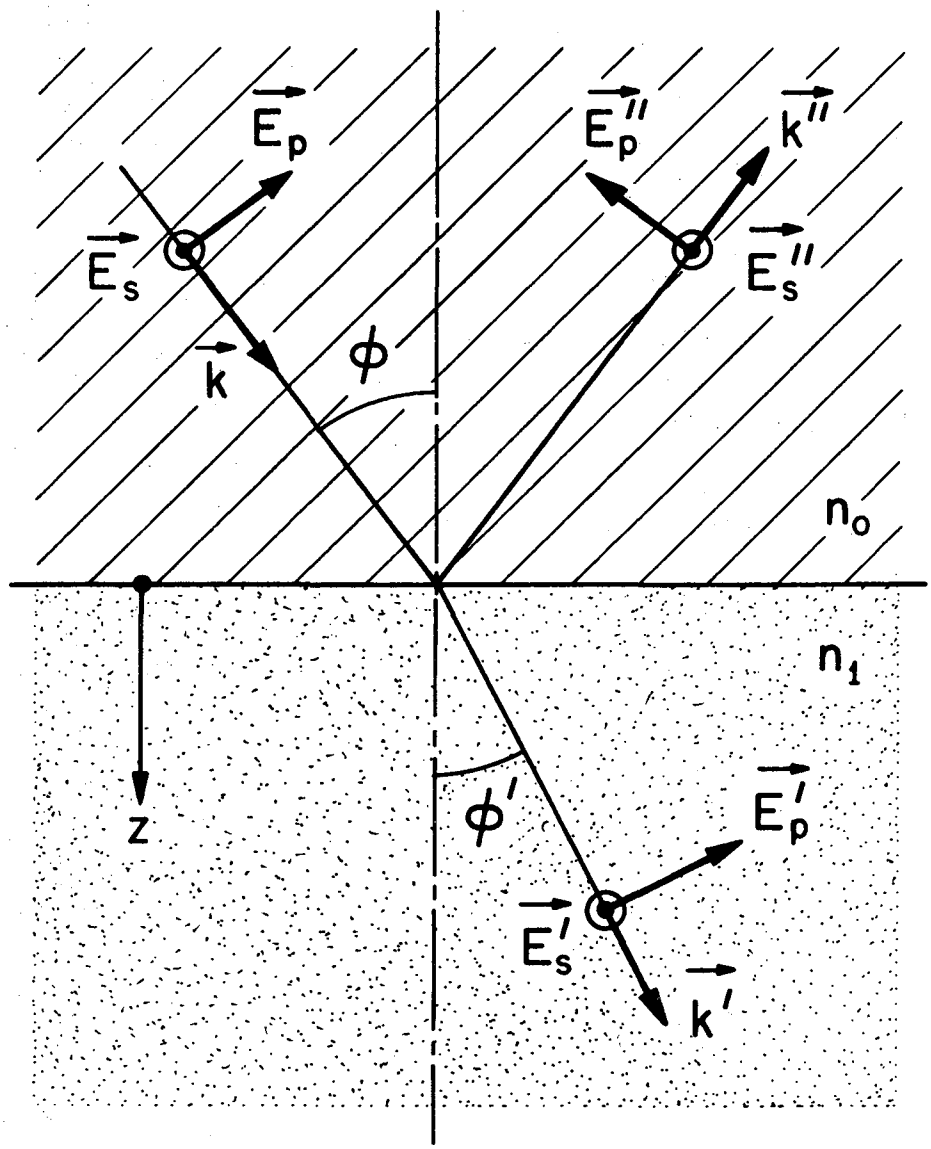

XBL 719-4286

Fig. 8

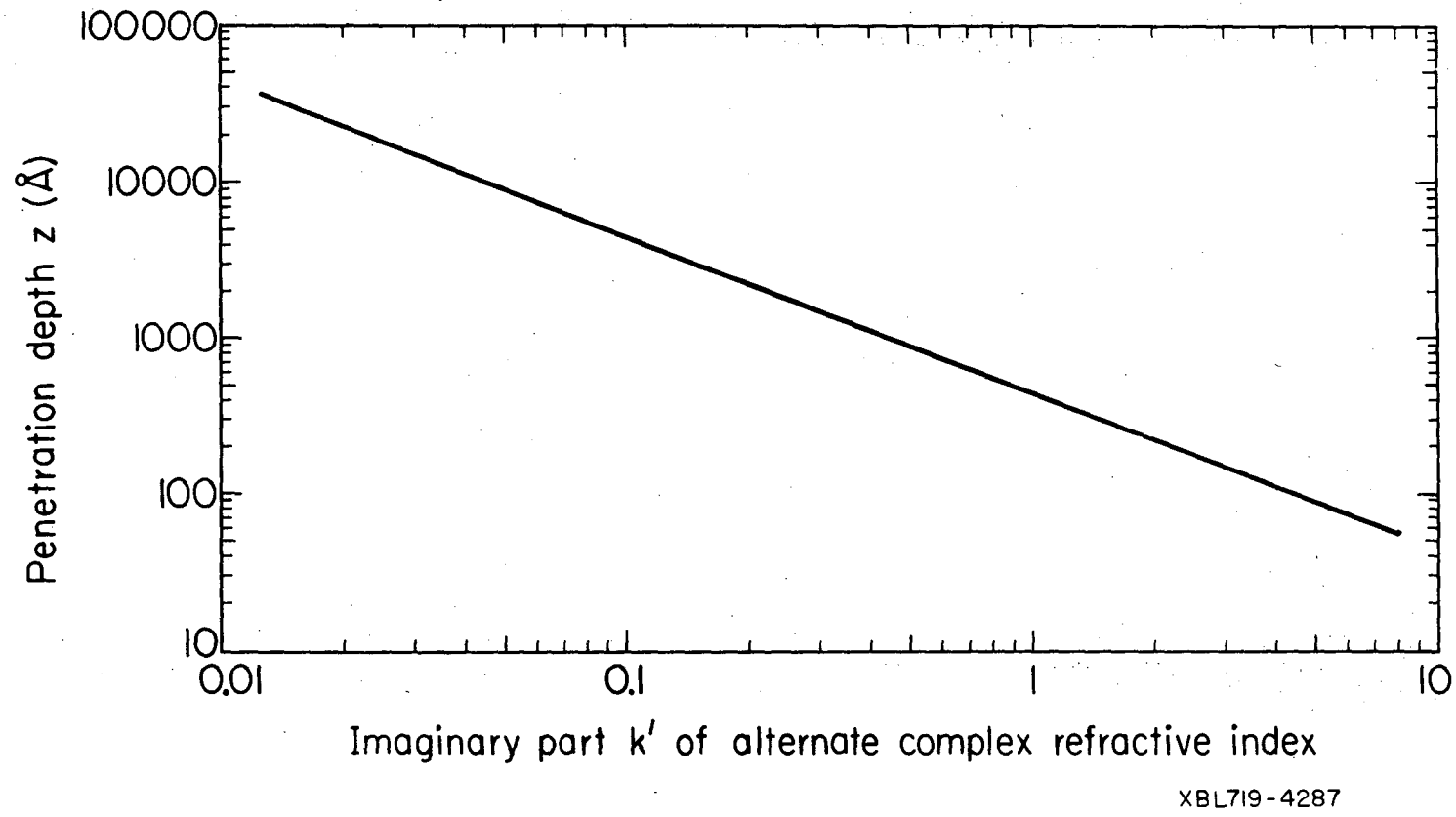
100000
10000
1000
100
10
Penetration depth z (Å)
0.01
0.1
1
10
Imaginary part k′ of alternate complex refractive index
XBL719-4287

Fig. 9

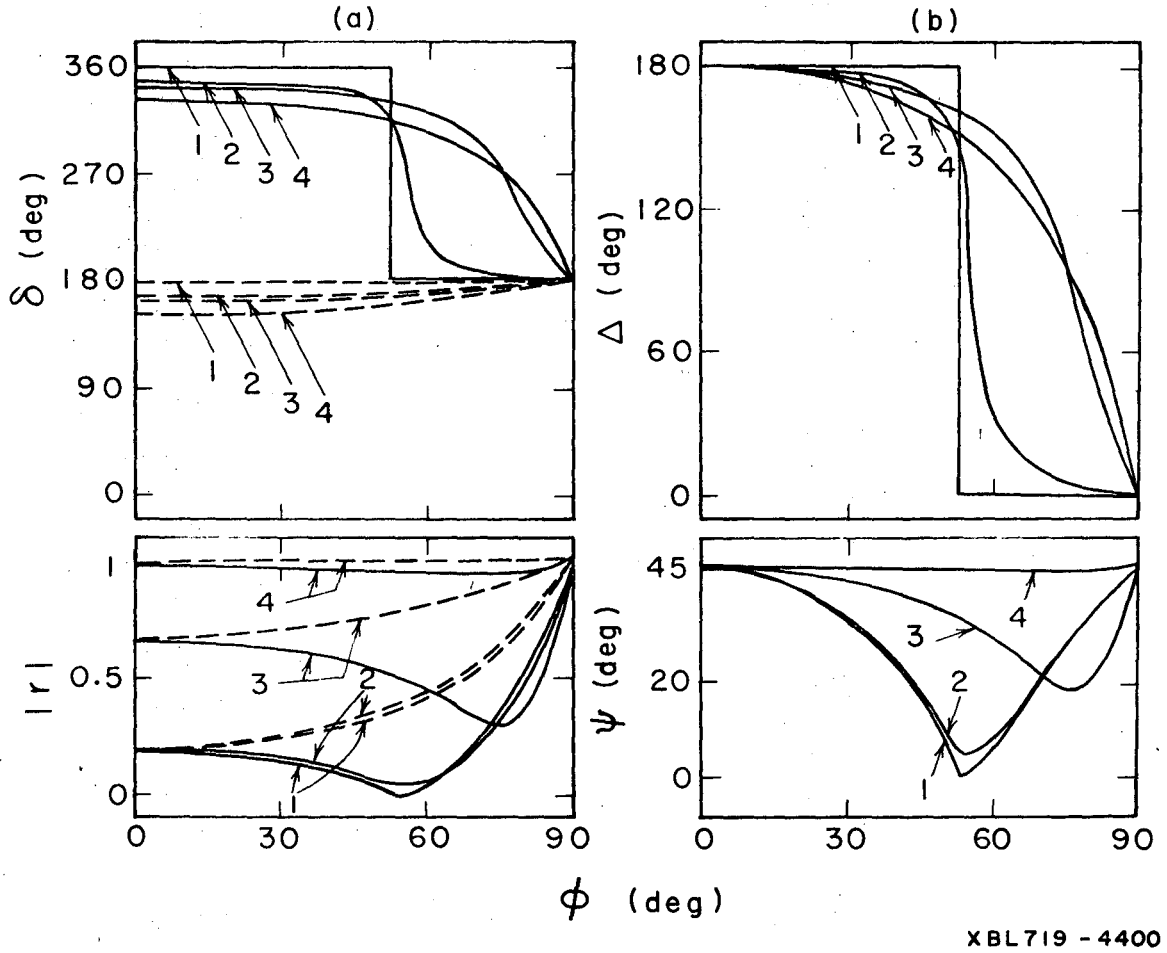
(a)
(b)
360
270
180
90
0
δ (deg)
1
2
3
4
180
120
60
0
Δ (deg)
1
0.5
0
|r|
45
20
0
ψ (deg)
0
30
60
90
φ (deg)
XBL719 - 4400

Fig. 10

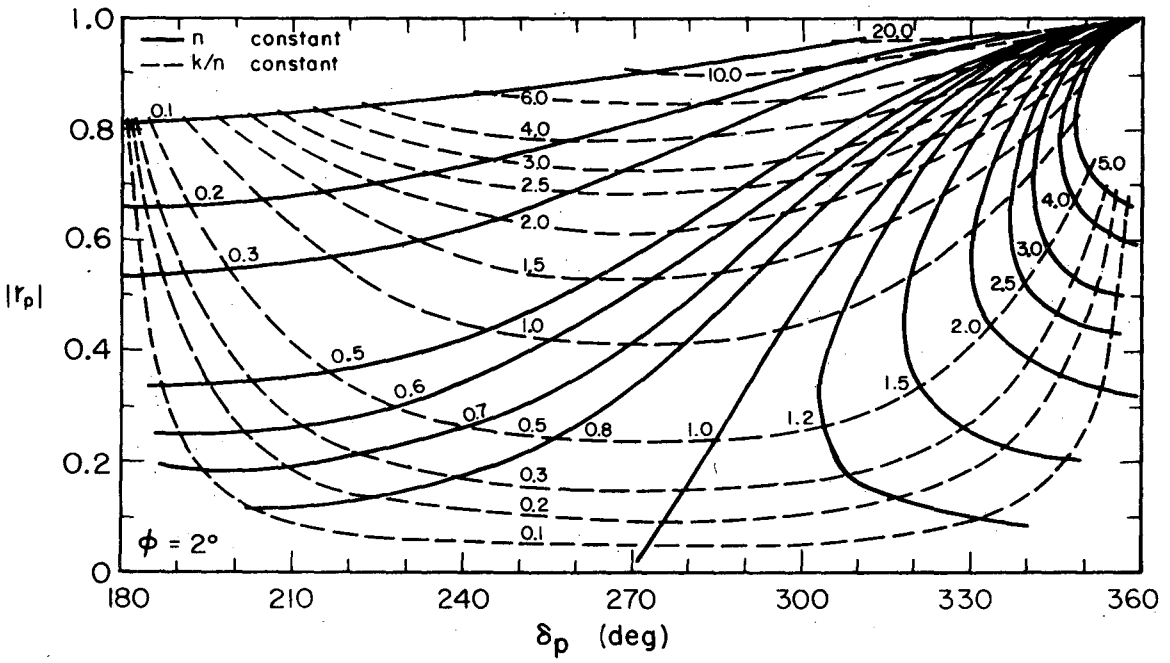

MUB 12901A

Fig. 11

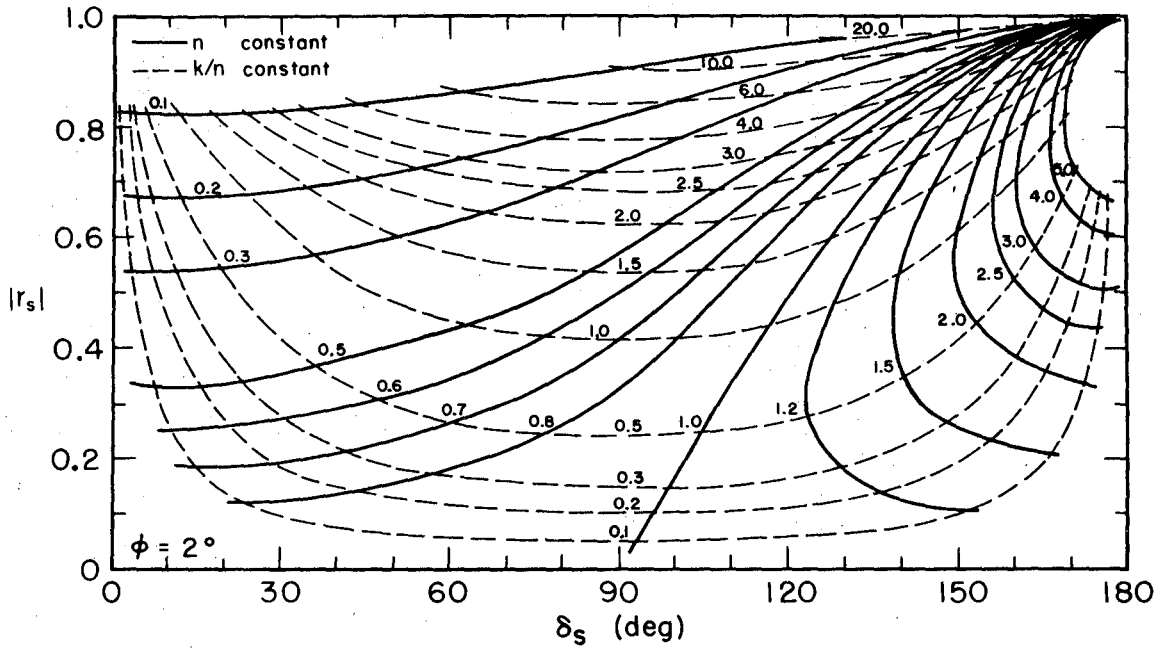

MUB 12900A

Fig. 12

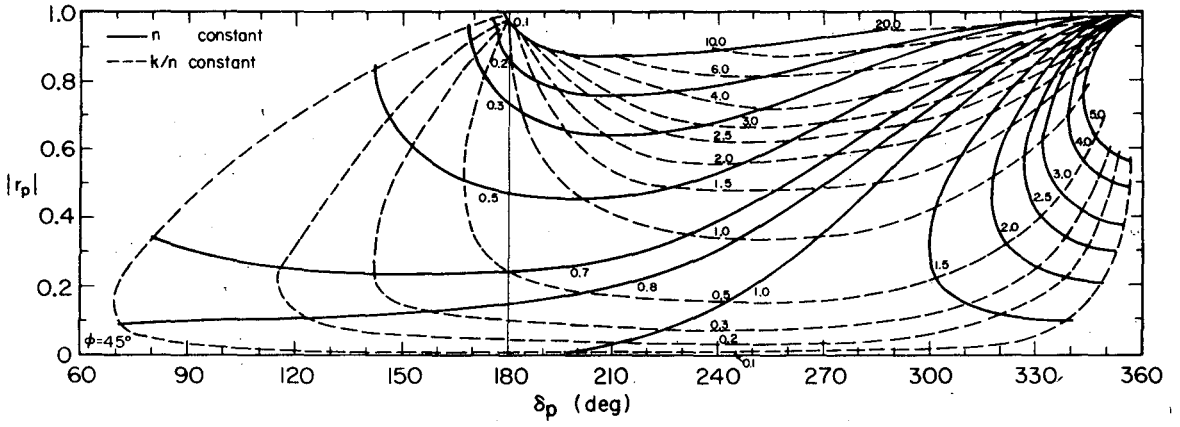

MUB 12909A

Fig. 13

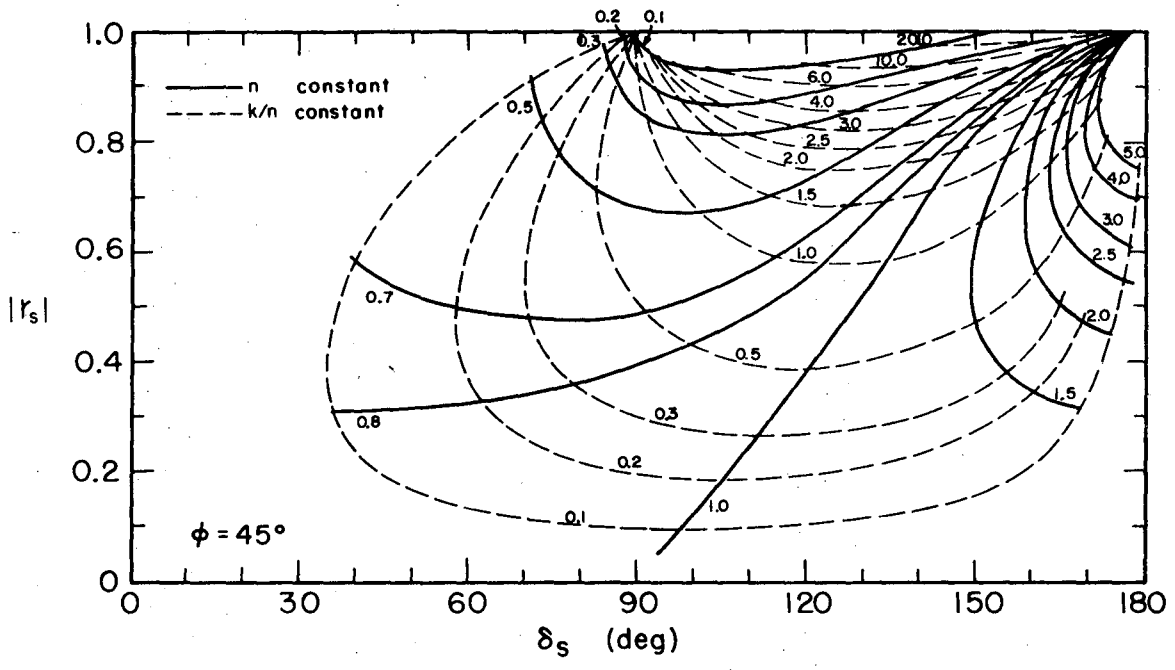

MUB 12904A

Fig. 14

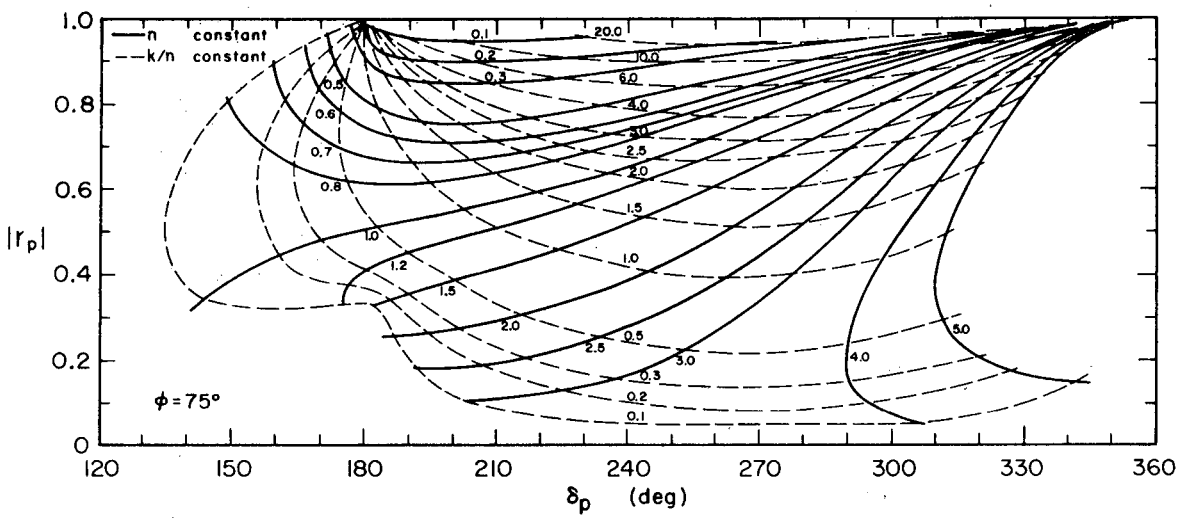

MUB 12908A

Fig. 15

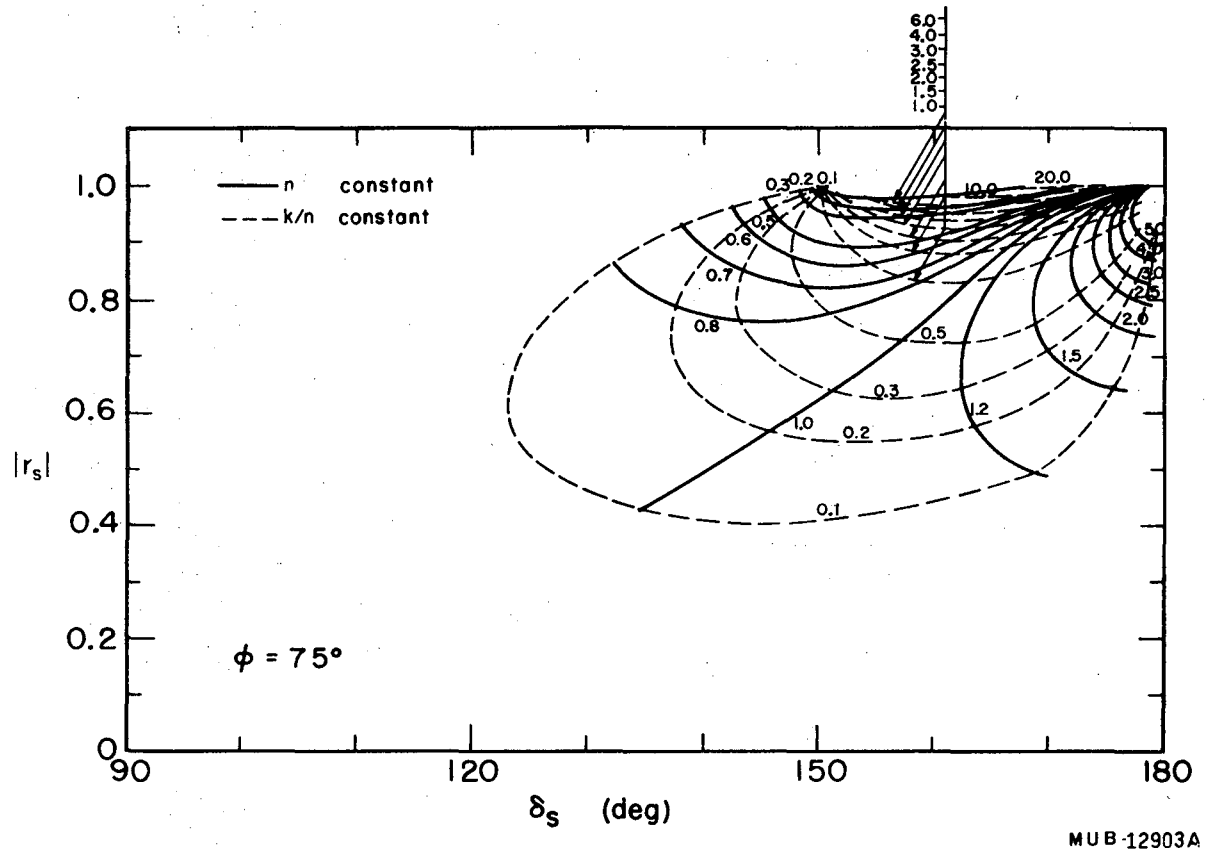

Fig. 16

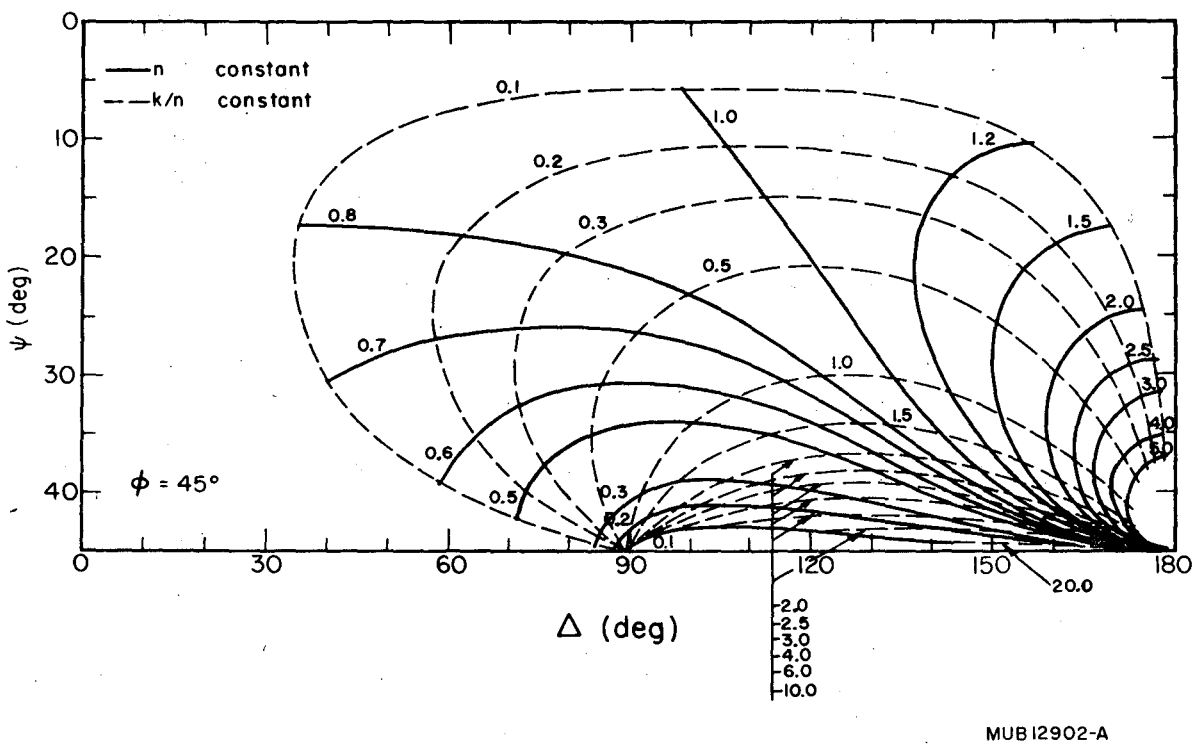
n constant
k/n constant
ψ (deg)
Δ (deg)
φ = 45°
0
10
20
30
40
0
30
60
90
120
150
180
0.1
0.2
0.3
0.5
0.7
0.8
1.0
1.2
1.5
2.0
2.5
3.0
4.0
6.0
10.0
20.0
MUB 12902-A

Fig. 17

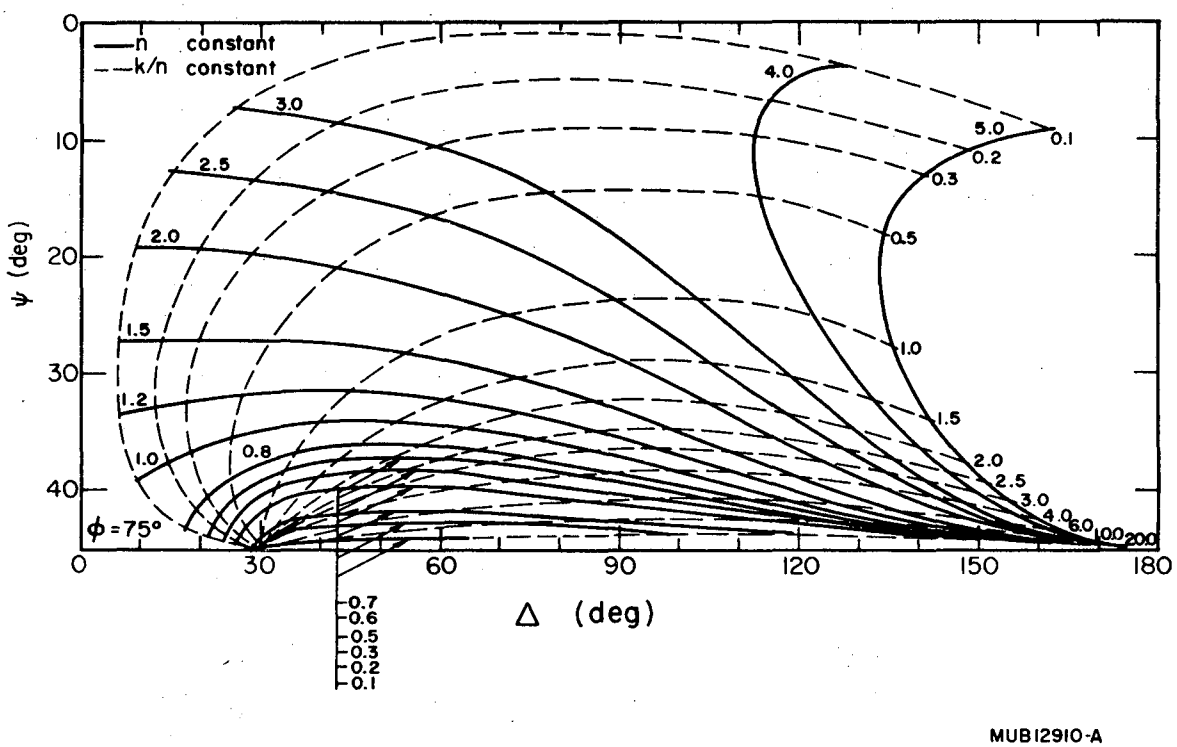
n constant
k/n constant
ψ (deg)
Δ (deg)
φ = 75°
0
10
20
30
40
0
30
60
90
120
150
180
3.0
2.5
2.0
1.5
1.2
1.0
0.8
4.0
5.0
0.1
0.2
0.3
0.5
1.0
1.5
2.0
2.5
3.0
4.0
6.0
10.0
20.0
0.7
0.6
0.5
0.3
0.2
0.1
MUB12910-A

Fig. 18

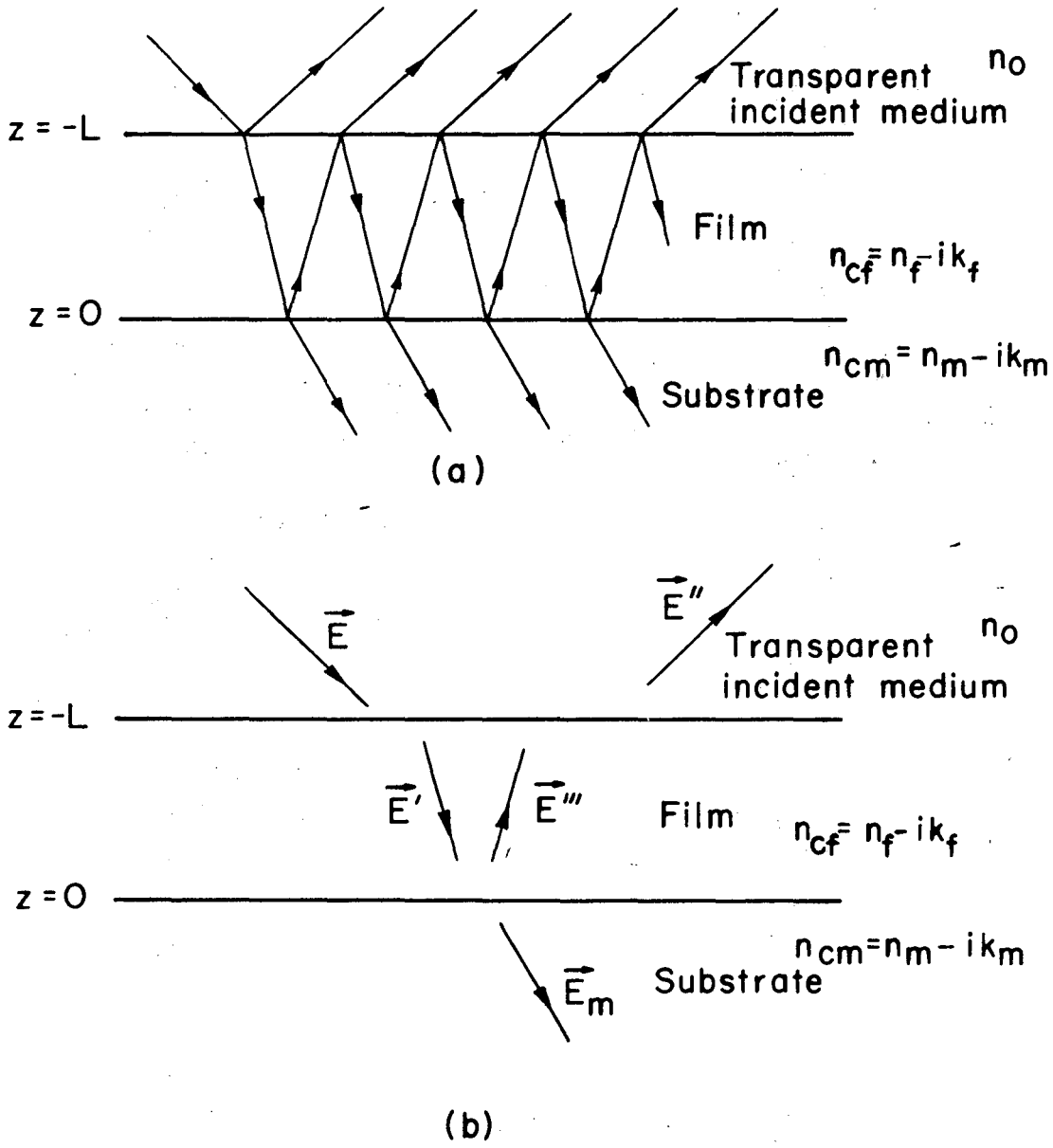

MUB-14178A

Fig. 19

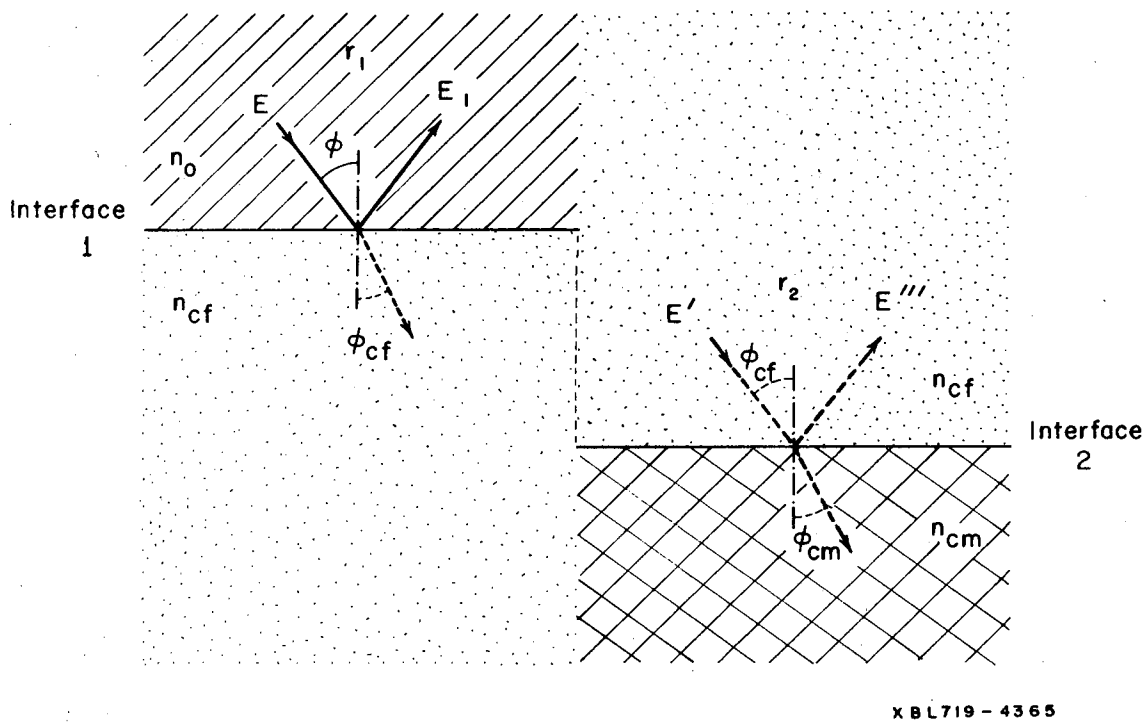
r1
E
E1
φ
no
Interface
1
ncf
φcf
E′
r2
E‴
φcf
ncf
Interface
2
φcm
ncm
XBL719-4365

Fig. 20

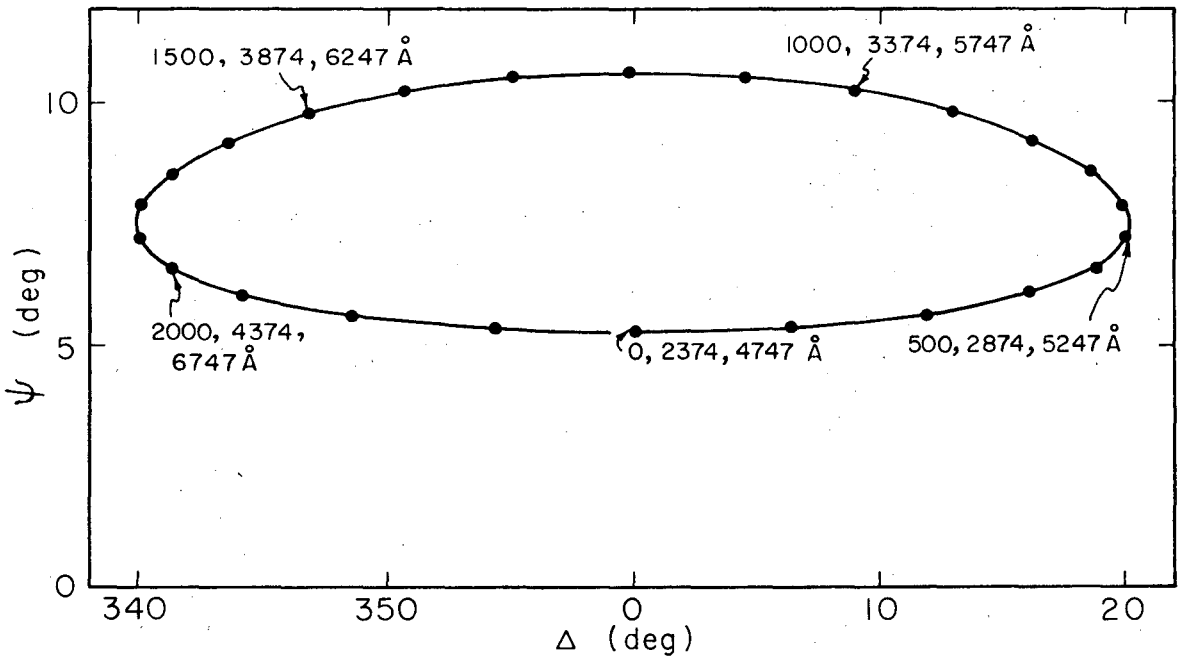

XBL719-4367

Fig. 21

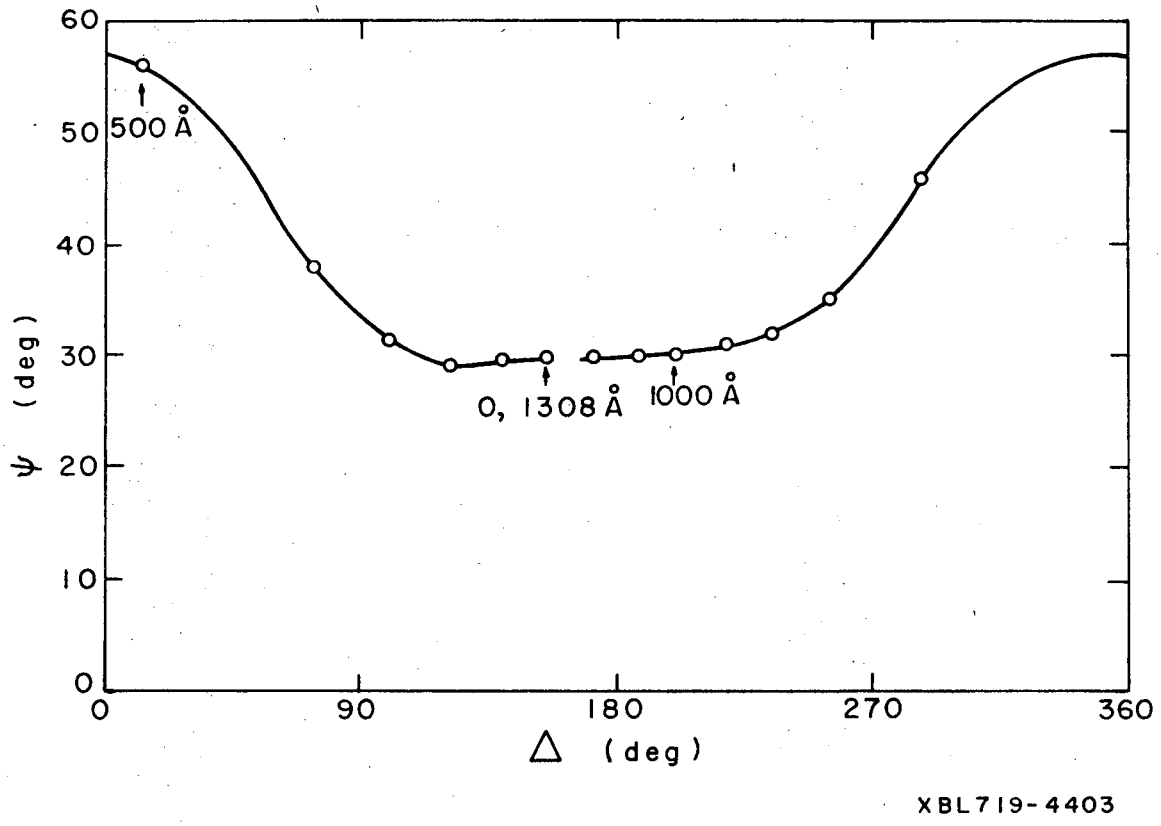
60
50
40
30
20
10
0
ψ (deg)
500 Å
0, 1308 Å
1000 Å
0
90
180
270
360
Δ (deg)
XBL719-4403

Fig. 22

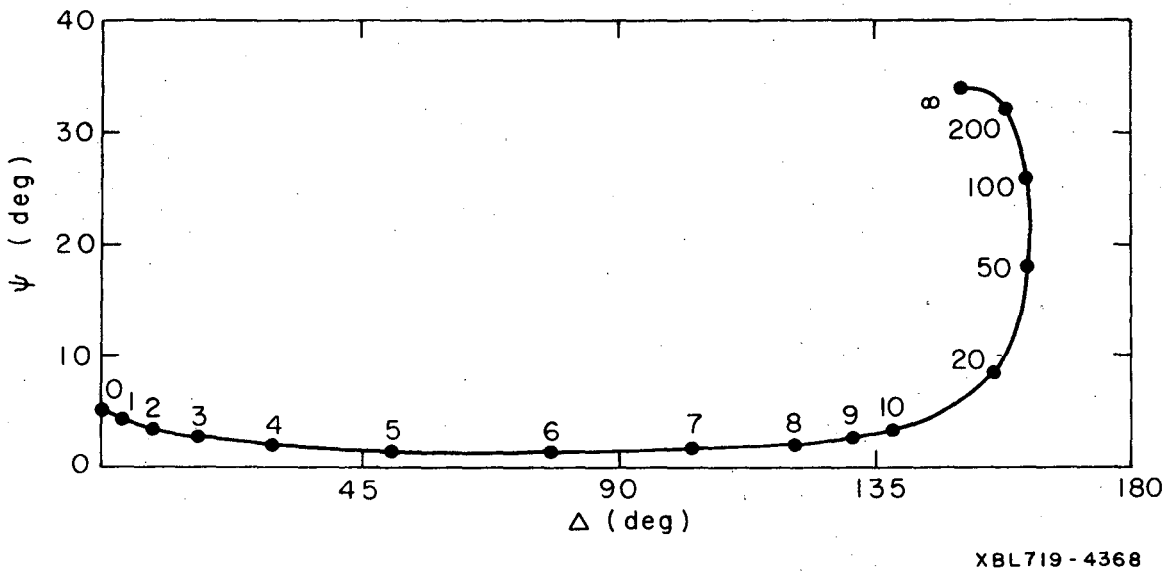
40
30
20
10
0
ψ (deg)
45
90
135
180
Δ (deg)
0
1
2
3
4
5
6
7
8
9
10
20
50
100
200
∞
XBL719-4368

Fig. 23

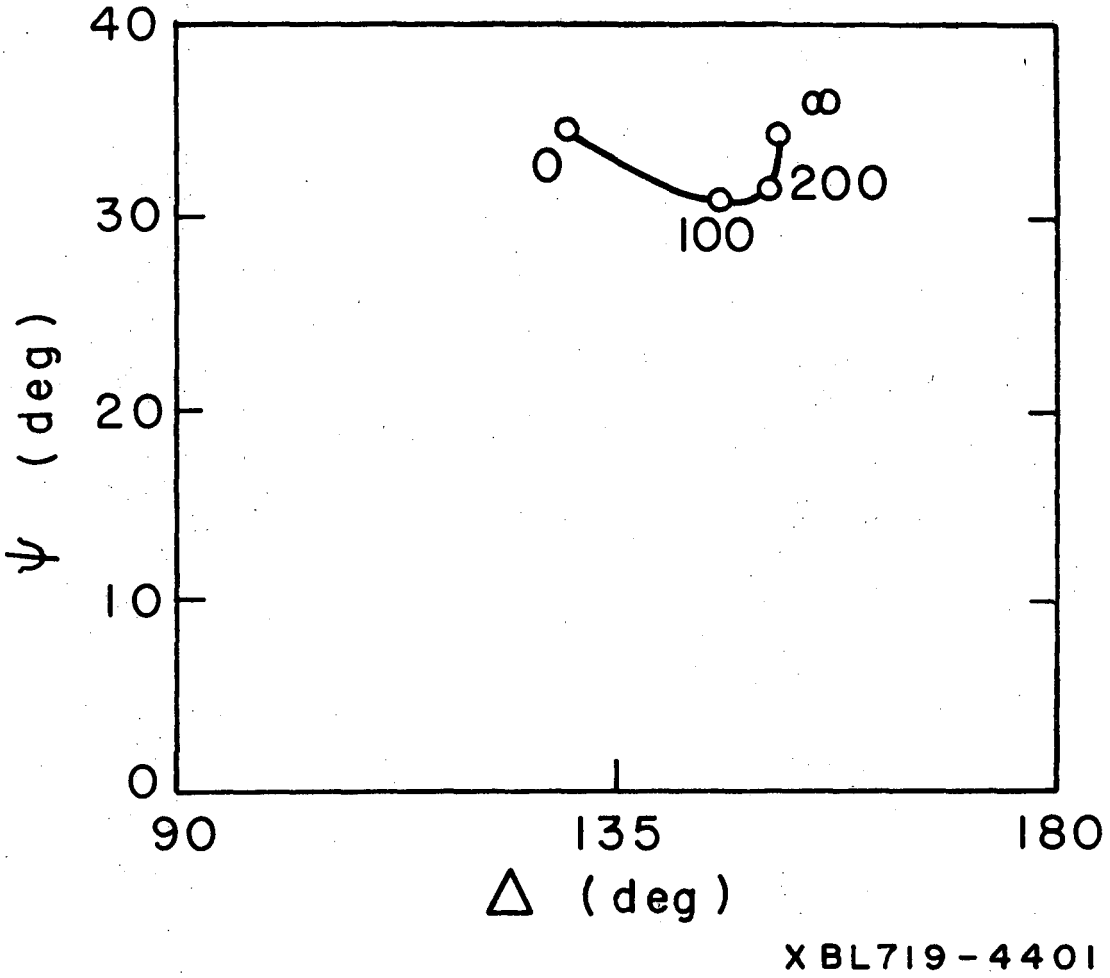

Fig. 24

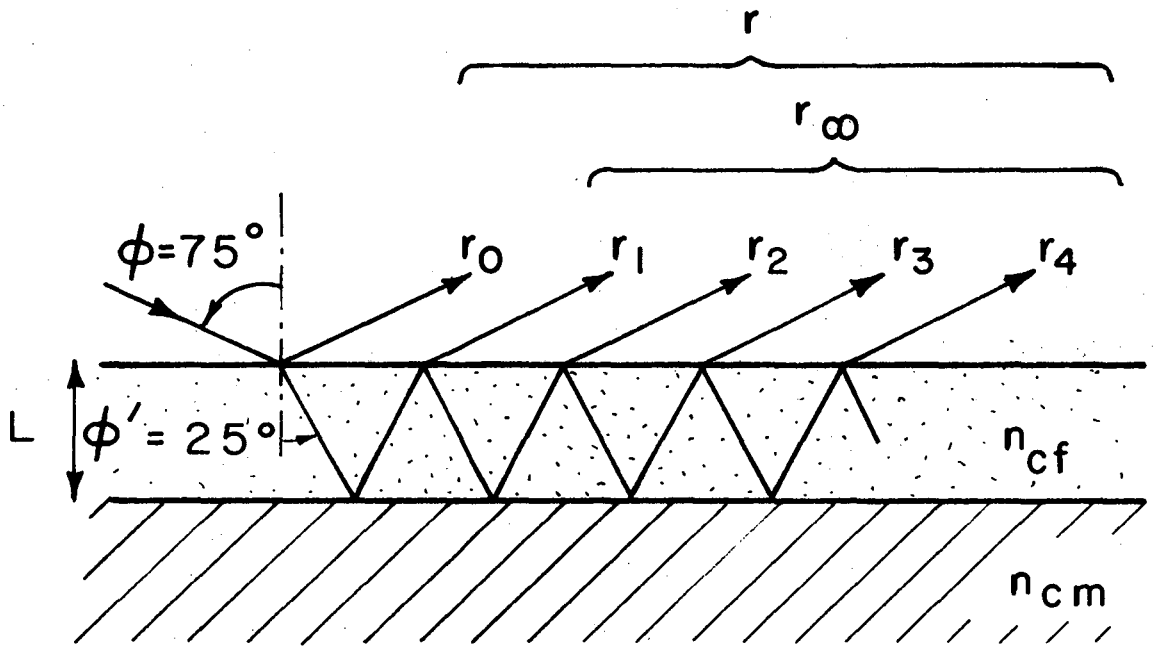

XBL719-4402

Fig. 25

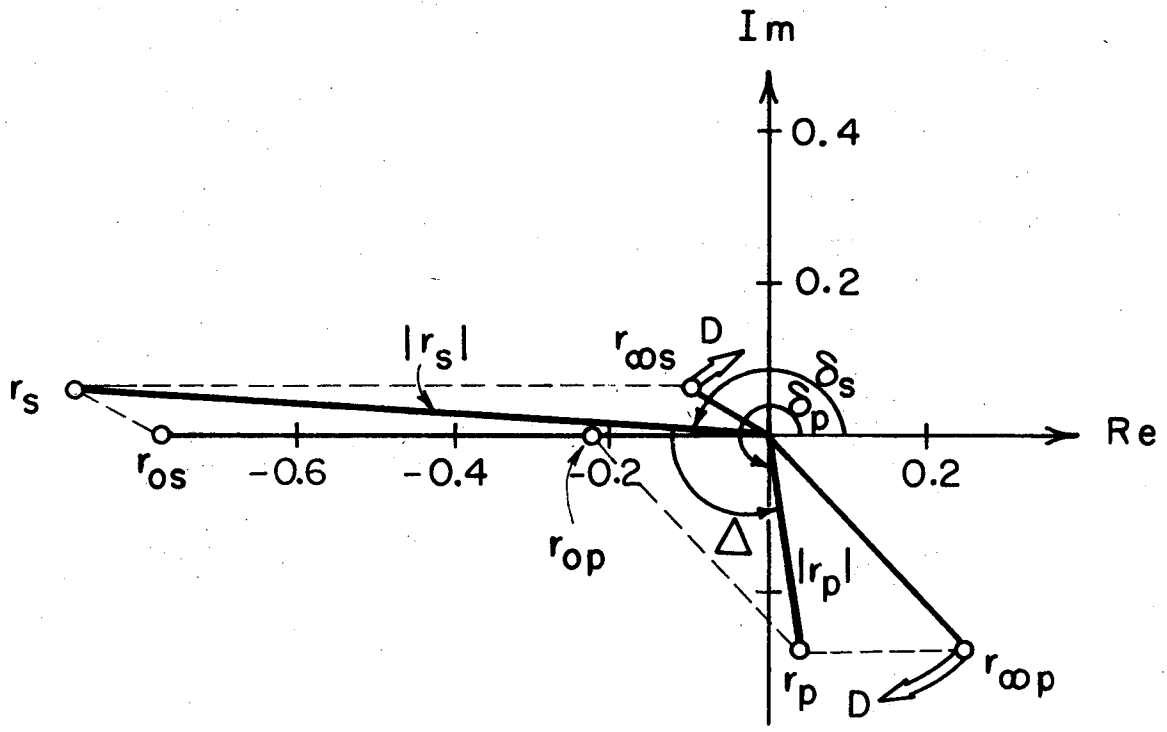

XBL719-4405

Fig. 26

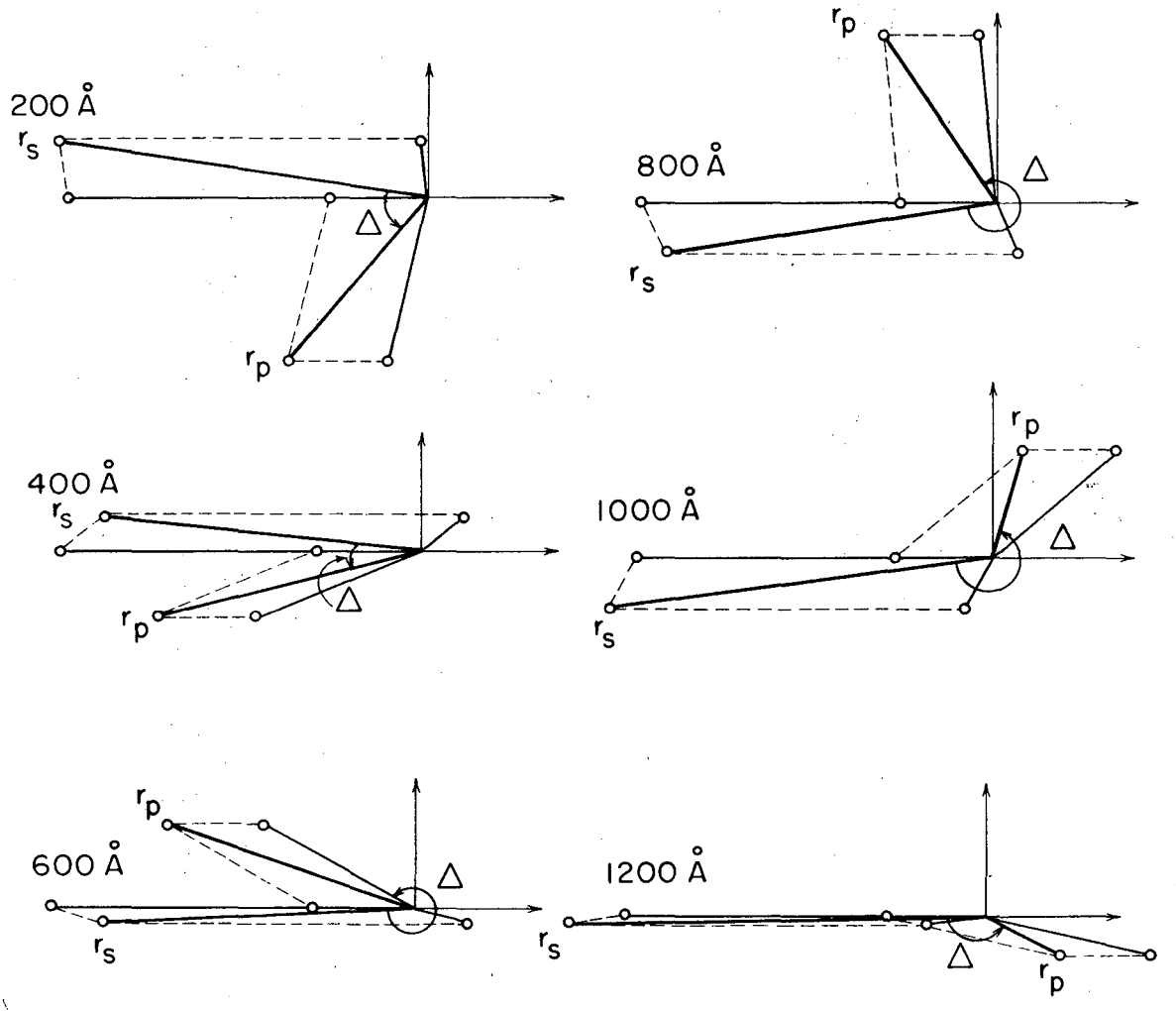

XBL719-4406

Fig. 27

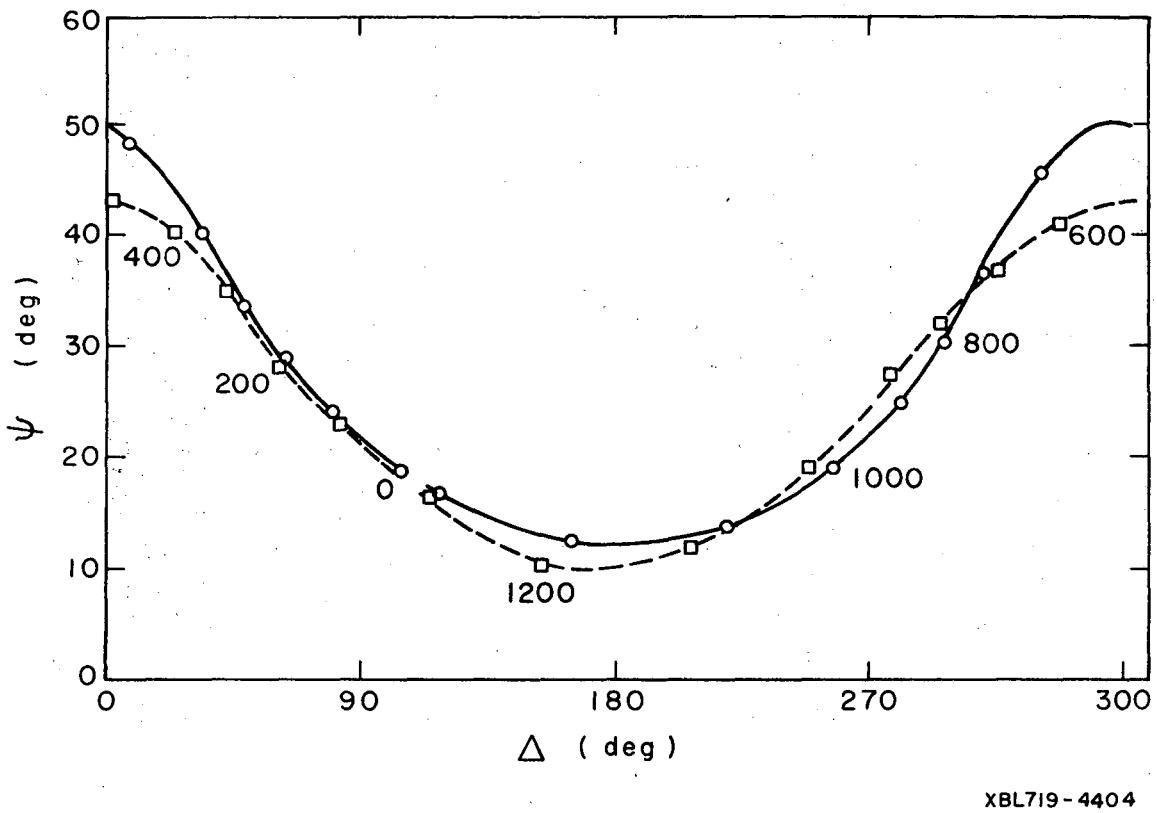
60
50
40
30
20
10
0
ψ (deg)
0
90
180
270
300
Δ (deg)
400
200
0
1200
1000
800
600
XBL719-4404

Fig. 28

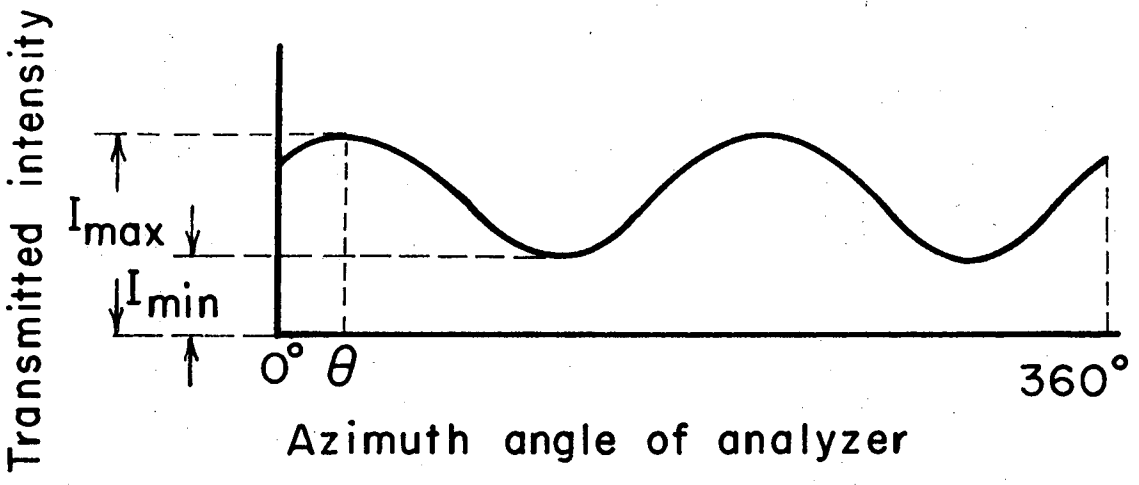

XBL719-4399

Fig. 29

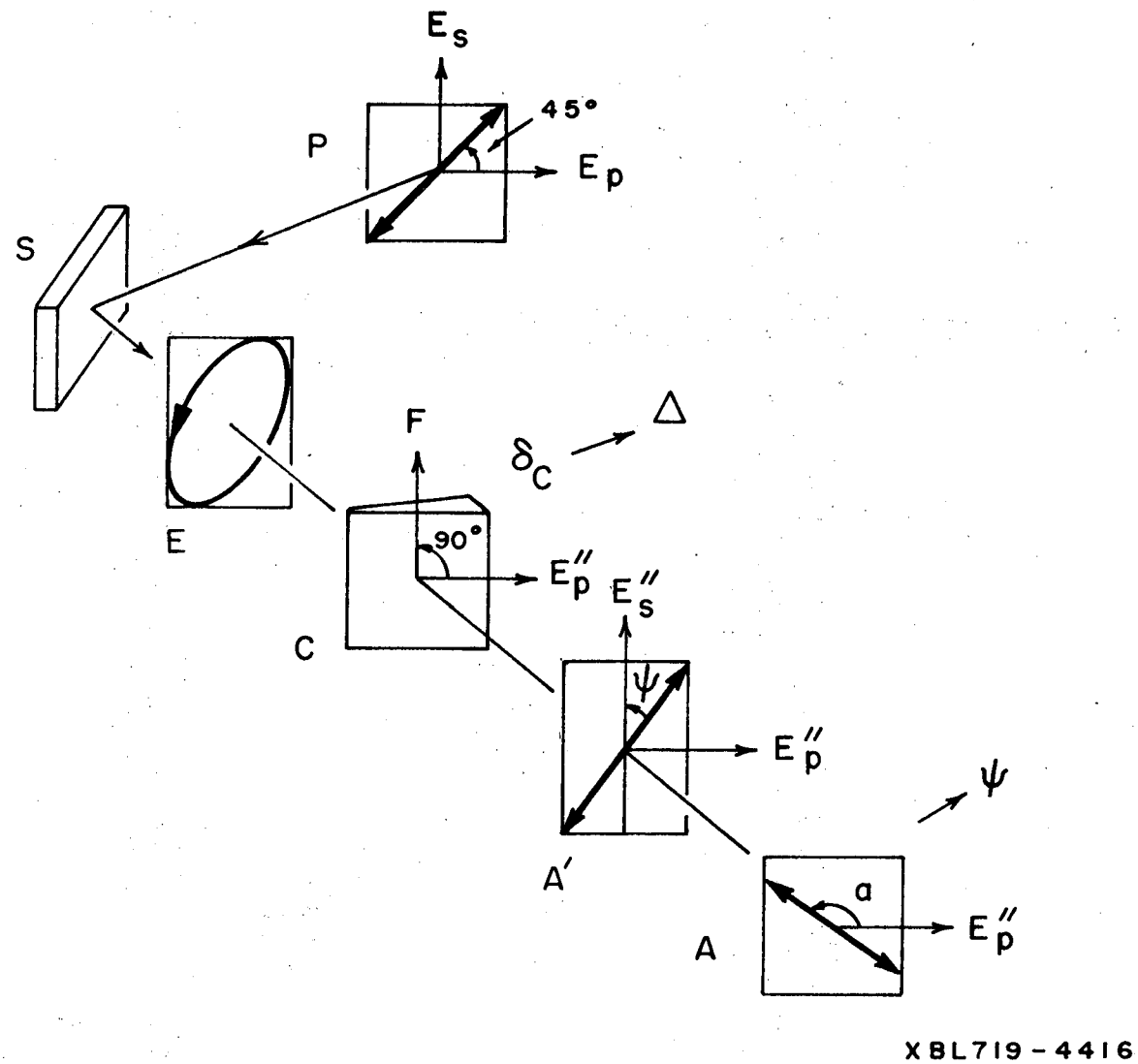
E_s
45°
P
E_p
S
E
F
δ_C
Δ
90°
E_p''
E_s''
C
ψ
E_p''
ψ
A′
a
A
E_p''
XBL719-4416

Fig. 30

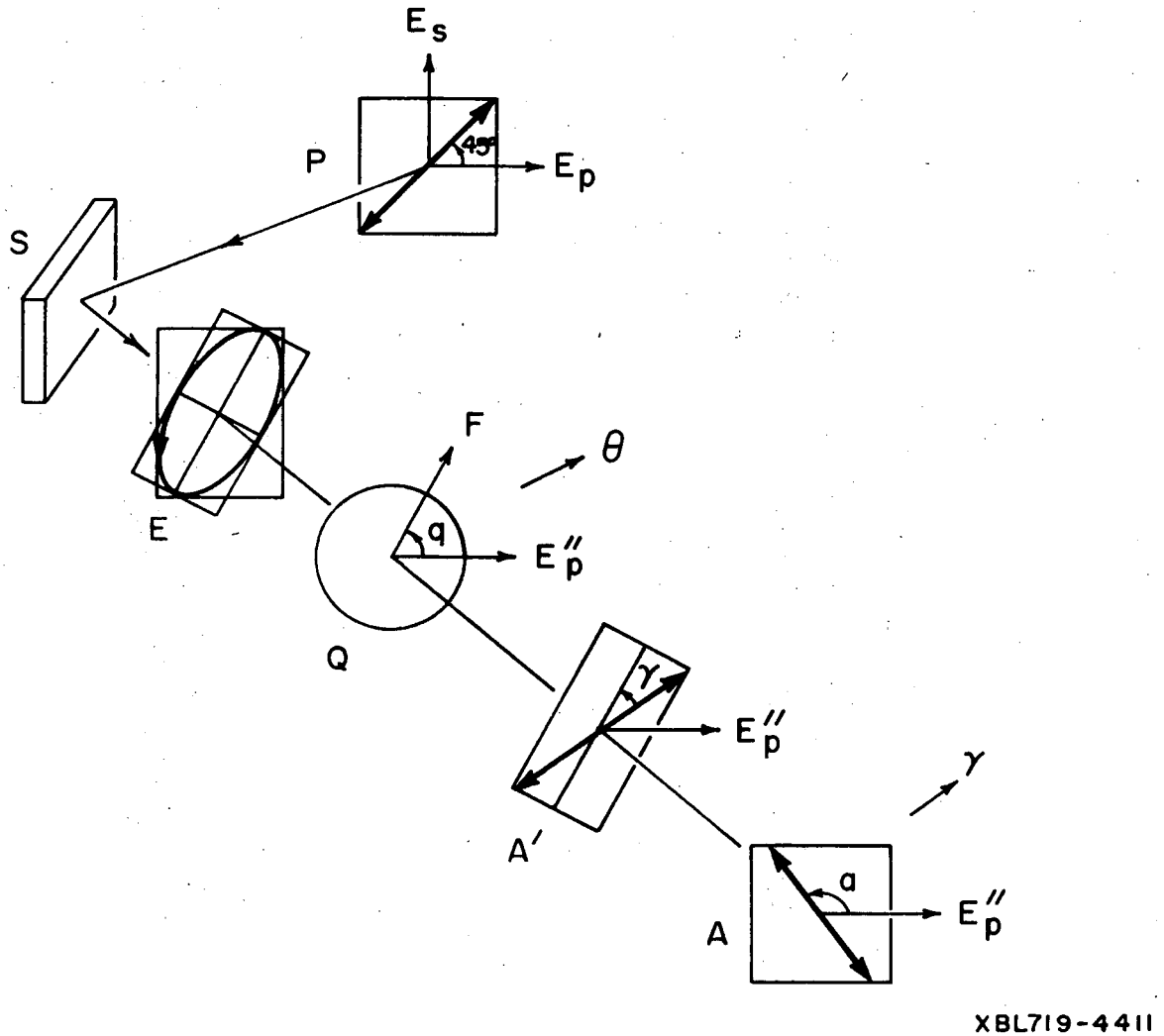

Fig. 31

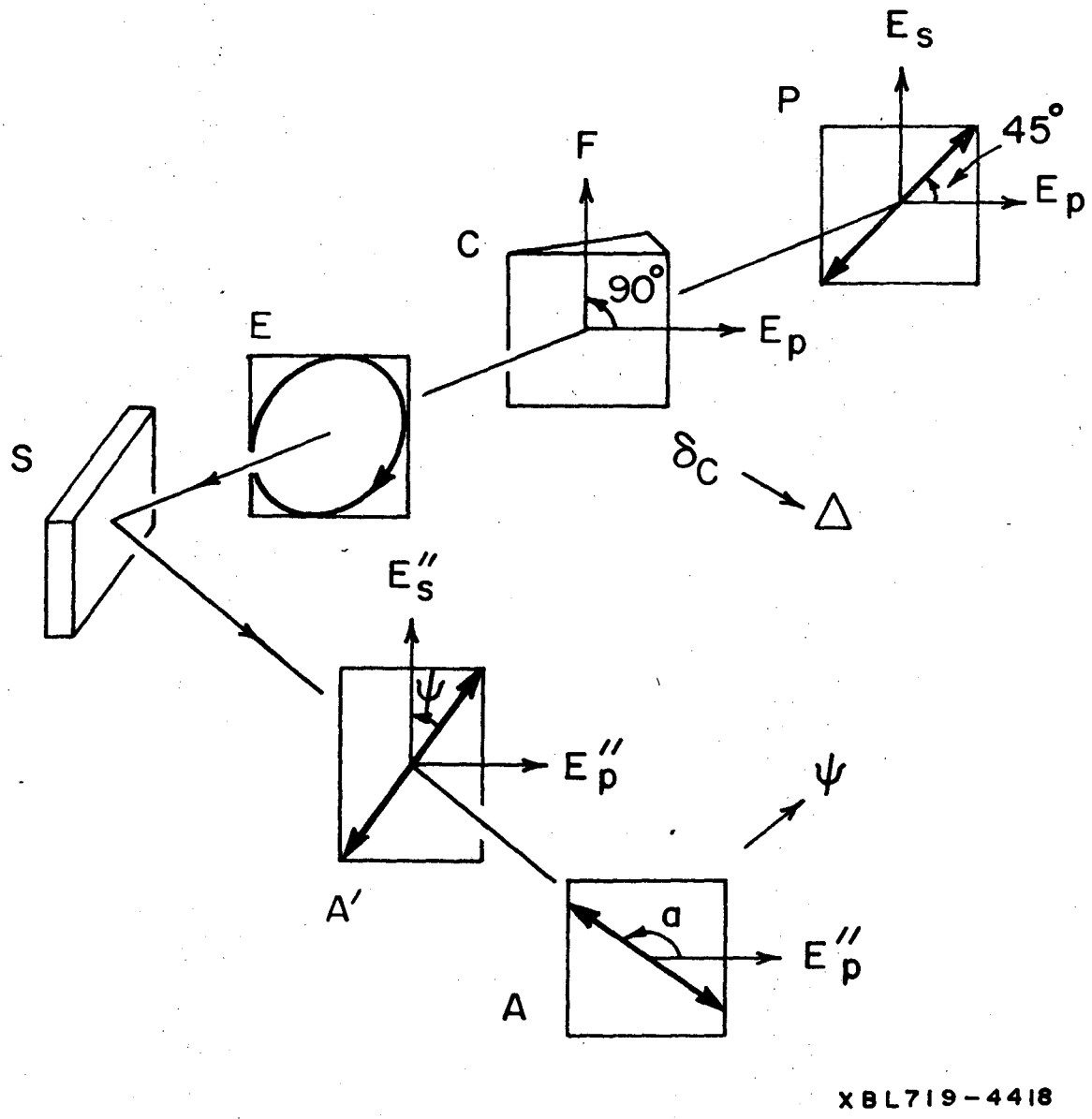

Fig. 32

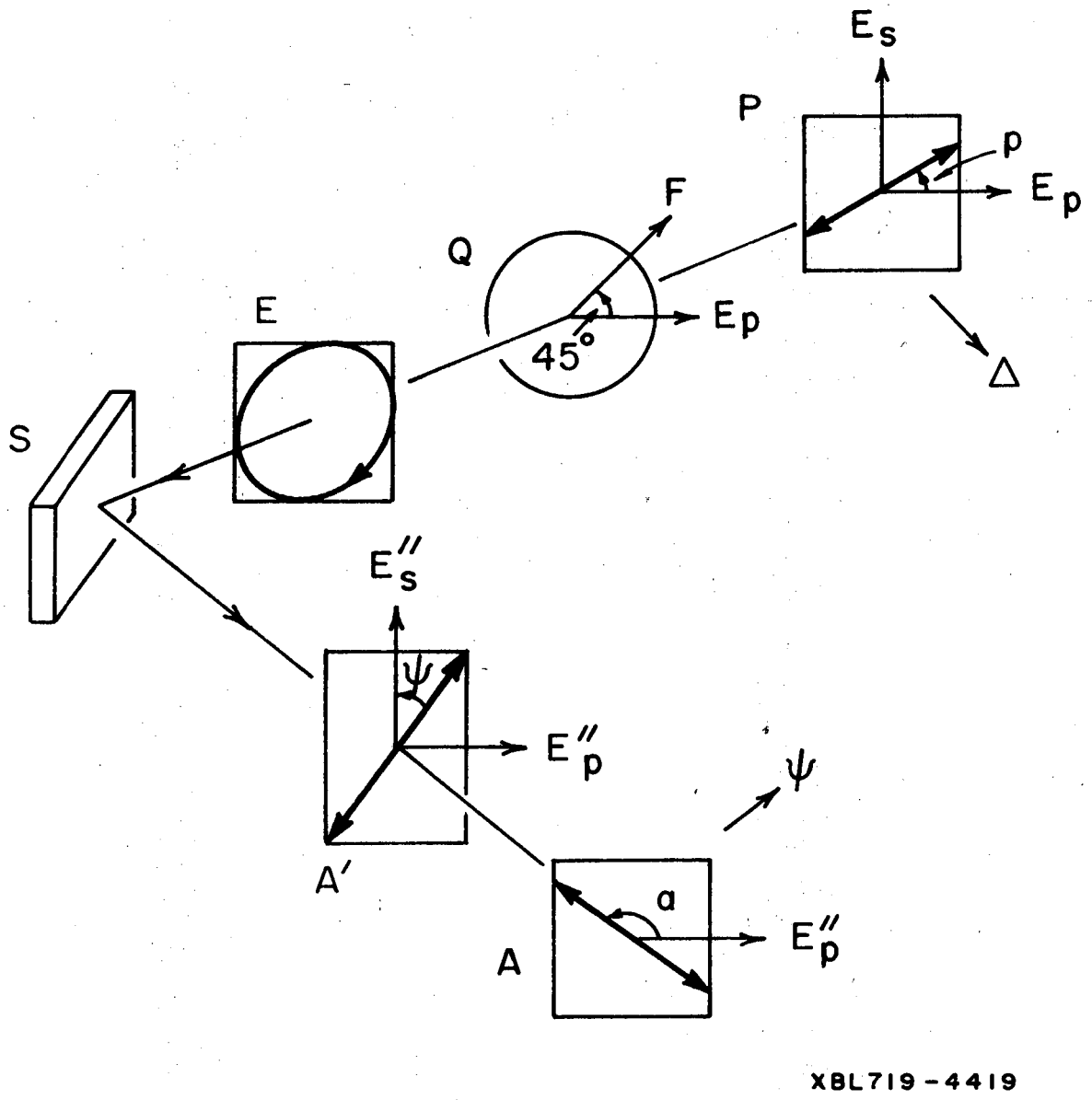

Fig. 33

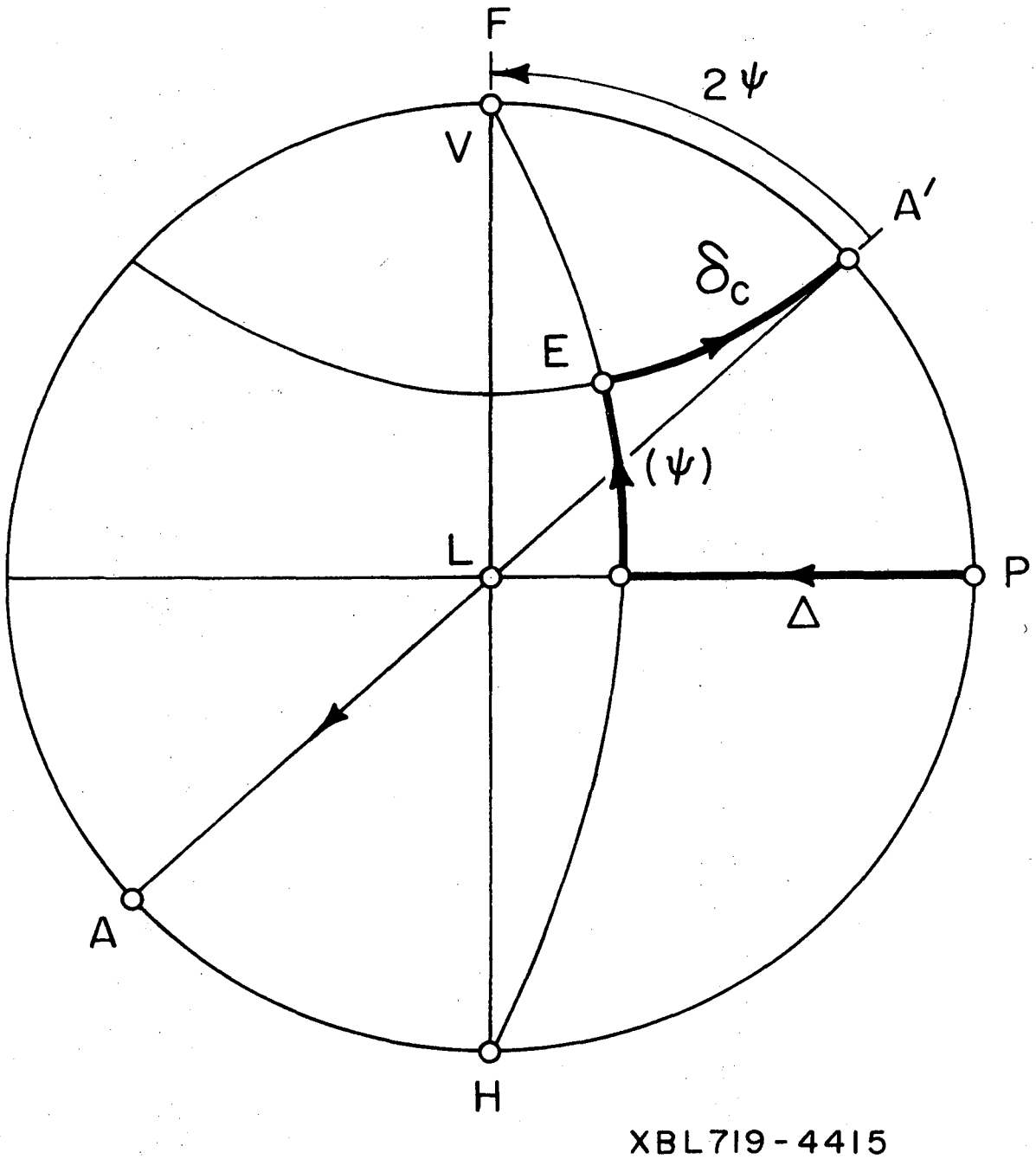

Fig. 34

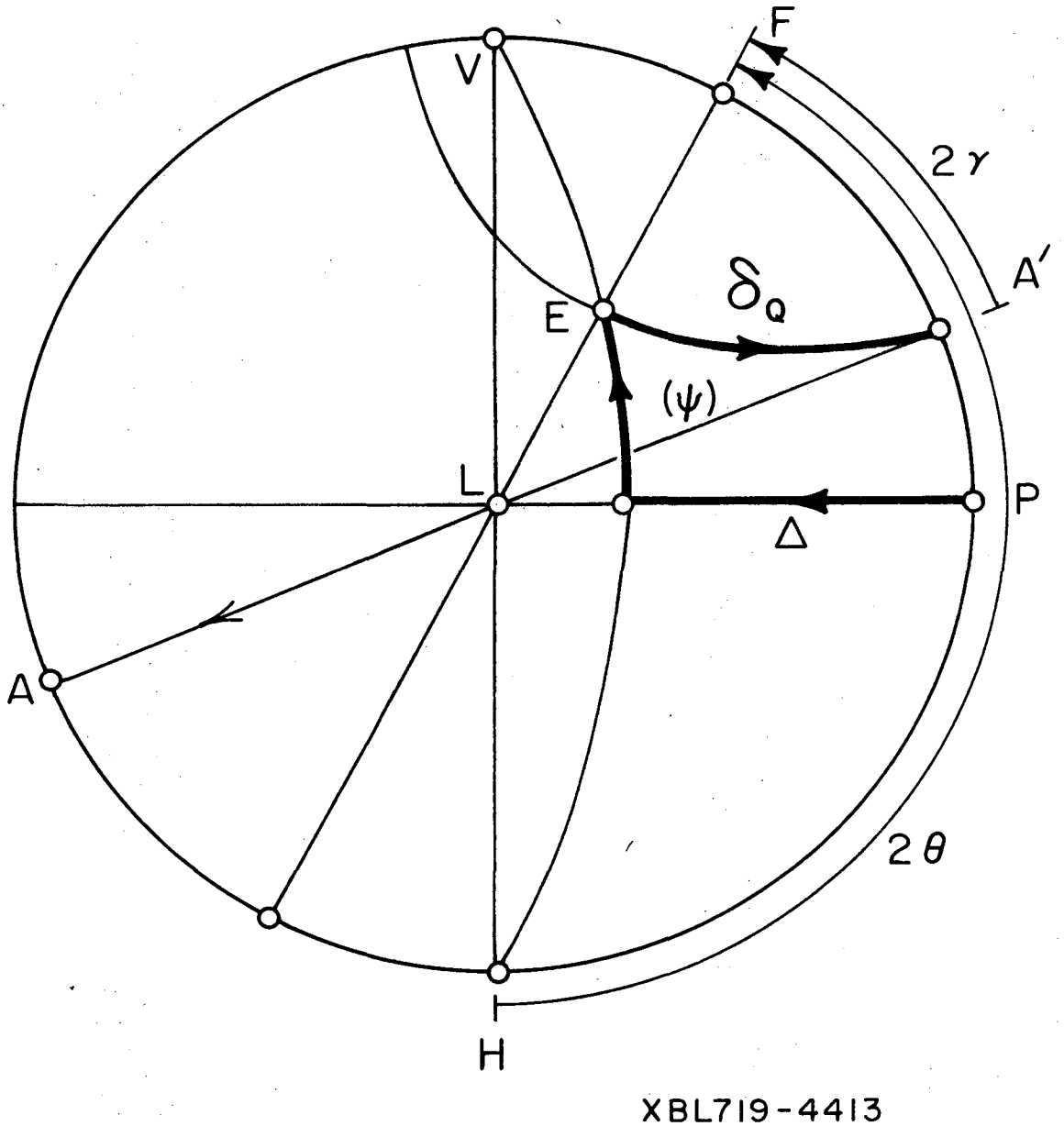

Fig. 35

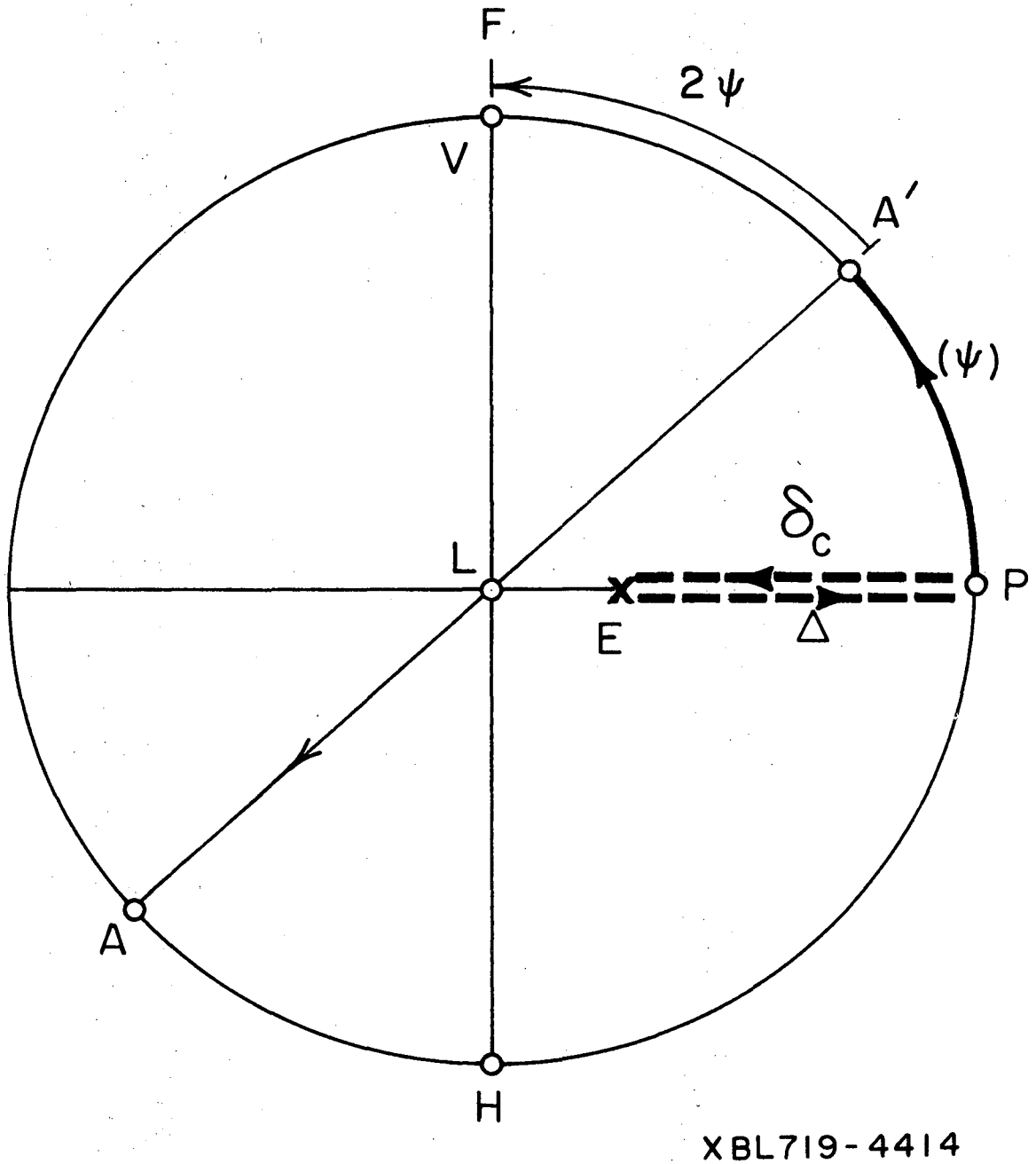

Fig. 36

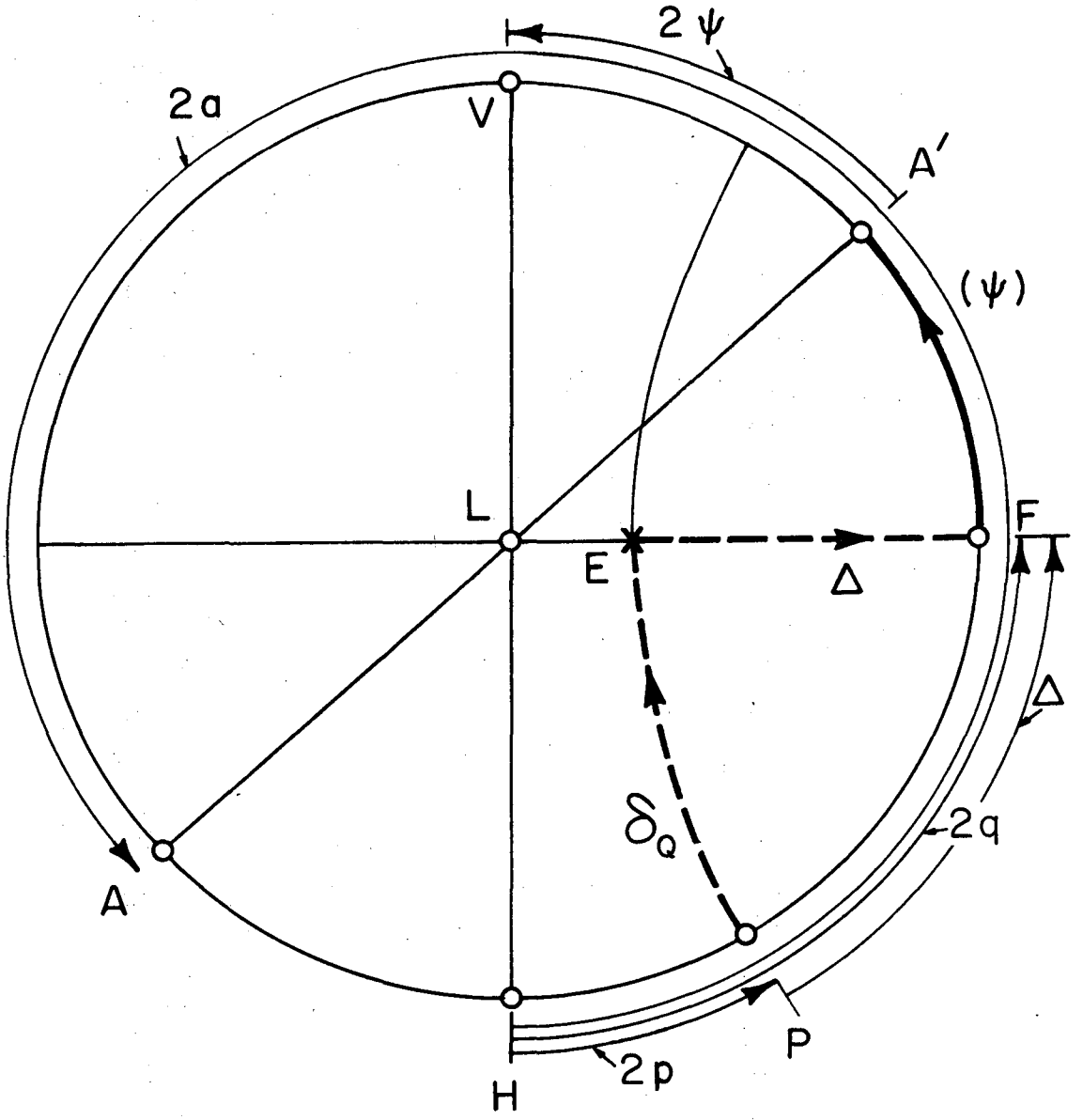

XBL719-4412

Fig. 37

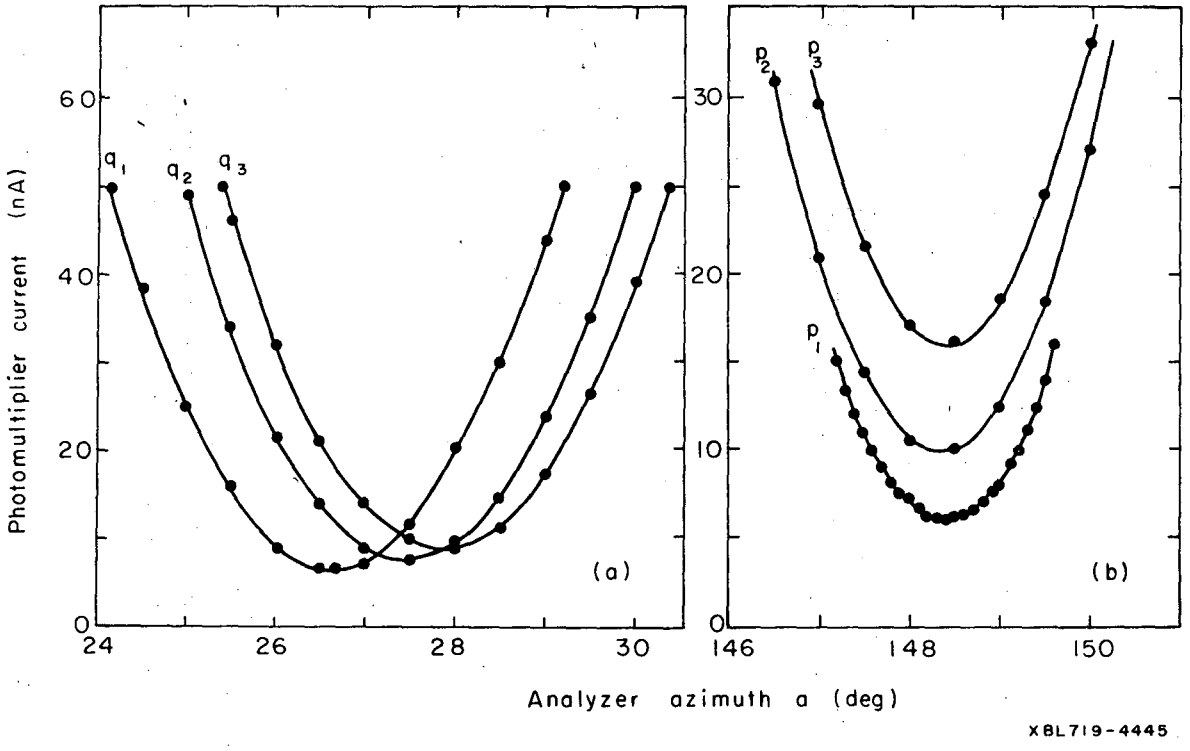
Photomultiplier current (nA)
60
40
20
0
24
26
28
30
q_1
q_2
q_3
(a)
30
20
10
0
146
148
150
p_2
p_3
p_1
(b)
Analyzer azimuth a (deg)
XBL719-4445

Fig. 38

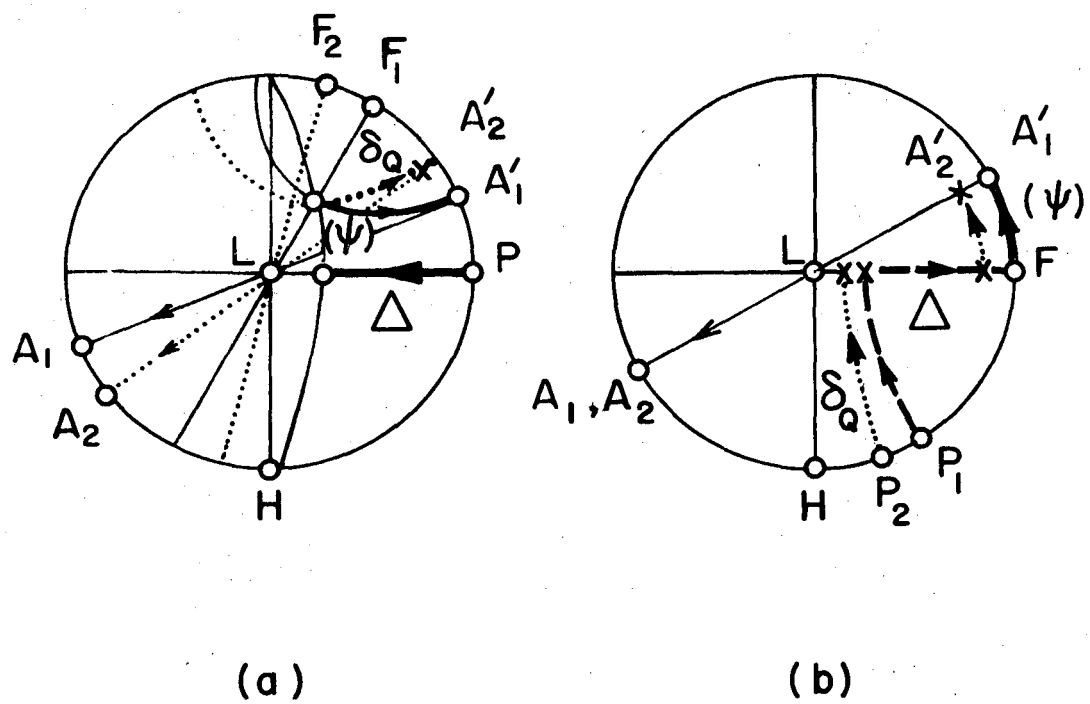

XBL719-4417

Fig. 39

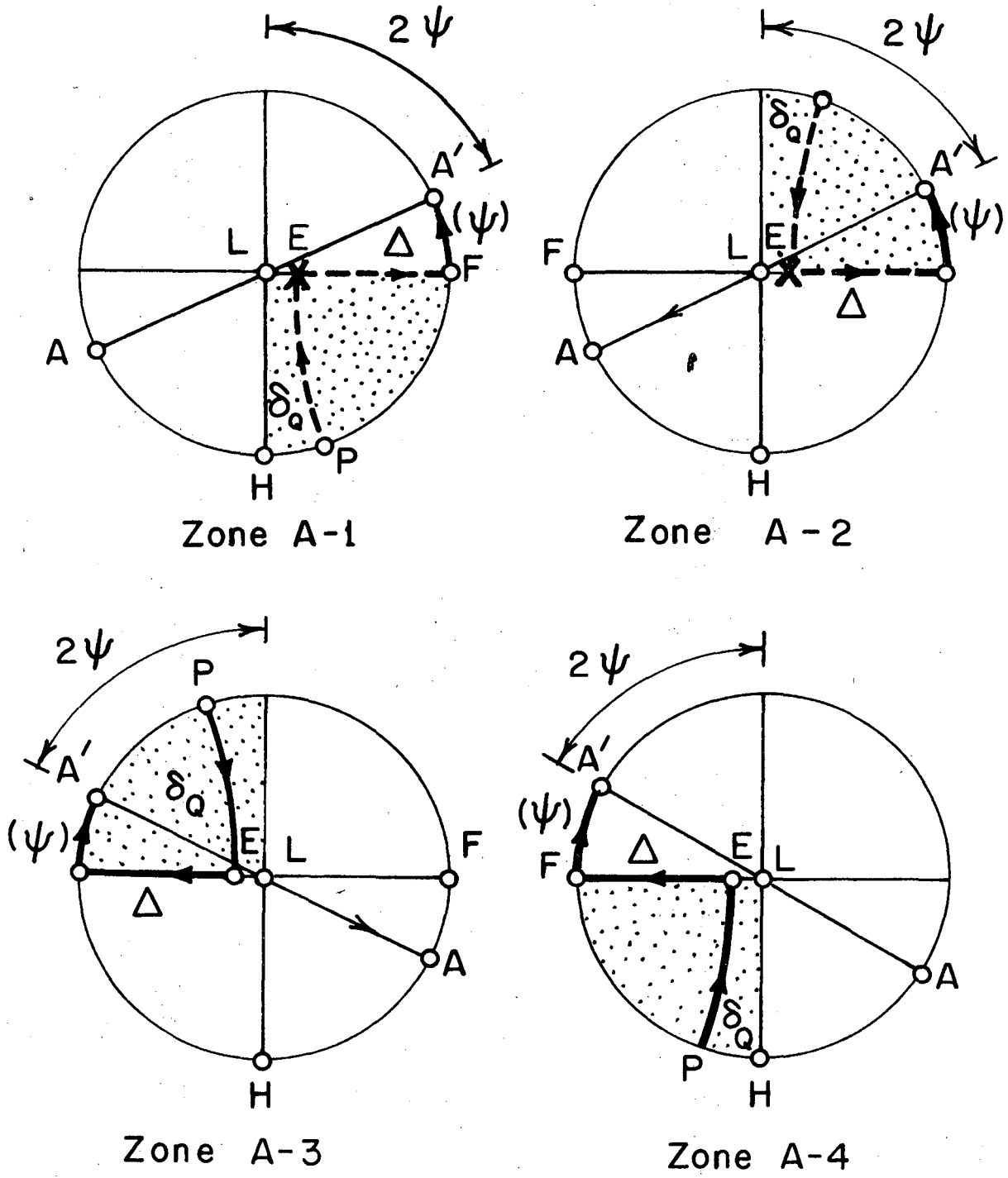

XBL719-4420

Fig. 40

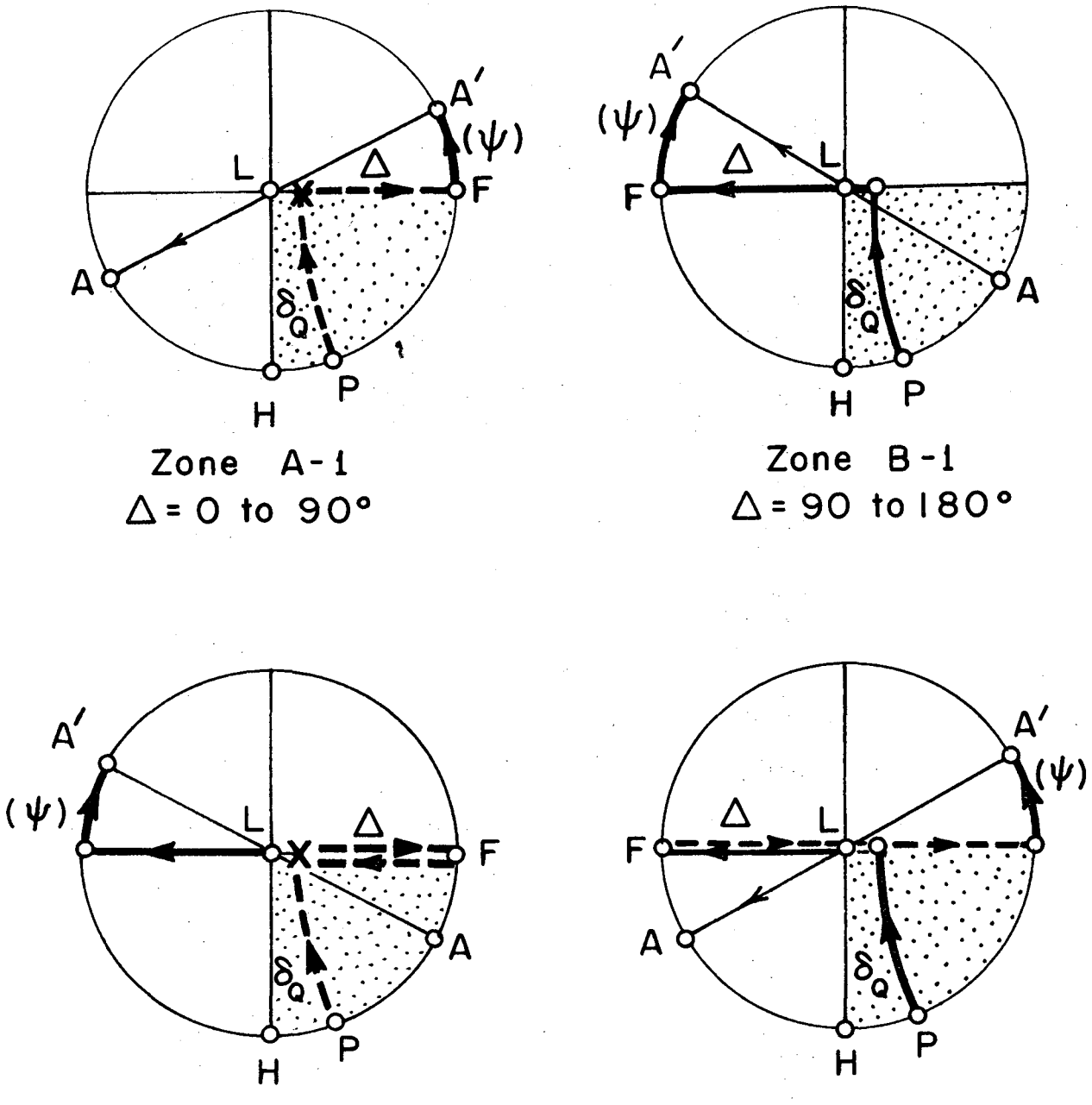

XBL719-4421

Fig. 41

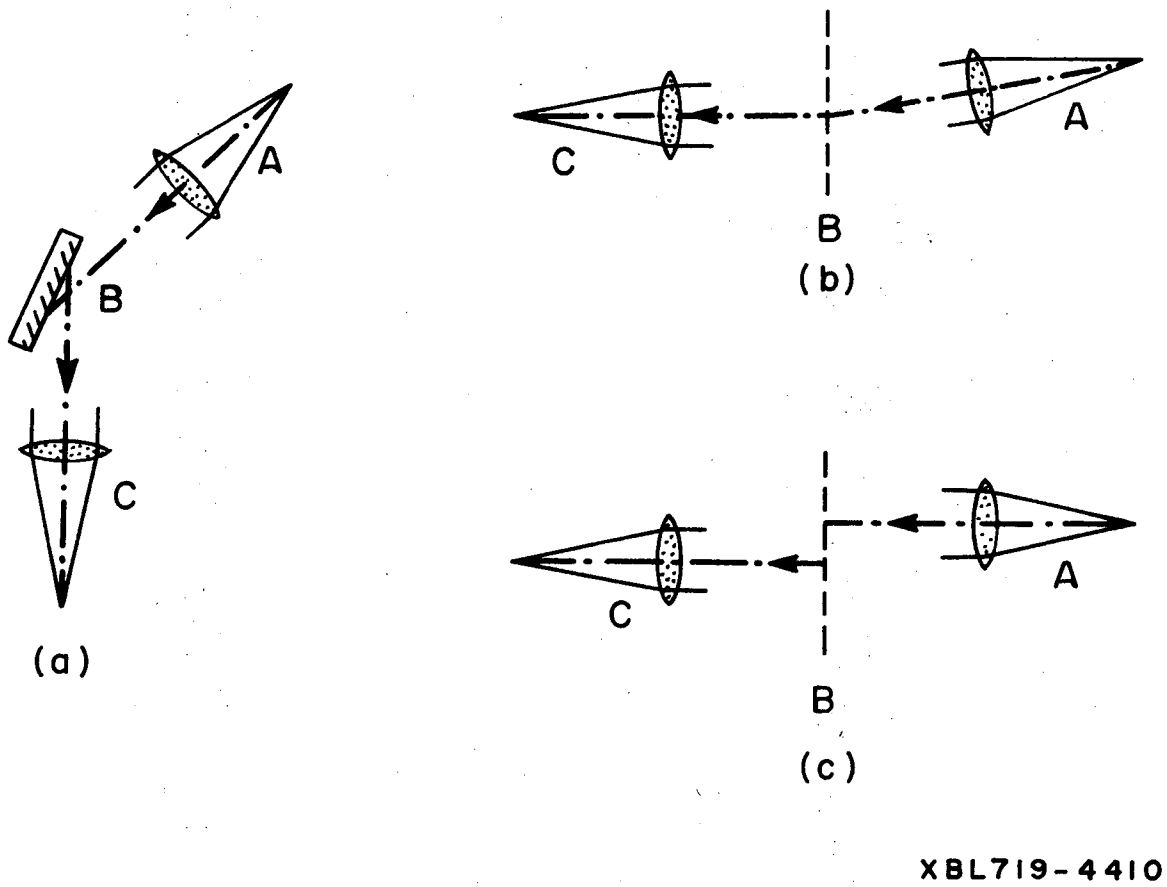

Fig. 42

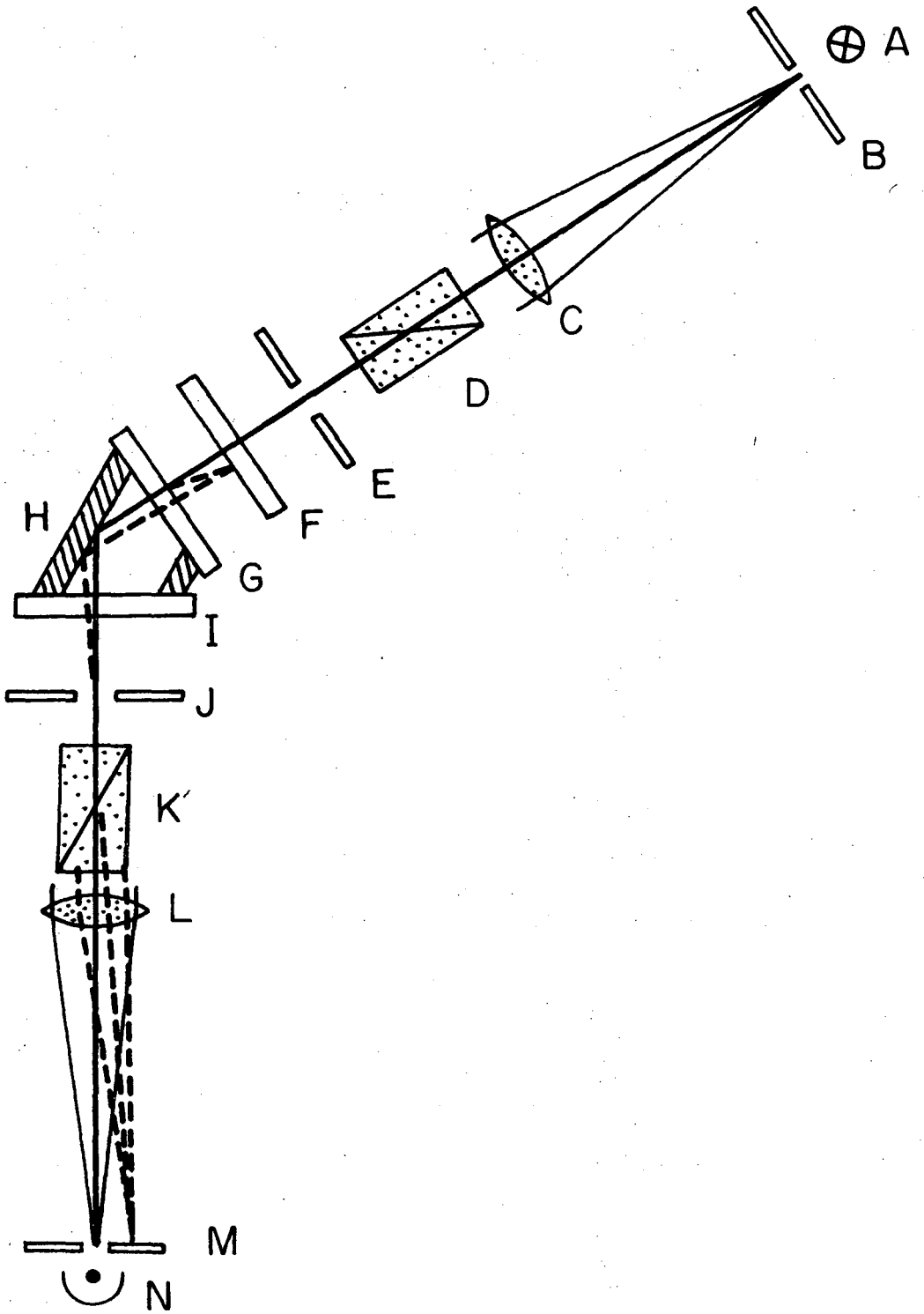

XBL719-4444

Fig. 43

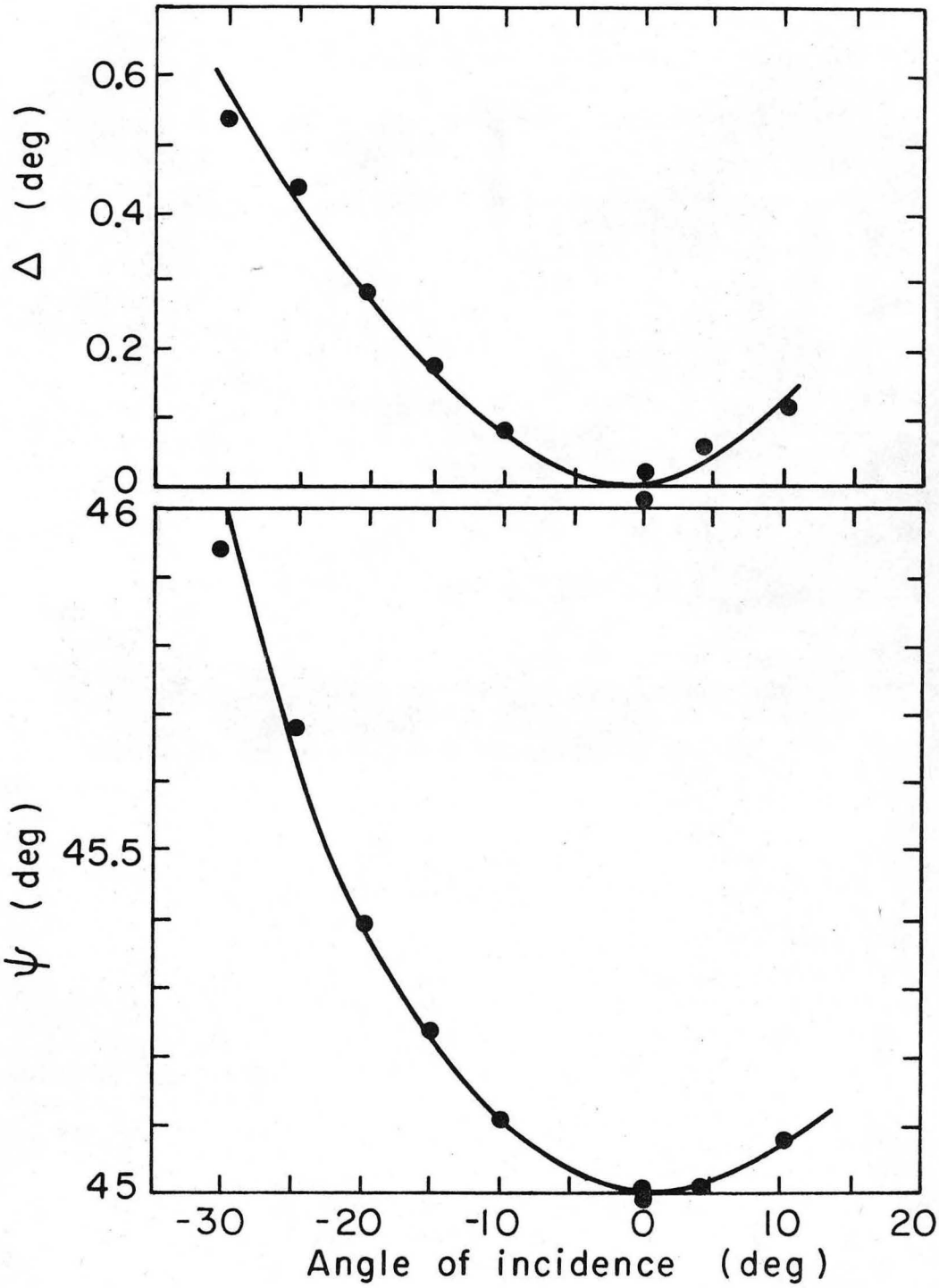

XBL719-4446

Fig. 44

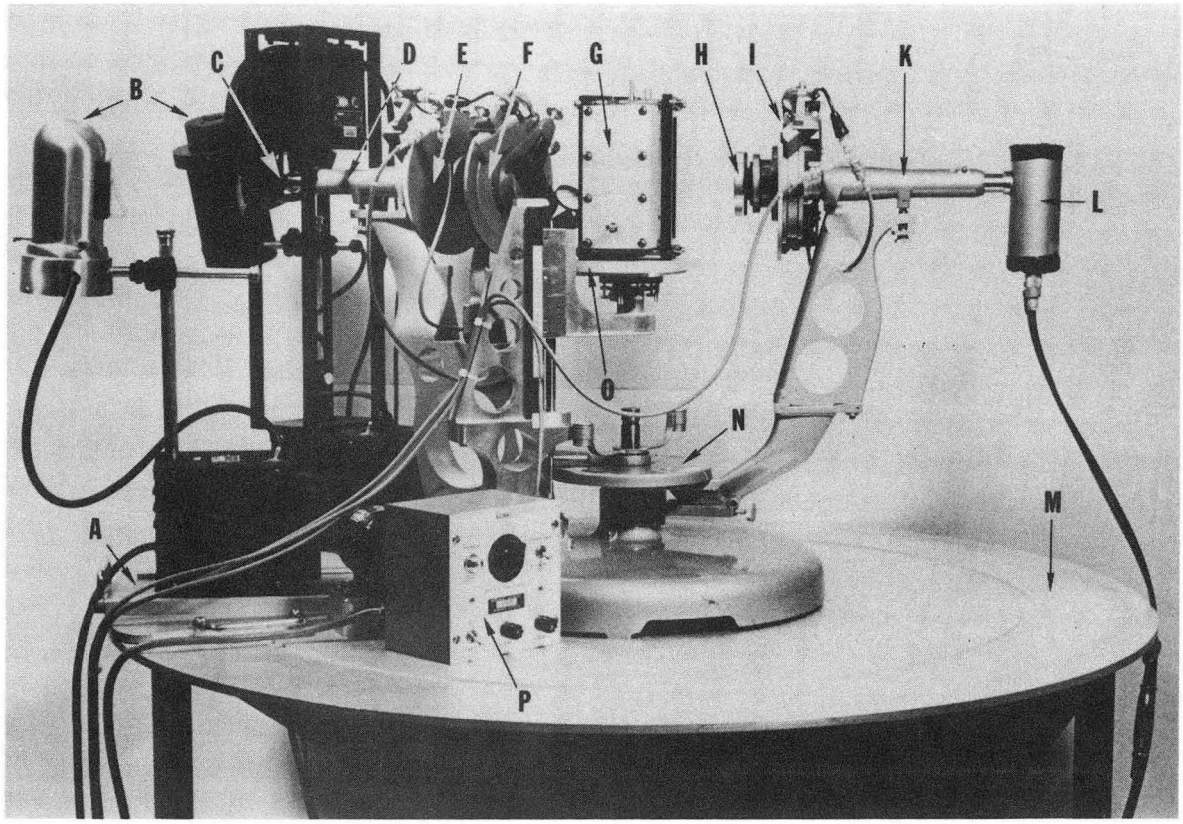

XBB 682-860

Fig. 45

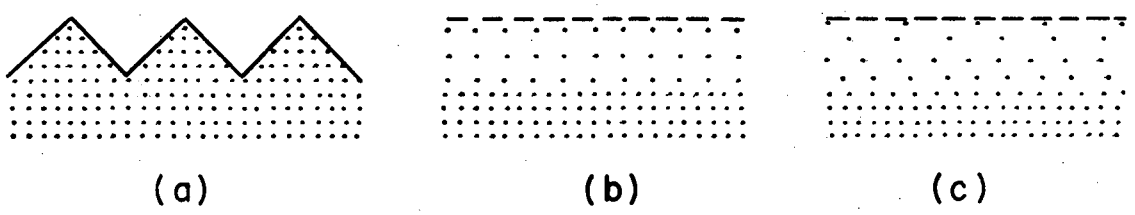

XBL 719-4442

Fig. 46

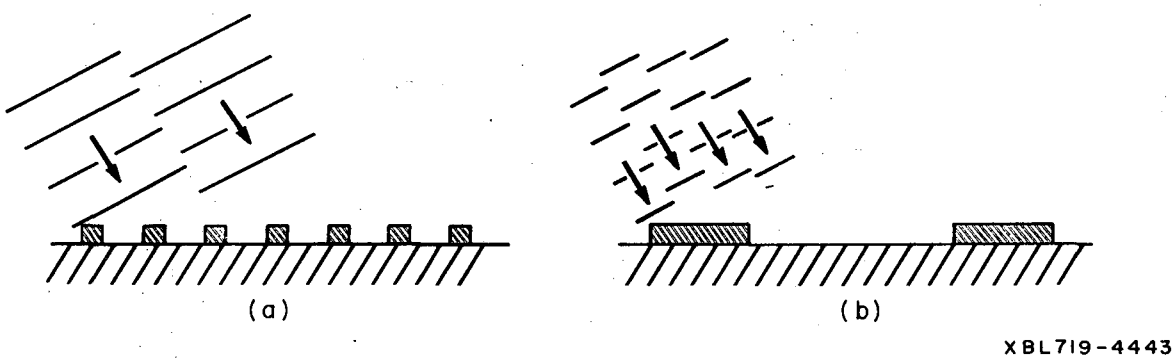

Fig. 47

LEGAL NOTICE

This report was prepared as an account of work sponsored by the United States Government. Neither the United States nor the United States Atomic Energy Commission, nor any of their employees, nor any of their contractors, subcontractors, or their employees, makes any warranty, express or implied, or assumes any legal liability or responsibility for the accuracy, completeness or usefulness of any information, apparatus, product or process disclosed, or represents that its use would not infringe privately owned rights.

TECHNICAL INFORMATION DIVISION
LAWRENCE BERKELEY LABORATORY
UNIVERSITY OF CALIFORNIA
BERKELEY, CALIFORNIA 94720